UNCLASSIFIED

DEPARTMENT OF PHYSICS

MEGATRON ACCELERATOR FINAL REPORT

April 15, 1961 - June 15, 1964

SIGNAL CORPS CONTRACT NR. DA 36-039-sc-87242(E)

ARPA Order Nr. 112-62, Project Code Nr. 3720

United States Army
Electronics Materiel Agency
Fort Monmouth, New Jersey

Information for Abstract Card
Department of Physics
Stevens Institute of Technology
Hoboken, New Jersey

Megatron Accelerator Final Report

K. C. Rogers, S. J. Lukasik, L. Ferrari

Final Report, April 15, 1961 - June 15, 1964
223 pp illustrated

Signal Corps Contract No. DA 36-039-sc-87242(E)
Unclassified

ARPA Order Nr. 112-62 Project Nr. 3720

This is the final report on the Megatron (plasma betatron) Project. Construction details of the accelerator are given, and methods of shaping and measuring the magnetic guide field are described. Methods of generating the plasma and its initial properties are listed. Application of the time-varying magnetic guide field results in the production of a runaway electron beam of peak energy 1 Mev and beam intensity approximately one ampere. Methods of detecting the runaway electrons are described, and the electron life histories are studied. It is found that ultimate destruction of the runaway electron beam results from a collective interaction of the beam electrons and the background plasma. The observations are compared with theoretical results of Field and Fried. Also included are the results of a computer study of early time collective effects in a cold plasma subjected to a rapidly rising betatron guide field.

TABLE OF CONTENTS

Introduction, "A Survey of the Megatron Project"
K. C. Rogers

"Behavior of Runaway Electrons in a Plasma Betatron"
L. A. Ferrari, K. C. Rogers

"Early-Time Collective Effects in a Plasma Betatron"
S. J. Lukasik, K. C. Rogers

Papers and Publications Produced on the Megatron

Personnel

Distribution List

A SURVEY OF THE MEGATRON PROJECT

In 1956, at the CERN Accelerator Conference[1], G. I. Budker suggested that the acceleration of electrons within a plasma by means of magnetic induction may be a way to create an intense (kiloampere) beam of relativistic electrons. His suggestion was accompanied by a preliminary report on a betatron device in which he claimed to have generated relativistic electron beams of approximately 20 amperes. The following year D. Finkelstein at Stevens in a brief note[2] outlined a mega-gauss betatron (Megatron) scheme for production of relativistic electrons in a plasma. The Megatron design was guided by the earlier work of Furth, Levine and Wanniek[3] on the production of very intense pulsed magnetic fields. At about the same time (1957) Finkelstein at Stevens initiated the construction of a low inductance rapid discharge capacitor bank (100 K Joule) suitable for driving an air-core betatron field coil. He was joined by K. C. Rogers in the work in early 1958 and a proposal for support of the work was submitted to the U. S. Atomic Energy Commission. Construction of the bank proceeded in 1958 under the direction of K. C. Rogers while D. Finkelstein spent a year at CERN. In the Spring of 1959 the Atomic Energy Commission awarded a one year contract to Stevens for construction of the plasma betatron accelerator. Work carried out under this contract was reported at the 1959 CERN Accelerator Conference and aroused considerable interest. Further support of the Stevens work was requested of the Advanced Research Projects Agency and was awarded through a plasma physics contract at Stevens with the United States Army Signal Corps. This agency took over support of the project until its termination in June 1964. Dr. Finkelstein joined the faculty of Yeshiva University in 1960

and terminated his connection with the project in 1961. Since that time the work has been carried out under the direction of K. C. Rogers.

Many technical problems arose during the course of the project and there were serious delays until they could be solved. The original scheme for generating the betatron field proved unworkable because of difficulties in producing the desired field shape. Another method was found, but this placed limitations on the maximum volts/turn that could be applied to the plasma. Construction of the low-inductance high voltage capacitor bank was difficult and slow because of dielectric breakdown problems. The most difficult and time consuming task was that of shaping the air-core betatron field so as to have all of the desired properties i.e., suitable vector potential well depth, freedom from azimuthal inhomogeneities, etc. The shape of pulsed magnetic fields varying on a microsecond time scale had to be measured with a precision of $\sim 0.1\%$. The production of large runaway electron beams in the plasma required that the betatron field be applied to a low density ($\sim 10^{10}$ cm^{-3}) plasma with no appreciable neutral particle background density. Production of a suitable plasma in the acceleration chamber required special techniques which in turn introduced problems of their own regarding betatron guide field perturbations. All of these problems were eventually solved and runaway electron beams were consistently produced with energies approaching the peak energy of the machine, approximately 1 Mev. (The machine peak energy was set by the dielectric strength of the flux guides in the betatron field coil.) However, they were disappointingly small (~ 1 ampere). In spite of the considerable care taken to optimize the conditions for runaway electron production the beam intensities produced remained small. The original design goal of the project was the production

of kiloampere electron beams with applied electric fields of 2×10^3 volts/cm. Dielectric strength limited the applied electric fields in our machine to ~ 20 volts/cm and resulted in beams of approximately one ampere. Even if our results could be extrapolated to the original design figure of 2×10^3 volts/cm, we would expect only 100 amperes of beam. The technical difficulties in achieving kilovolt/cm applied electric fields in a betatron guide field are so great that we do not consider it reasonable to attempt to meet them.

Our results further show that the runaway electron beams created in the plasma eventually are destroyed by collective effects. The beam survives to nearly the end of the acceleration cycle before its destruction however, so that the electrons are accelerated to approximately the peak energy of the machine. We conclude that our results offer little encouragement for further development of plasma betatrons as sources of intense relativistic electron beams.

Many colleagues and students have contributed from time to time to this project. This final report was prepared by L. Ferrari, S. J. Lukasik, and K. C. Rogers, but it rests heavily on the many contributions of G. Brucker, J. R. M. Coulter, D. Finkelstein, H. Huber, A. Jermakian, C. T. Lunghard, I. Mansfield, and G. Zepko.

K. C. Rogers

1. G. I. Budker and A. A. Naumov, CERN Symposium on High Energy Accelerators and Pion Physics (Geneva, 1956).

2. D. Finkelstein, The Megatron, NYO-7735 (1957), D. Finkelstein, The Megatron, Second U. N. International Conference on the Peaceful Uses of Atomic Energy, Geneva (1958).

3. H. P. Furth, and R. W. Wanniek, Rev. Sci. Instr. 27, 195 (1956), H. P. Furth, M. A. Levine, and R. W. Wanniek, Rev. Sci. Instr. 28, 949 (1957).

"Behavior of Runaway Electrons

in a Plasma Betatron"

L. A. Ferrari and K. C. Rogers

ABSTRACT

BEHAVIOR OF RUNAWAY ELECTRONS IN A PLASMA BETATRON

Runaway electrons generated by induction acceleration in a plasma betatron with axially symmetric guide field $B_z(r,z,t)=B_0(R_0/R)^n \cdot f(z)\sin 2\pi t/\tau$ ($n=0.6$, $\tau=16\mu$sec, $R_0=4.8$ cm) together with auxiliary azimuthal guide field $B_\theta(R)=(k/r)$, ($2\ kG \leq B_\theta(r) \leq 5kG$) have been studied for a wide range of induction electric fields E_θ ($2.5\ v/cm \leq (E)_\theta \leq 26 v/cm$). Experiments have been carried out in argon and krypton at ambient pressures of 0.5-2 Torr. The ratio of the applied electric field to the critical electrical field for runaway was typically ~ 500 so that most of the electrons should run away. Runaway currents of $\sim$ 1A were observed immersed in a background conduction current of 25-100 A. The runaway electrons strike the vacuum chamber walls at a time t_x after betatron acceleration has begun. The resulting x-rays are detected with a scintillation counter. The x-ray time t_x has been measured as a function of E_θ and B_θ for several half-cycles of the guide field. It is found that t_x decreases with E_θ but increases with B_θ. It is also found that t_x depends on the relative orientation of E_θ with respect to B_θ. This is shown to be due to a small transverse magnetic field associated with the B_θ guide field. The small runaway current is consistant with that determined from the self electric field generated by the adiabatic constriction of the runaway stream or the Negative-Mass-Instability.

The reason for the beam disruption and subsequent x-ray emission are unexplained but the mechanism of Field and Fried appears to describe the process.

The betatron guide field was generated in a low inductance (50×10^{-9} h) single-turn coil using flux-concentrators. Techniques used to construct the flux-concentrators and measure the resulting pulsed magnetic field distribution are also described.

Lawrence A. Ferrari, Author

Professor Kenneth C. Rogers
Thesis Advisor

Department of Physics
Stevens Institute of Technology
Castle Point Station
Hoboken, New Jersey
May, 1965

TABLE OF CONTENTS

		PAGE
I	Introduction	I
II	Theory of Runaway Electrons	8
III	Equations of Motion for Single Particles	
	3.1 In an idealized betatron field	II
	3.2 In a betatron field with azimuthal inhomogenities	I6
	3.3 In a betatron field and additional azimuthal magnetic field	I8
	3.4 Just after turn-on of the betatron field	2I
IV	The Magnetic Field	
	4.1 General considerations	26
	4.2 Field Coil Design	29
	4.3 The Flux Concentrators	30
	4.4 Difference Amplifier Technique for Measuring the Magnetic Field	3I
	4.5 Shaping the Field	33
	4.6 Radial Distribution	36
	4.7 The Vector Potential	37
	4.8 Azimuthal Field Measurements	39
	4.9 Results of Magnetic Field Measurements	40
	4.10 Summary	45
V	Additional Apparatus and Plasma Generation	
	5.1 The B_e Field	46
	5.2 The Vacuum System	50
	5.3 Plasma Generation	5I
VI	Diagnostics	
	6.1 Electron Density	57
	6.2 Electron Temperature	68
	6.3 The Runaway Current	69
	6.4 X-Ray Measurements	8I
	6.5 X-Ray Absorbtion Measurements	83
	6.6 Electric Field Measurements	86
VII	Results and Analysis of X-Ray Emission Time	88
VIII	Summary	I2I
IX	Conclusions	I22

X	Acknowledgement	I23
XI	Appendix #I Transient Penetration of a Magnetic Field into a Conductor	I24
XII	Appendix #2 Error Produced by a Small Lateral Displacement of a Single Turn Coil	I28
XII	Appendix #3 Electric Quadrupole Coil Design	I30
XIV	References	I32

INTRODUCTION

In 1956 Budker[1] suggested that the principle of magnetic self-focusing of a relativistic stream, first discovered by Bennett[2], might be used to build a new type of high energy particle accelerator. This principle is based on the fact that it takes a relatively small amount of positive charge added to an intense relativistic electron beam to replace the Coulomb repulsion by strong attraction. The magnetic self focusing produces electromagnetic radiation which then damps the transverse oscillations of the electrons. This would then cause the beam to shrink to a thin thread with very large electric and magnetic fields on the surface.

Budker proposed that the self magnetic field of the beam so formed could then be used as the guid field for the acceleration of ions. The electrons would travel large distances while the beam diameter was shrinking, therefore it was obvious that a circular type of particle accelerator such as a betatron would be necessary to hold the electrons a, while the stream was shrinking and b, while the ions were being accelerated.

Budker envisioned a circulating beam current of 17,000 amp (obtained when the number of electrons per length of stream equal to the classical radius of the

electron was equal to one) however, beam current calculations by Finkelstein and Maisonnier[3] and finally by Schmidt[4] showed that the beam diamagnetism would limit the maximum beam current in plasma betatrons to several hundred amperes.

In spite of this drastic reduction in maximum beam current from that envisioned by Budker the plasma betatron is a device which still warrants interest. Fainberg[5] in his review article lists approximately twenty different instabilities that can be generated by the passage of a charged particle stream through a plasma. The energy lost by the beam particles in exciting oscillations can be considerable; when the number of particles per bunch $N_b \approx 10^7 - 10^8$ the energy loss can be as high as $10^3 - 10^4$ ev/cm. per bunch. Since this energy loss can be so large it is obvious that these interactions may play an important role in plasma physics and hence be worthy of study. In a plasma betatron the electrodes which are present in most beam-plasma studies are absent. This coupled with the toroidal geometry enables a very long path length for the circulating electrons. In principle it is also possible to accelerate the electrons to any velocity between their initial thermal velocity and essentially the velocity of light. The magnetic guide fields are sufficiently simple so that the single particle motion can be studied analytically

and thus may help to understand the experimental behavior of the device.

Plasma betatrons with low inductance as well as high inductance can be constructed.[6] High inductance plasma betatrons consist of a symmetric arrangement of a group of single turn coils arranged geometrically so that the resulting magnetic field in the median plane between them satisfies the betatron condition.[7-10] A low inductance plasma betatron is constructed within a single turn solenoid. For the latter case the vacuum magnetic field, which is essentially uniform must be distorted (shaped) in a cylindrically symmetric fashion until a betatron field is obtained. The possibility of utilizing the high magnetic field that can be generated in such a coil for a small orbit accelerator has been pointed out by Furth, Levine and Waniek[11] and also by Finkelstein.[12]

The betatron studied by Linhart and Reynolds[7] and Skarsgard at CERN[8], has an azimuthal magnetic field in addition to the betatron field. Results were discouraging since runaway currents of only ≈ / amp were generated.

Drees at Bonn[9] has constructed a high inductance plasma betatron that uses a high-frequency quadrupole electric field for additional stabilization. The maximum runaway current observed in this devise is only ≈ ½ amp.

(10)
Shepherd and Skarsgard have studied a plasma betatron similar to the CERN machine. Again the runaway current is of the order of a few amperes.

The low inductance plasma betatron, the subject of this study, is considerably more difficult to construct than the high inductance type. The advantage of this type of betatron is that the low inductance ($\approx 60 \times 10^{-9}$ h) will in principle allow the field at the orbit to reach several kilogauss in 10^{-6} sec or less and it is for this reason that this type was chosen for this study rather than the high inductance device. Although the low inductance is highly desirable in a plasma betatron, the construction of the field coil and allied apparatus poses more experimental problems than are encountered in the high inductance type. Among these are: a, obtaining a high precision magnetic field shape in a small device, b, voltage insulation because of the combination of small size and high electric fields, c, production of a highly ionized low density plasma in a small vacuum chamber, d, a high degree of azimuthal uniformity in the plasma density is also required, therefore, the plasma must be generated within the torus, e, all measurements are more difficult because of the small size, f, the time required to build up a steady curre layer in the field-coil takes

about three half cycles of the betatron field, therefore, magnetic field measurements with A.C. excitation cannot be used (appendix #1). Other techniques for making precise measurements of the spatial distribution of a pulsed magnetic field had to be developed.

Construction of a low inductance plasma betatron at Stevens Institute of Technology was initiated in 1957 by Prof. D. Finkelstein. The present betatron, which is quite different from the device originally designed by Finkelstein, gradually evolved to its present state because of the technical problems encountered in the earlier ideas.

In this report we describe the construction and operating characteristics of a low inductance plasma betatron. A cylindrically symmetric magnetic field distribution that satisfies the betatron condition is obtained by placing flux concentrators at appropriate positions within the interior of a single turn solenoid. In addition to the betatron field there is an azimuthal magnetic field that is required for runaway production.

It is observed in this experiment as well as in the other plasma betatrons that beam disruption and subsequent x-ray emission begins before the end of the acceleration cycle has been reached. The runaway electrons hit the walls of the vacuum chamber without benefit of the beam

disturbing techniques used in ordinary betatrons. The time at which x-ray emission starts, and the number of runaway electrons have been studied as functions of the various experimental parameters.

We find that the runaway current is limited to about one ampere by either one of two mechanisms; the self electric field that is generated by the adiabatic collapse of the runaway stream or the Negative Mass-Instability.

The streaming velocity appears to be limited by a beam plasma interaction that has been treated theoretically by Field and Fried (see section #2).

The maximum electron energy at the onset of x-ray emission was approximately 350 kev. Although some x-ray emission occurs at the peak of the acceleration cycle indicating that the full energy of the machine was reached ($\approx$ 1.3 mev) the intensity was greatest at the beam disruption time. If we choose the experimental parameters that give the greatest x-ray energy for a given accelerating field strength, we find that $E_0 \approx 70$ v/cm is required if the electrons are to have a kinetic energy of 1 mev when they strike the walls of the vacuum chamber. This electric field is about three times greater than the experimentally applied fields. The extrapolated runaway current with E_0 =70 v/cm is only 5 amperes.

In section #2 we present a brief review of the theory of runaway electrons. Section #3 deals with the single particle motion in a betatron magnetic field and in a combined betatron and azimuthal magnetic field. The particle motion just after the betatron field is turned on is also discussed here.

In section #4 the generation of a betatron magnetic field using flux concentrators is described. Techniques for making precise measurements of pulsed magnetic fields are also described in this section.

Section #5 deals with the generation of the B_θ field and the method used for preionization. The electron density, electron temperature, runaway current, x-ray measurements, and electric field measurements are described in section #6.

Finally the results of the measurements are analyzed and discussed in section #7.

II THEORY OF RUNAWAY ELECTRONS

The subject of electron runaway in ionized gases has been studied by many authors.[13-19] In all of the calculations the electric field E_c, which accelerates an electron by its thermal velocity in one collision period, enters as a parameter. If the applied electric field $E \ll E_c$ then the resulting current is linearly related to the perturbing field. The stationary methods of solution of the collision dominated Boltzman equation ie.,

$$\frac{\partial f}{\partial t} + \frac{e}{m}\vec{E}\cdot\frac{\partial f}{\partial \vec{v}} = \left(\frac{\partial f}{\partial t}\right)_{coll.} \qquad 2.1$$

$$\left(\frac{\partial f}{\partial t}\right)_{coll} >> \frac{e}{m}\vec{E}\cdot\frac{\partial f}{\partial \vec{v}}$$

are assumed to yield correct answers provided the average random electron speed is much larger than the electron drift velocity. In this limit the electrical conductivity follows the well known $T^{3/2}$ law (Spitzer conductivity). The calculations are based on the assumption that a steady-state velocity distribution is attained several mean-free collision times after the electric field is turned on.[13-18] The present calculations relax this last restriction on the problem, ie., a time dependent solution of eq. (2.1) is sought. In the next paragraphs we give the essential results of all the runaway electron calculations rather than discuss the work contained in each paper separately.

When $E/E_c \ll 1$, the application of the external electric field causes the electron distribution function to be only slightly disturbed from its initial equilibrium situation. If the distribution function resembles a Maxwellian, ie, if it has a high energy tail, there will always be some electrons with velocities large enough to runaway no matter how small the applied field is. As far as the main bulk of electrons are concerned, the application of the electric field causes heating, thereby enabling more electrons to move into the runaway region. The velocity of any given electron gradually increases with time. Thus all the electrons eventually runaway.

When $E/E_c \gg 1$ the electric field term in the Boltzman equation dominates, all the electrons runaway immediately, and the runaway current increases linearly with time according to

$$j = n_c q v = n_o q^2 \frac{E}{m} t \qquad (2.2)$$

Recently Field and Fried[19] have attacked the problem of electron runaway in a way that is very different from the previous calculations. Instead of the conventional Fokker-Planck collision term for the right-hand side of 2.1 they assume that $\left(\frac{\partial f}{\partial t}\right)_{coll.}$ arises from the generation of ion acoustic waves. The calculation is done in the $E/E_c \gg 1$ limit. Thus initially $\left(\frac{\partial f}{\partial t}\right)_{coll.}$ is of the same

order of magnitude as the conventional collision term so that the current density $\vec{j}$ increases linearly with time. As soon as it passes a small threshold

$$j \approx n_e c \nu_{THERMAL} \left(\frac{m_e}{m_i}\right)^{1/2}$$

however, the $\left(\frac{\partial f}{\partial t}\right)_{COLL.}$ term begins to rise exponentially and eventually becomes comparable with the driving term. The current density reaches a maximum and then decreases rapidly in time.

To summarize, for efficient runaway production the induction electric field E_θ should be much larger than E_c, where

$$E_c \approx 1.4 \times 10^{-12} \frac{n_e (\#/cm^3)}{T_e (ev.)} \quad v/cm.$$

In this experiment the ratio of E_θ/E_c is very large, typically 500 so that all the electrons should runaway immediately. Furthermore the coulomb collision time is $\approx 10^{-5}$ sec. ($n_e = 10^{11}/cm^3$, T_e = 10 eV.). This is more than twice as long as the acceleration cycle, hence the runaways will move through the backround plasma in a collisionless way.

Further discussion of the work by Field and Fried will be left to section #7.

III EQUATIONS OF MOTION FOR SINGLE PARTICLES

In this section we derive the equations of motion for single particles in an axially symmetric betatron magnetic field and in a betatron field with an additional azimuthal guide field.

3.1 The non-relativistic Lagrangian for a charged particle with mass m, and charge q in a magnetic field with vector potential $\vec{A}$ is given by

$$L = \frac{1}{2} m \vec{v} \cdot \vec{v} + q \vec{v} \cdot \vec{A} \qquad 3.1$$

In cylindrical co-ordinates (r, θ, z) the Lagrangian takes the form

$$L = \frac{1}{2} m \left(\dot{r}^2 + r^2 \dot{\theta}^2 + \dot{z}^2 \right) + q \dot{r} A_r + q r \dot{\theta} A_\theta + q \dot{z} A_z \qquad 3.2$$

The equations of motion for the particle are given by Lagrange's equations:

$$\frac{d}{dt} \left(\frac{\partial L}{\partial \dot{q}_i} \right) - \frac{\partial L}{\partial q_i} = 0 \qquad 3.3$$

Where the q_i's are the generalized co-ordinates. Thus the r, θ and z equations of motion are

$$\frac{d}{dt} \left(m \dot{r} + q A_r \right) = m r \dot{\theta}^2 + q \dot{r} \frac{\partial A_r}{\partial r} + q \dot{\theta} \frac{\partial}{\partial r} (r A_\theta) + q \dot{z} \frac{\partial A_z}{\partial r}$$

$$\frac{d}{dt} \left(m \dot{z} + q A_z \right) = q \dot{r} \frac{\partial A_r}{\partial z} + q r \dot{\theta} \frac{\partial A_\theta}{\partial z} + q \dot{z} \frac{\partial A_z}{\partial z}$$

$$\frac{d}{dt}\left(m r^2 \dot\theta + q r A_\theta\right) = q \dot r \frac{\partial A_r}{\partial \theta} + q r \dot\theta \frac{\partial A_\theta}{\partial \theta} + q \dot z \frac{\partial A_z}{\partial \theta} \quad 3.4$$

If we perform the differentiation with respect to time and make use of $\vec B = \nabla \times \vec A$, equations 3.4 become

$$\begin{aligned} m\ddot r &= m r \dot\theta^2 - q \dot z B_\theta + q r \dot\theta B_z \\ m\ddot z &= q \dot r B_\theta - q r \dot\theta B_r \\ m r \ddot\theta + 2 m \dot r \dot\theta &= - q \dot r B_z + q \dot z B_r \end{aligned} \quad 3.5$$

(we have neglected the time dependence of $\vec A$)

The first field configuration we will study will be just the betatron field. For this situation $B_\theta = 0$ so that eq's (3.5) reduce to

$$\begin{aligned} m\ddot r &= m r \dot\theta^2 + q r \dot\theta B_z \\ m\ddot z &= - q r \dot\theta B_r \\ m r \ddot\theta + 2 m \dot r \dot\theta &= - q \dot r B_z + q \dot z B_r \end{aligned} \quad 3.6$$

Before we analyze the equations of motion any further it will be helpful if we first derive the necessary conditions for an equilibrium orbit. Only one component of the vector potential, A_θ , is necessary to generate an axially symmetric betatron field. Thus the Lagrangian (3.2) reduces to

$$L = \tfrac{1}{2} m \left(\dot r^2 + r^2 \dot\theta^2 + \dot z^2\right) + q r \dot\theta A_\theta \quad 3.7$$

We will assume that A_θ is cylindrically symmetric and we will also assume that A_θ is time independent. Since A_θ is symmetric, the θ - component of the canonical momentum $P_\theta \equiv \frac{\partial L}{\partial \dot{\theta}}$ will be a constant of the motion. We choose $P_\theta = 0$. Thus

$$P_\theta = \frac{\partial L}{\partial \dot{\theta}} = m r^2 \dot{\theta} + q r A_\theta = 0 \qquad 3.8$$

Solving for $(r\dot{\theta})$ in eq. 3.8 and substituting into eq.(37), the Lagrangian becomes

$$L = \frac{1}{2} m (\dot{r}^2 + \dot{z}^2) - \frac{q^2}{2m} A_\theta^2(r,z) \qquad 3.9$$

Thus with this Vector Potential, the r, z equations of motion are:

$$m \ddot{r} + \frac{q^2}{m} A_\theta \frac{\partial A_\theta}{\partial r} = 0$$

$$m \ddot{z} + \frac{q^2}{m} A_\theta \frac{\partial A_\theta}{\partial z} = 0 \qquad 3.10$$

Therefore at the equilibrium orbit both $\frac{\partial A_\theta}{\partial r}$ and $\frac{\partial A_\theta}{\partial z}$ must vanish. The familiar $2:1$ betatron condition is obtained by calculating the magnetic flux Φ that links the equilibrium orbit with radius $r = r_0$.

$$\Phi = \iint_S \vec{B} \cdot d\vec{S} = \langle B \rangle \pi r_0^2 \qquad 3.11$$

where $\langle B \rangle$ is the average value of the magnetic field within the orbit. We also have that

$$\Phi = \iint_S \vec{B} \cdot d\vec{S} = \iint_S (\nabla \times \vec{A}) \cdot d\vec{S} = \oint \vec{A} \cdot d\vec{l}$$

$$\Phi(r_0) = A_\theta(r_0)[2\pi r_0] \qquad 3.12$$

where $A_\theta(r_0)$ is the value of the vector potential at the equilibrium orbit. From $\vec{B} = \nabla \times \vec{A}$

$$B_z = \frac{1}{r}\frac{\partial}{\partial r}(r A_\theta) = \frac{\partial A_\theta}{\partial r} + \frac{A_\theta}{r} \qquad 3.13$$

Since $\left(\frac{\partial A_\theta}{\partial r}\right)_{r=r_0} = 0$, we have

$$B_z(r_0) = \frac{A_\theta(r_0)}{r_0} \qquad 3.14$$

thus

$$\Phi(r_0) = \langle B \rangle \pi r_0^2 = 2\pi r_0 A_\theta(r_0) = 2\pi r_0^2 B_z(r_0)$$

finally

$$B_z(r_0) = \frac{1}{2}\langle B \rangle \qquad 3.15$$

Now we return to the equations of motion 3.6 to calculate the particle orbits. The "z" component of the magnetic field in the neighborhood of the equilibrium orbit is assumed to be of the form (20)

$$B_z = B_z(r_0)\left(\frac{r_0}{r}\right)^n = B_0\left(\frac{r_0}{r}\right)^n \qquad 3.16$$

The radial field component associated with this B_z is obtained from $\nabla \times \vec{B} = 0$ i.e.,

$$B_r = -\frac{n}{r} B_0 \left(\frac{r_0}{r}\right)^n z \qquad 3.17$$

Now we linearize the equations of motion ie., we let

$$r = r_0 + x, \quad \dot{\theta} = \omega_0 + \dot{\psi}, \quad z = z$$

where $|x| << r_0$ and $\dot{\psi} << \omega_0 = -qB_0/m$

To first order, we find that

$$\begin{aligned} \dot{\psi} &= -\frac{\omega_0}{r_0} x \\ \ddot{z} &= -\omega_0^2 n z \\ \ddot{x} &= r_0 \dot{\psi} \omega_0 + \omega_0^2 n x \end{aligned} \qquad 3.18$$

finally, the radial and vertical equations of motion become

$$\begin{aligned} \ddot{x} + \omega_0^2 (1-n) x &= 0 \\ \ddot{z} + \omega_0^2 n z &= 0 \end{aligned} \qquad 3.19$$

The solutions of the radial equation will be harmonic provided $n < 1$. Similarly the solutions of the " z " equation will be harmonic if $n > 1$. Hence we have arrived at the familiar "weak focusing condition", ie., in a weak focusing field (a betatron field), the field index "n" at the orbit must lie between 0 and 1 .

3.2 At this point we will digress from the main purpose of this section to calculate the effect that azimuthal inhomogeneities in the guide field have on the betatron orbits. This is a very important consideration in the design of the betatron field because as we shall show, azimuthal inhomogeneities increase the amplitude of both the radial and vertical betatron oscillations thereby placing restrictions on the vacuum chamber cross-section.

We assume that the z-component of the magnetic field is given by (21)

$$B_z = B_0 \left(\frac{r_0}{r}\right)^n \left[1 + \sum_{m=1}^{\infty} \delta_m \sin (m\theta + \alpha_m) \right] \qquad 3.20$$

And that

$$B_r = -\frac{n}{r} B_z z = -\frac{n}{r} z B_0 \left(\frac{r_0}{r}\right)^n + \sum_{l=1}^{\infty} \psi_l \sin (l\theta + \gamma_l) \qquad 3.21$$

The equations of motion for the radial and vertical directions are now

$$\ddot{x} + \omega_0^2 (1-n)\, x = -\rho_0 \omega_0^2 \sum_{m=1}^{\infty} \delta_m \sin(m\omega_0 t + \alpha_m)$$

$$\ddot{z} + \omega_0^2 n z = \omega_0^2 \frac{\rho_0}{B_0} \sum_{\ell=1}^{\infty} \psi_\ell \sin(\ell\omega_0 t + \beta_\ell)$$

3.22

where $\theta = \omega_0 t$

The complete solution to the radial equation is

$$x = A \sin\left[\omega_0 (1-n)^{1/2} t\right] + B \cos\left[\omega_0 (1-n)^{1/2} t\right]$$

$$+ \sum_{m=1}^{\infty} \frac{\rho_0 \delta_m}{m^2 - (1-n)} \sin(m\omega_0 t + \alpha_m)$$

3.23

The constants "A" and "B" are determined by initial conditions.

The solution to the "z" equation is obtained from eq. (23) by simply replacing $(1-n)$ by (n) and

δ_m by $\left(\frac{\rho_0}{B_0}\right) \psi_m$ in all terms, ie.,

$$z = C \sin(\omega_0 n t) + D \cos(\omega_0 n t)$$

$$+ \frac{R_0}{B_0} \sum_{l=1}^{\infty} \frac{\psi_l}{(l^2 - n^2)} \sin(l\omega_0 t + \gamma_l)$$

Thus we see that the harmonics that will give the largest displacement from the equilibrium orbit are those with low "n" values, i.e., $n = 1, 2, 3$. The higher n-values will not play an important role because of the $1/n^2$ dependence.

Equations 3.23 will be used later on to calculate the particle displacements in the field coil.

3.3 We will now study the solutions of the equations of motion (3.5) when in addition to the betatron magnetic field, there is an azimuthal guide field $B_0(r)$. For this case eq.'s 3.5 retain their full form with B_z & B_r the same as before. The linearized equations of motion about the equilibrium orbit R_0 [22] are

$$\ddot{x} + \omega_0^2 (1-n) x = \omega_c \dot{z}$$

$$\ddot{z} + \omega_0^2 m z = -\omega_c \dot{x}$$

$$\dot{\psi} = -\frac{\omega_0}{\lambda_0} x$$

3.24

where $\omega_c = \delta B_\theta / m$, and B_θ is the magnitude of the azimuthal field at $\lambda = \lambda_0$. The solutions of eq (3.24) are assumed to be of the form.

$$x_\omega \propto \eta_\omega e^{i\omega t}, \quad z_\omega \propto \lambda_\omega e^{i\omega t}$$

3.25

substituting (3.25) into (3.24) we get the pair of equations

$$-\omega^2 x + \omega_0^2 (1-m) x - i\omega\omega_c z = 0$$

$$-\omega^2 z + \omega_0^2 m z + i\omega\omega_c x = 0$$

3.26

The condition for a non-trivial solution is that the determinant of the co-efficients vanish, ie.,

$$\begin{vmatrix} \omega_0^2 (1-m) - \omega^2 & -i\omega\omega_c \\ i\omega\omega_c & \omega_0^2 m - \omega^2 \end{vmatrix} = 0$$

3.27

Thus "w" is determined by the solution of

$$\omega^4 - \left[\omega_0^2 + \omega_c^2\right]\omega^2 + \omega_0^4\, n(1-n) = 0 \qquad 3.28$$

Finally

$$\omega^2 = \tfrac{1}{2}\left(\omega_0^2 + \omega_c^2\right) \pm \tfrac{1}{2}\left\{\left[\omega_0^2 + \omega_c^2\right]^2 - 4\,\omega_0^4 n(1-n)\right\}^{1/2} \qquad 3.29$$

Thus in general the electron motion is harmonic with frequencies that are complicated functions of ω_0 and ω_c . However, when $\omega_c >> \omega_0$ the roots of 3.29 become

$$\omega_1^2 \approx \frac{\omega_0^4}{\omega_c^2}\, n(1-n) \qquad 3.30$$

$$\omega_2^2 \approx \omega_c^2\left[1 - \frac{\omega_0^4}{\omega_c^4}\, n(1-n)\right] \qquad 3.31$$

From (3.26) we find that

$$\frac{x}{\beta} \approx \left(\frac{n}{1-n}\right)^{1/2} \qquad 3.32$$

when $\omega = \omega_1$, and $\frac{x}{\beta} \approx 1$ with $\omega = \omega_2$ 3.33

The motion is, therefore, composed of two elementary motions (Fig.#I), one being nearly a cyclotron motion with angular frequency $\omega_1 \approx \omega_c$ and the other a slow elliptic motion whose angular frequency is

$$\omega_1 \approx \frac{\omega_0^2}{\omega_c}\left[n(1-n)\right]^{1/2} \qquad 3.3b$$

3.4 In the preceeding section we have studied the motion of charged particles under the combined influence of axially symmetric betatron and azimuthal magnetic fields (B_z and B_θ). The motion was studied for the static case, i.e., both B_z and B_θ remained unchanged during the times of interest. For the case when $B_\theta >> B_z(r_0)$ it was found that the motion in the (x,z) plane was composed of two elementary motions (Fig.#1), a nearly cyclotron motion with $\omega_2 \approx \omega_c$ and a slow elliptic motion with $\omega_1 \approx \frac{\omega_0^2}{\omega_c}\left[n(1-n)\right]^{1/2}$. This solution is correct as long as both $B_z(r_0) + B_\theta$ are sufficiently large. However, this is not always the case for a plasma betatron. The time scale of the present experiment is as follows: B_θ is approximately trapezoidal in shape and lasts for about 100 μ sec. B_z on the other hand rings with a period of 16 μ sec . Therefore during an acceleration cycle (a quarter period), $B_z(r_0)$ rises from zero to its maximum value, while

B_θ is essentially unchanged. The equations of motion discussed in the previous section are not valid when $B_z = 0$. When $B_z = 0$ eq.'s(3.24)reduce to

$$\ddot{x} = \omega_c \dot{z}$$

$$\ddot{z} = -\omega_c \dot{x} \qquad 3.35$$

Eq.'s(3.35)are the equations of motion for a charged particle in a uniform magnetic field which is not the case for B_θ since $B_\theta \propto 1/r$.

Since eq.'s(3.24)are valid when $B_z > 0$ and not valid when $B_z = 0$ we now seek to determine a time t_{cr} such that the equations of motion are valid for all $t > t_{cr}$ and further more we must also investigate the electron motion for $t < t_{cr}$.

The solution to (3.24) with a time varying B_z is very difficult to do analytically, however, we will make an estimate the range of validity in the following way.

The terms $\omega_0^2(1-n)x$ and $\omega_0^2 n z$ in the equations of motion are measures of the focusing force produced by the betatron field. If the B_θ field was independent of "r" the equations of motion would be valid for all time including t=0. Therefore the equations of motion should be valid for all times that the magnetic focusing

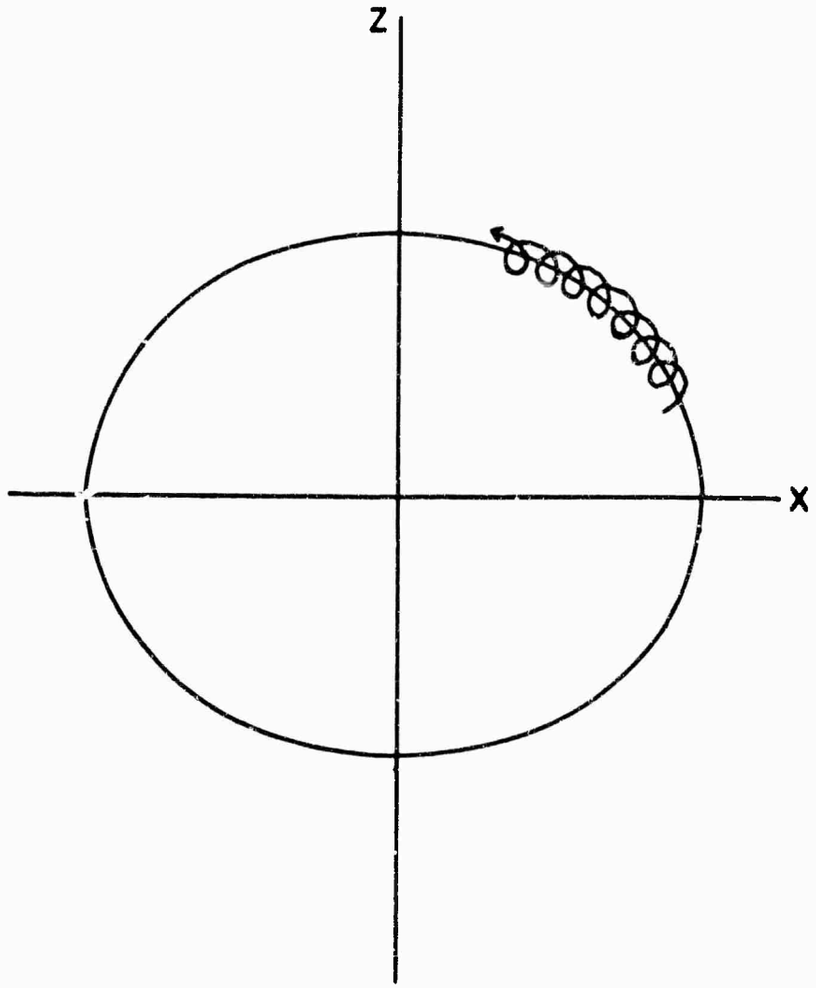

ELECTRON MOTION IN THE (X,Z) PLANE

FIG.# 1

BLANK PAGE

terms are larger than the higher order terms in the expansion of B_θ about the equilibrium orbit. If the first two terms of the expansion of B_θ are retained the equations of motion become, for $B_z > 0$, (consider only the radial equation).

$$\ddot{x} + \omega_0^2 (1-n)\, x = \omega_c \dot{z} \left(1 - \cdot / \Omega_0\right) \qquad 3.36$$

then the solution (3.31) and (3.34) should be valid when

$$\omega_0^2 (1-n) >> \omega_c \dot{z}/\Omega_0 \qquad 3.37$$

Since $\omega_0 = -\frac{q}{m} B_z(\Omega_0) \sin \Omega t$ eq. (3.37) reduces to

$$t >> t_v = \frac{1}{\Omega} \sin^{-1} \left\{ \frac{m}{q} \frac{B_\theta}{B_z^2} \frac{\dot{z}}{(1-n)} \right\}^{1/2} \qquad 3.38$$

Typical experimental parameters are: B_θ =5 k gauss, $n = \frac{1}{2}$, B_z =1 k gauss and Ω =0.39x10^6 rad/sec. If we assume $\dot{z}$ is the velocity of a 10 volt electron, then t_v is

$$t_v \approx 7 \times 10^{-8} \text{ SEC.}$$

We must now investigate the motion for $0 < t < t_{sr}$ to make sure that all the electrons will not drift out of the acceleration region during this time. For times less than t_{sr} the electrons will drift in the B_θ field with their guiding center velocity which is given by (23)

$$\vec{V_D} = \frac{1}{2} \frac{m(\dot{x}^2 + \dot{y}^2)}{q B^4} \left(\vec{B} \times \nabla \frac{B^2}{2} \right) + \frac{m v_{\parallel}^2}{q B^4} \left(\vec{B} \times \nabla \frac{B^2}{2} \right) \qquad 3.39$$

where $v_{\parallel} = \frac{q}{m} E_\theta t$ is the particle velocity parallel to B_θ. Since $v_{\parallel}$ increases more rapidly than either $\dot{x}$ or $\dot{y}$ we will neglect the first term in eq. (39), then in a pure B_θ field the drift is in the "z" direction and is equal to

$$v_D = \frac{m v_{\parallel}^2}{q B_\theta(r_0) R_0} = \frac{q E_\theta^2 t^2}{m B_\theta(r_0) R_0} \qquad 3.40$$

The distance that an electron travels during the time t_{sr} is

$$z = \int_0^{t_{sr}} v_D \, dt = \frac{q}{m} \frac{E_\theta^2}{B_\theta R_0} \int_0^{t_{sr}} t^2 \, dt \qquad 3.41$$

$$z = \frac{q}{m} \frac{E_\theta^2}{B_\theta(r_0) R_0} \frac{t_{sr}^3}{3} \qquad 3.42$$

With E_θ = 20 v/cm, r_0 = 5 cm, t_r = 7×10^{-8} sec. and B_θ =5 k gauss, we find that

$$z \approx 0.3 \text{ CM.} \qquad 3.43$$

Since the inside diameter of the vacuum chamber is $\approx$ 1.5 CM. we can expect that the magnetic focusing forces will be large enough to stop the "z" drift of most of the electrons before they hit the vacuum chamber walls. This transverse drift during the time $0 < t < t_r$ will cause the loss of some particles to the walls but certainly not all of them. Therefore, the fact that the equations of motion are not valid for the entire part of the acceleration cycle does not seem to lead to any disasterous effects.

IV THE MAGNETIC FIELD

4.1 General considerations:

Probably the major difficulty encountered in the design of a betatron particle accelerator is that of the magnetic guide field. If the magnetic guide field is "right", then properly injected particles will usually be accelerated to the full energy of the machine. A plasma betatron, in addition to being subject to all the difficulties that are encountered in electron betatrons, will be at the mercy of any collective effects that may develop during the acceleration cycle. We have therefore paid a great deal of attention to the betatron guide field in this experiment, with the hopes that we might be able to separate single particle effects from collective effects.

The degree of precision with which the guide field must be measured can be estimated from the vector potential well depth. The vector potential well depth $\int$ is defined as:

$$\int \equiv \frac{A_\theta(r_0+\delta r) - A_\theta(r_0)}{A_\theta(r_0)} \qquad 4.1$$

where r_0 is the equilibrium orbit radius and δr is a small displacement from r_0 .

if we assume that the "n"-value is uniform in the orbit region then it is easy to show that the well depth is given by (to second order)

$$\delta = \frac{1}{2}(1-n)\left(\frac{\delta r}{r_0}\right)^2 \qquad 4.2$$

With n=0.5 and r_0 =2", the well depth at δr =0.2" (determined by the vacuum chamber size) is

$$\delta = \frac{1}{2}\left(1-\frac{1}{2}\right)\left(\frac{.2}{2}\right)^2 = 0.25\times10^{-2}$$

$$\delta = 0.25\ \%$$

Since the well depth in a betatron turns out to be very small an accuracy of $\pm$ 0.1 % in all magnetic field measurements was decided upon. A further complication arises because of the time that it takes to build up a steady current layer in the coil. A simple calculation of the magnetic field penetration time into a conductor for the frequencies we are interested in ($\approx$ 65 k c) shows that at least one complete cycle of the betatron field is required to build up a steady state "skin depth" in the field coil, (see appendix # 1). This means that the field distribution in the coil on the second half cycle will probably be different from that on the first. At the start of the third half-cycle (fifth quarter period)

the magnetic field distribution will be close to its steady state A.C. value.

Therefore if the betatron field is determined with continuous A. C. excitation, it is quite likely that the field distribution on the first half-cycle may not satisfy the betatron condition. We have therefore made all magnetic field measurements under pulsed operations. In fact all of the magnetic measurements were made under some of the conditions that were used for experiments with plasma.

4.2 Field Coil Design

The design of the plasma betatron field-coil has been determined largely by considerations of magnetic field shape and accessability rather than mechanical strength. Fortunately, the final design is sufficiently simple so that both mechanical and magnetic requirements are easily satisfied.

The coil shown in Figs. #2&3 is machined from two blanks of zirconium-copper (99.85% Cu, 0.15% Zr) supplied by the Philadelphia Bronze and Brass Company. The blanks, originally work hardened, were recovered by heat treating for four hours at 600° F and then oven cooled for 24 hours to prevent distortion during machining and aging.

Alignment of the four "C's" in the vertical direction is by precision ground alumina spacers resting in jig bored wells. Proper separation between the two halves of the coil is maintained by inserting insulating spacers into the gaps at the current feed points.

The physical dimensions of the coil, inside diameter 4.875", separation between halves 0.750", overall height 8.750", were arrived at after magnetic measurements in a mock-up coil indicated that, with flux-concentrators, the betatron condition might be satisfied in this type of arrangement.

4.3 The Flux Concentrators

Flux concentrators make use of the fact that good conductors tend to exclude time varying electromagnetic fields from their interior. The physical mechanism for the exclusion of the flux is quite simple. A time changing magnetic field has associated with it an induction electric field. The electric field in the conductor generates eddy currents that are just large enough to cancel the applied magnetic field.

Each flux concentrator is composed of 16 copper discs 1/16" thick with an outside diameter of 4.813" ± 0.001" and an inside diameter of 1.5000" ± .0005". A .020" slot in each discs permits magnetic flux to enter the central hole. (Fig.#5) The discs are insulated from each other by a .010" thick mylar sheet. Each of the 16 copper pieces and mylar insulators is coated with Emerson & Cummings 1264 epoxy resin and then mounted on a mandrel which maintains allignment between the discs. The mandrel is designed so that no disc is out of alignment from any other by more than 0.001". The entire assembly is then clamped and allowed to harden. Staggering the gaps in alternate layers reduces the azimuthal field inhomogeneities that are caused by the slots in the discs.

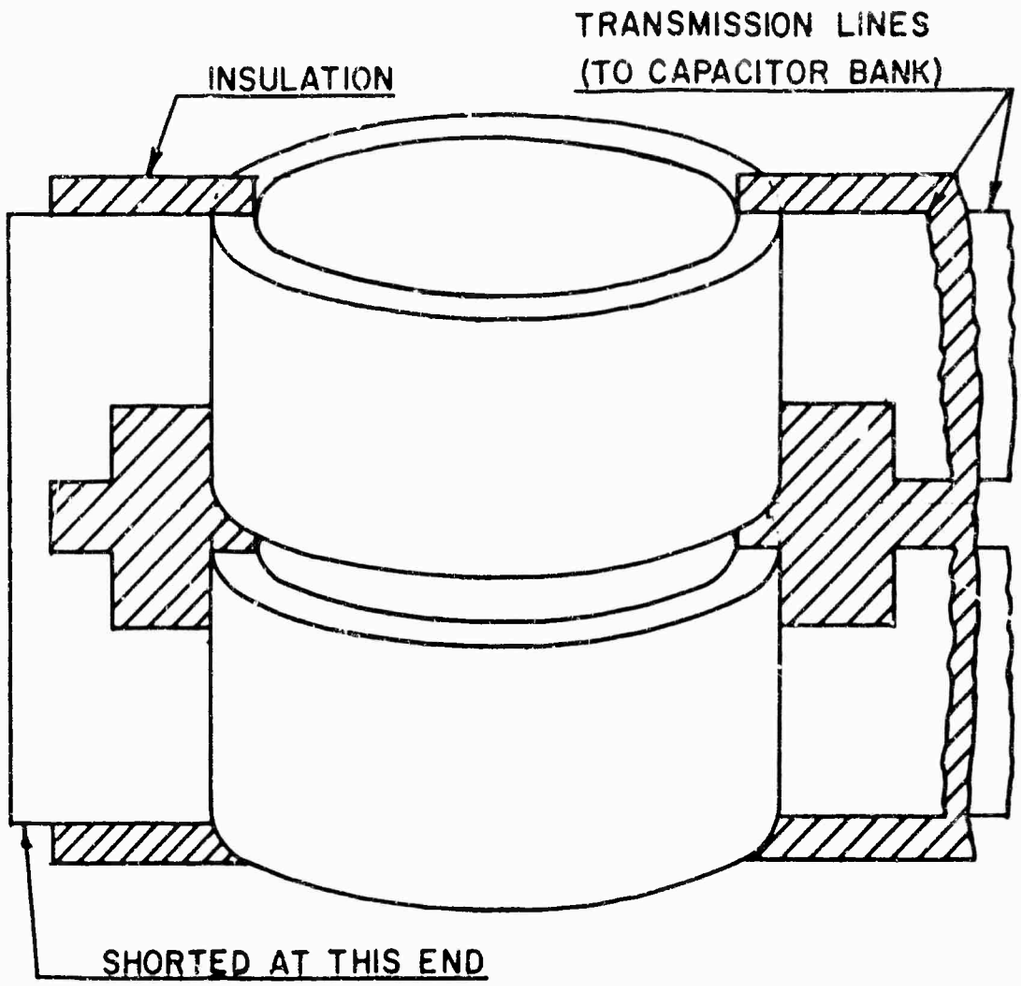

FIELD COIL

FIG. # 2

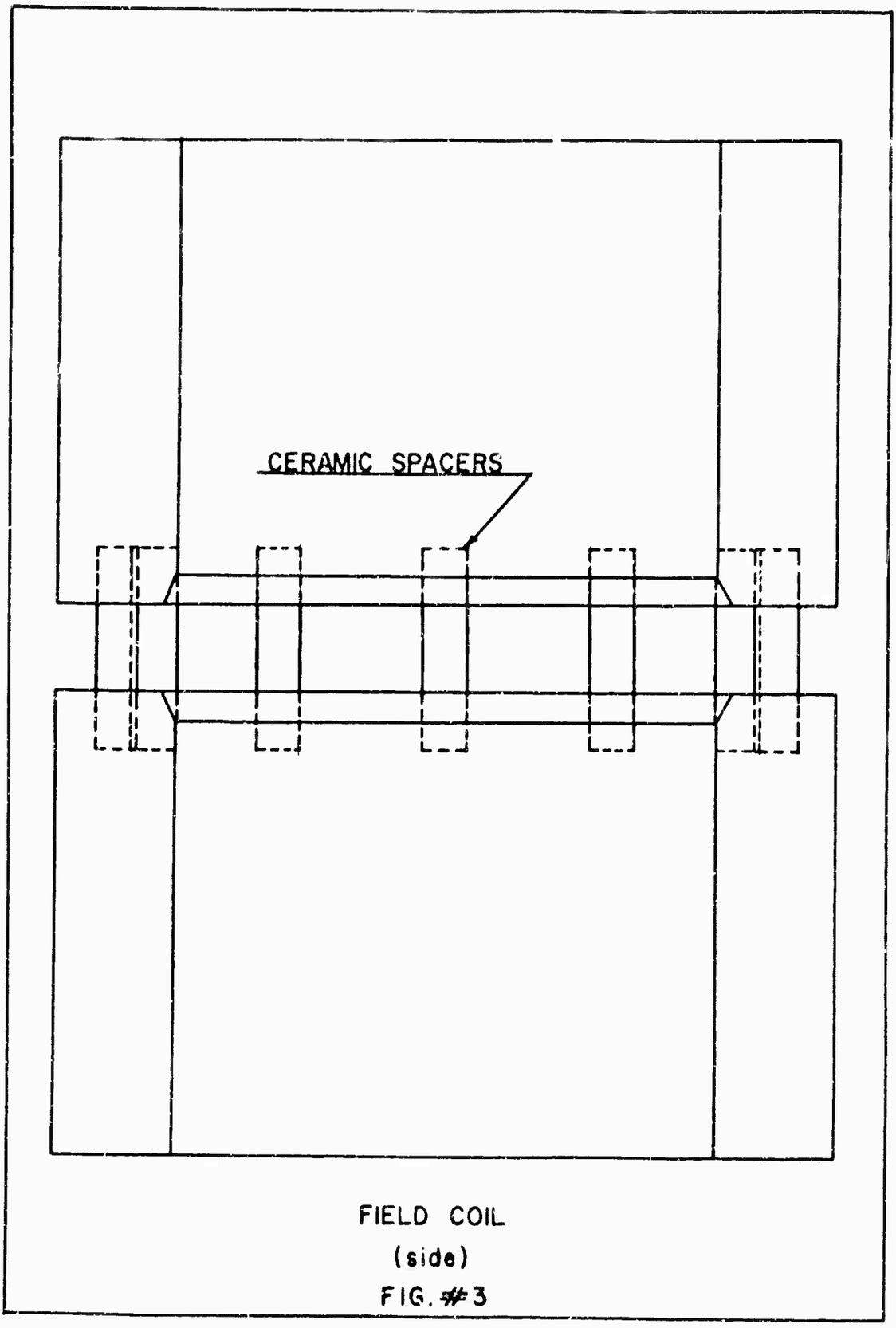

FIELD COIL

(side)

FIG. #3

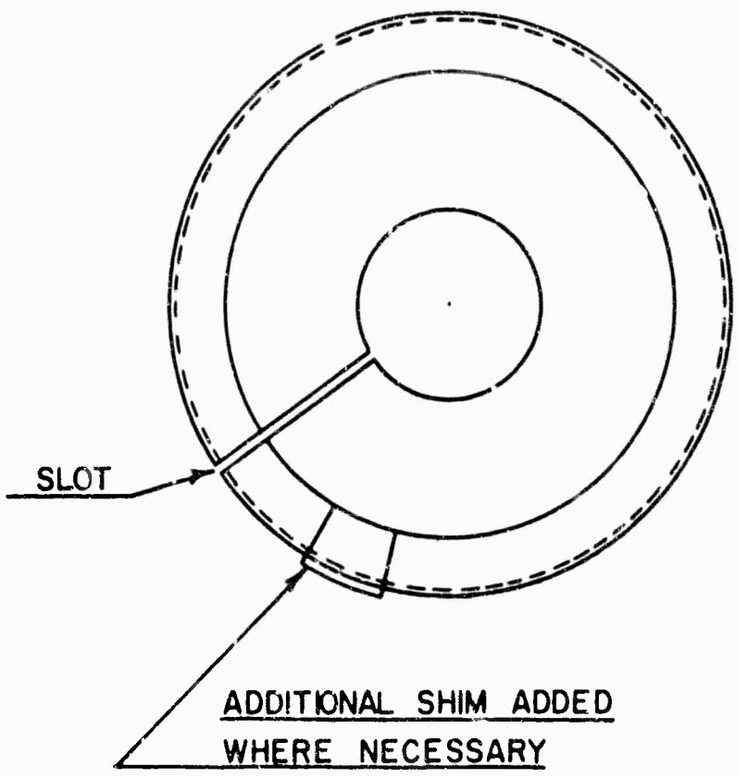

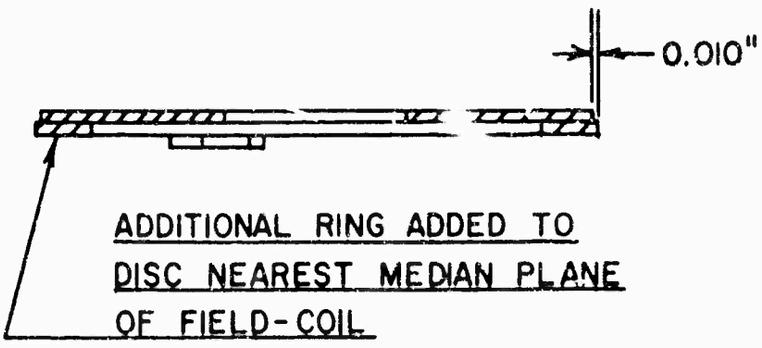

FLUX CONCENTRATOR DISCS

FIG. # 5

BLANK PAGE

4.4 Difference Amplifier Technique For Measuring The Magnetic Field

All of the magnetic field measurements were made with two magnetic pick-up loops. One of the probes, fixed in space, was used to monitor the current through the field-coil. The second probe (in some cases a moving probe) was used to map the magnetic field. Each signal was integrated in an R-C network and fed into a Tektronix Type Z differential preamplifier mounted in a Tektronix Type 555 dual beam cathode-ray oscilloscope. The difference between each pick-up loop signal and the variable D.C. bias voltage built into the preamp. was recorded on polaroid film.(In principle it is possible to see a change of 5 mv. in a 100 volt signal).

The current through the field-coil varied from 5-10% between successive capacitor bank discharges because of the uncertainty in the charging voltage. Under these conditions one must keep discharging the capacitor bank at each probe position until the signals from both pick-up coils were "on screen". Installation of the capacitor bank voltage measuring circuit shown in Fig.4 removed this difficulty. With this circuit it was possible to discharge the capacitor bank so that signals from both the fixed probe and moving probe were "on screen" every

discharge. The circuit is balanced so that there is zero current in the middle leg when a calibrated high voltage source is connected across the input (in our case a John Fluke Precision H.V. Supply, with a 0.1% accuracy). The bridge will then indicate zero current when the capacitor bank voltage reaches the voltage used for balance. With an RCA ultra sensitive microammeter in the middle leg it is possible to see a difference of one part in 4000 in th charging voltage. Normally the capacitor bank would be allowed to overcharge approximately 10 to 75 volts. The charge was then allowed to leak off. Switch S was opened, disconnecting the microammeter, and simultaneously generating a pulse which initiated the bank discharge.

This entire process was repeated at least three times at each probe position. All the data (in a given set of circumstances) were then normalized to the same value of field-coil current (provided the location of the fixed coil was not changed). The spread in the data obtained this way was typically ± .05%.

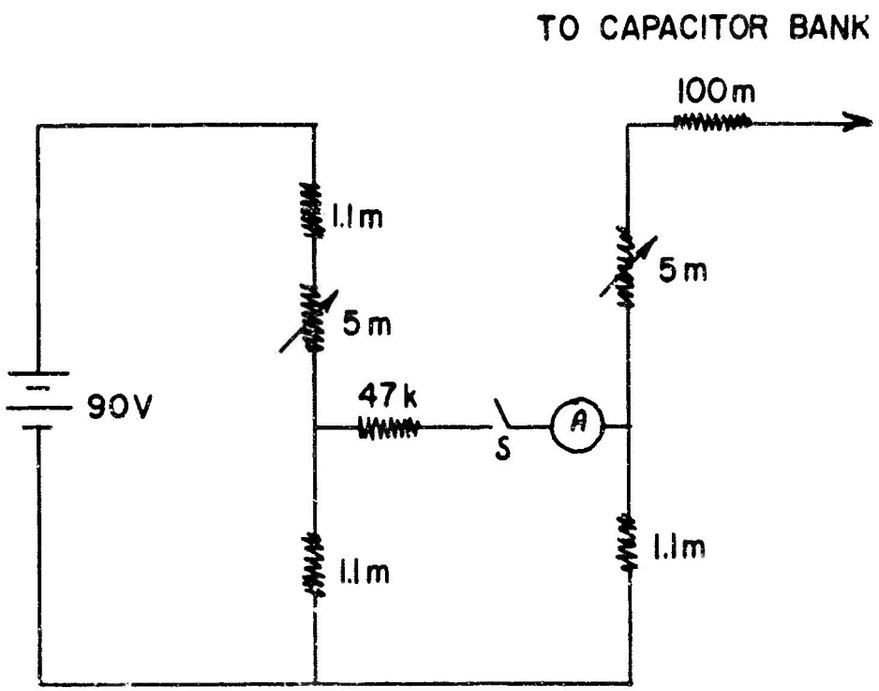

CAPACITOR BANK VOLTAGE

MONITORING CIRCUIT

FIG. # 4

BLANK PAGE

4.5 Shaping the Field

The radial distribution of the z-component of the magnetic field in the median plane of the field coil is determined by the following field-coil and flux concentrators parameters

a= The diameter of the central hole in the flux concentrators

b= The separation between the flux concentrators and the interior wall of the field coil

c= The height of the flux concentrators themselves

d= The vertical gap between the two halves of the field-coil

e= The axial spacing between the two flux concentrators.

Suitable choices for dimensions "a" through "d" were determined by magnetic field measurements in a model field-coil.

In order to discuss the roles the different parameters play in determining the field distribution, it is convenient to introduce the parameter "G". G is defined as the ratio of the magnetic field strength $B_z(o,o)$ on the axis of the field coil in the median plane, to the field at the equilibrium orbit radius. With the present geometry the vector potential has a minimum, with the "n" value between zero and one at R_o =1.9 inches for

values of G between 4 and 5.

Field distributions with G>5 generate a vector potential that decreases monotonicaly in the orbit region. For a given set of flux concentrators "G" decreases with increasing "e". In general the larger "a" is with respect to the inside diameter of the field coil the smaller G will be. The dimensions "b", "d" and "e" control the fine details of the magnetic field in the orbit region, i.e., the "n"-value. Once a set of flux concentrators has been constructed the only parameter that can be changed easily is "b". This is accomplished by adding an additional ring to the innermost flux-concentrator disc (see fig.5). Obviously this procedure only works when "b" is to be made smaller. An increase in the value of "b" or a decrease in "d" will cause the "n"-value to become negative for values of (r) greater than the equilibrium orbit radius.

In the few preceeding paragraphs we have described in general terms the roles the various parameters play in determining the radial profile of the magnetic field in the coil. A more quantitative description would require an extensive set of magnetic measurements covering many different values of all the parameters, most of which did not lead to a suitable betatron field.

Since we are only interested in those experimental situations that produce an acceptable betatron field shape, a thorough set of magnetic measurements was not made until it was reasonably clear that a given set of parameters would produce the desired result. Table #1 lists the values of the different parameters which produced a betatron field in the median plane of the field coil.

Table # 1

a= 1.500"

b= 0.031"

c= 1.250"(approximate)

d= 0.750"

e= 1.750"

4.6 Radial Distribution

The radial distribution of the "z" component of the magnetic field $B_z(R)$ in the field-coil was measured with a small pick-up coil (1/8" O.D.x1/16" high) that was constrained to move along a diameter. The pick-up coil was mounted on one end of a length of bakelite rod that had a square cross-section (0.250" x 0.250"). A probe holder that could be mounted in the gap between the two halves of the field coil had 14 radial grooves machined into it. The grooves were machined so that the probe rod could move no more than $\pm$ .002" in either of the vertical or lateral directions. Alignment of the probe holder with the geometric axis of the field coil was accomplished by drilling holes for the alumina ceramic spacers that are used for vertical alignment of the field coil. The vertical positioning of the probe holder was done by adding shims until the desired "z" position was reached (most of the measurements were done at z=o", the geometric mid-pleane of the coil). Radial motion and position was obtained by connecting the probe rod to a precision screw thread (10 threads /cm). The screw thread was graduated in units of (1/200 mm) so that precise radial positioning could be maintained.

4.7 The Vector Potential

The vector potential $A_\theta(r)$ in the field-coil was obtained two different ways. First, by numerically integrating the expression

$$A_\theta(r) = \frac{1}{r}\int_0^r B_z(r')\, r'\, dr' \qquad 4.3$$

where $B_z(r')$ is the radial distribution of the magnetic field, and secondly, by measuring the voltage induced in a series of single turn pick-up coils concentric with the geometric axis of the field coil. The first method, because it is more time consuming was only used to check the second, and then only after the single turn coils had indicated that a vector potential minimum existed.

The desired accuracy of our magnetic measurements, ($\pm$ .1%) requires that the radius of each of the pick-up coils be known to at least $\pm$ .001". The single turn coils were made of 0.007" copper wire which was glued into 0.007" grooves machined in a piece of plexiglass. The diameter of each groove was measured with an optical comparater and found to be within $\pm$0.0005" of the nominal value. A

length of micro-dot cable was connected to each loop via a 1/16" x 1/16" radial slot machined in the plexiglass under the wires. This type of connection allows the perturbation at the connection to be minimized.

A second source of error arises if there is a lateral displacement of the set of pick-up coils with respect to the axis of the machine. One can show (appendix #2) that the fractional error in the signal from a pick-up coil with radius "r" due to a lateral displacement "a" is given by

$$\frac{\delta V}{V} \approx \frac{1}{4}(1-n)\left(\frac{a}{r}\right)^2 \qquad 4.4$$

If we assume that $n=\frac{1}{2}$, and take r=2" then with a=.010"

$$\frac{\delta V}{V} = \frac{1}{8}\left(\frac{10^{-4}}{4}\right) = 3.1\times10^{-6}$$

$$\frac{\delta V}{V} = 3\times10^{-4}\,\%$$

The lateral displacement of 0.010" assumed above would only result from a severe mis-alignment in the field-coil. The measured displacement is $\approx$ .006". Since the error due to small lateral displacements is extremely small, it has been neglected in all of our treatment of the experimental data.

4.8 Azimuthal Field Measurements

The azimuthal variation of the magnetic guide field $B_z(R)$ was measured along the equilibrium orbit radius. The probe O.D. was 1/8" and its height was 1/16". The probe was mounted in a plexiglass disc that was free to rotate in a shallow well machined into another piece of plexiglass. Alignment of the probe holder in the radial and vertical directions was done exactly the same as it was for the radial probe.

The shallow well holder was also used to locate the single turn pick-up coils in the field coil.

4.9 Results of the Magnetic Field Measurements

The radial distribution of the betatron guide field $B_z(r,\theta)$ on the first half-cycle is shown in Fig.#6. The "n"-value, measured at twelve different azimuths is displayed in Fig.#7. The vector potential $A_\theta(r)$ that corresponds to the guide field of Fig.#6 is shown in Fig.#8. The minimum in A_θ, hence the equilibrium orbit, occurs at r=1.9". The vector potential at the peak of the second half-cycle is also shown in Fig.#8. As we can see, A_θ on the second half-cycle is not the same as it was on the first. All of the magnetic measurements that we have described so far have been made at the peaks of the field on the respective half-cycles. The fact that the vector potential at the peak of the second half-cycle is different from that on the first raises the question of whether or not the field shape is correct during the entire first quarter period. With the differential amplifier techniques previously discussed it is possible to measure only peaks (in time) with high precision hence a different procedure had to be used. As a first step in this direction an x-y densitometer was constructed so that the amplitude of the signal from a magnetic pick-up loop (recorded on Polaroid film) could be measured as a function of time.

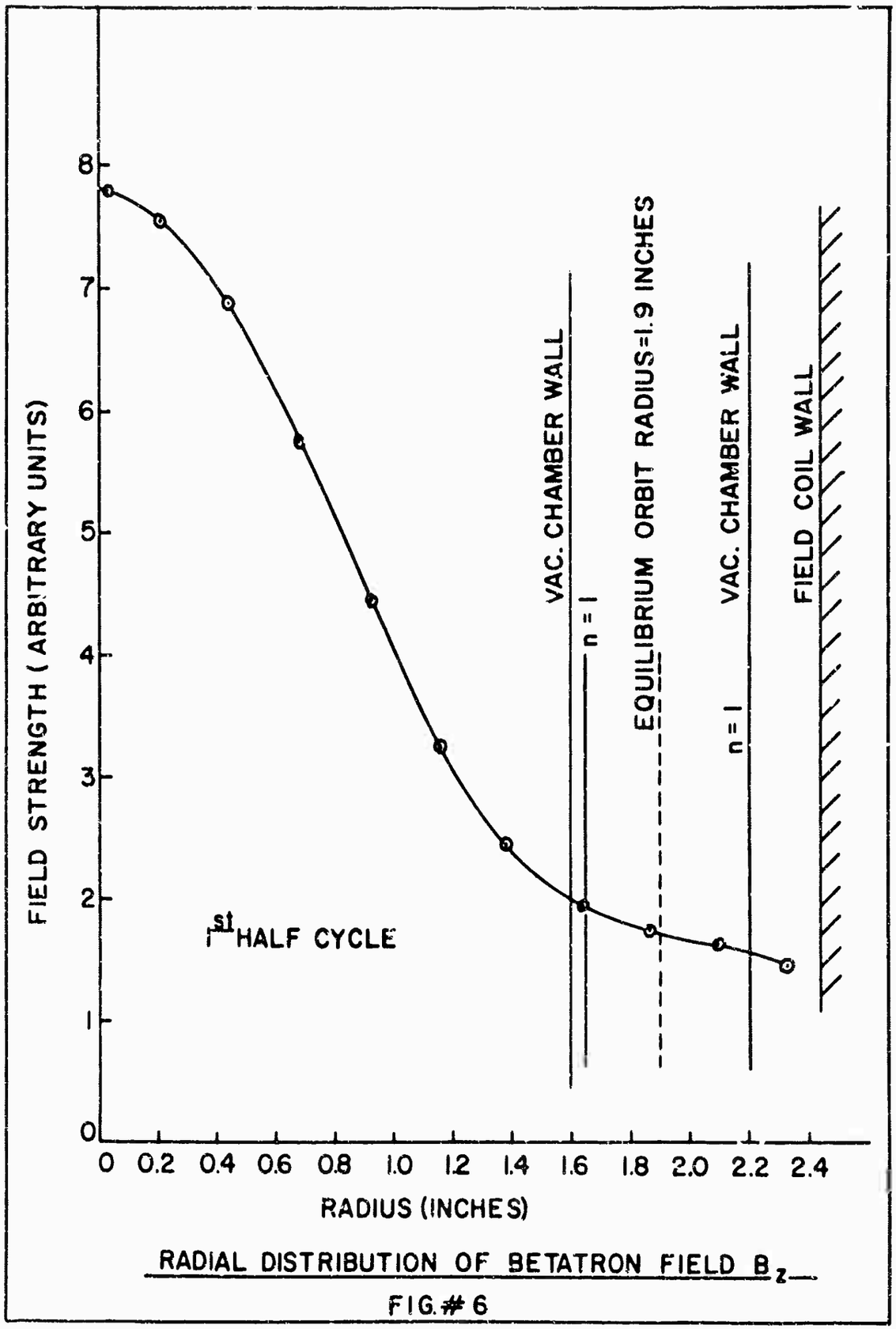

RADIAL DISTRIBUTION OF BETATRON FIELD B_z

FIG.# 6

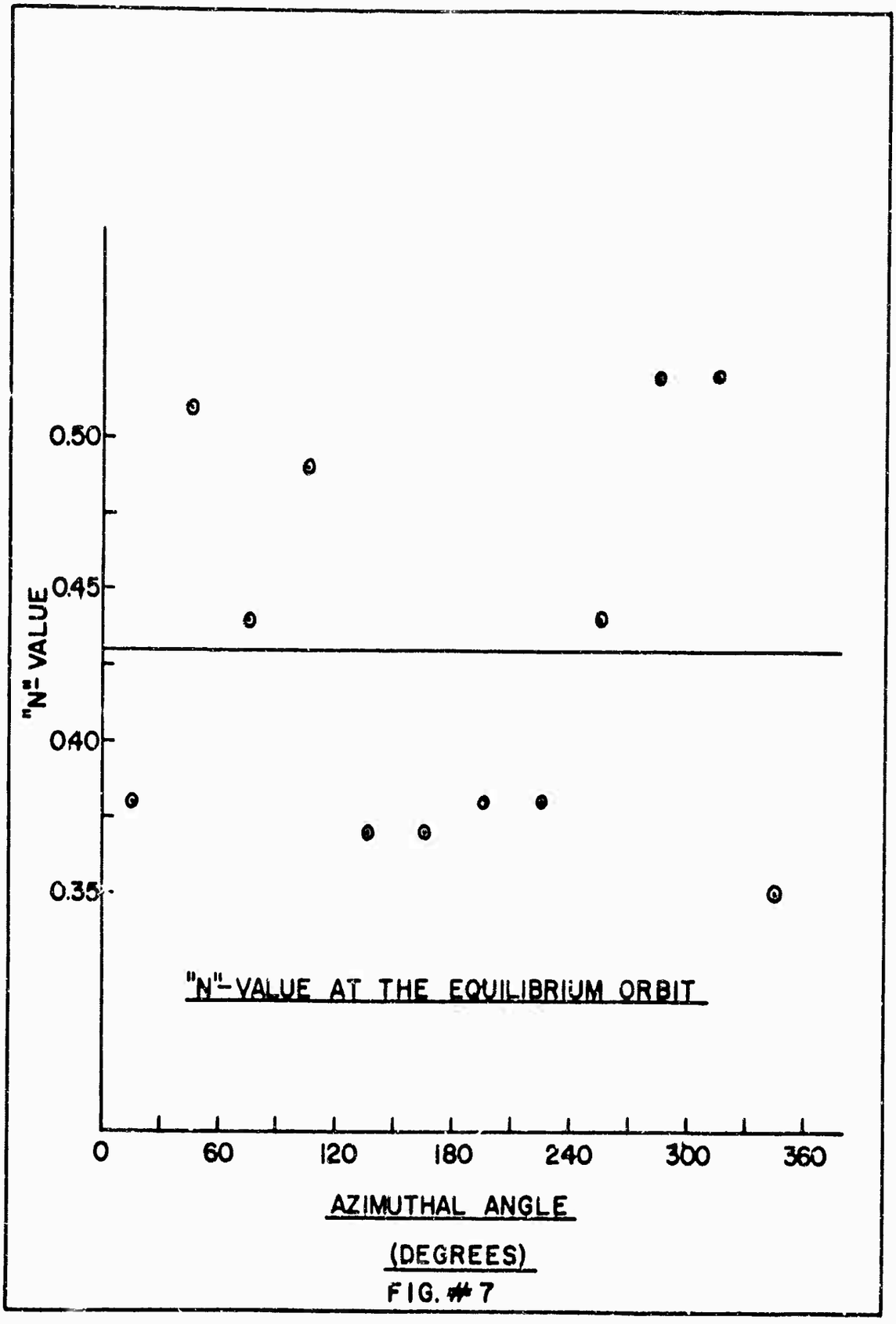
0.50
0.45
0.40
0.35
"N"- VALUE
"N"-VALUE AT THE EQUILIBRIUM ORBIT
0
60
120
180
240
300
360
AZIMUTHAL ANGLE
(DEGREES)

FIG. #7

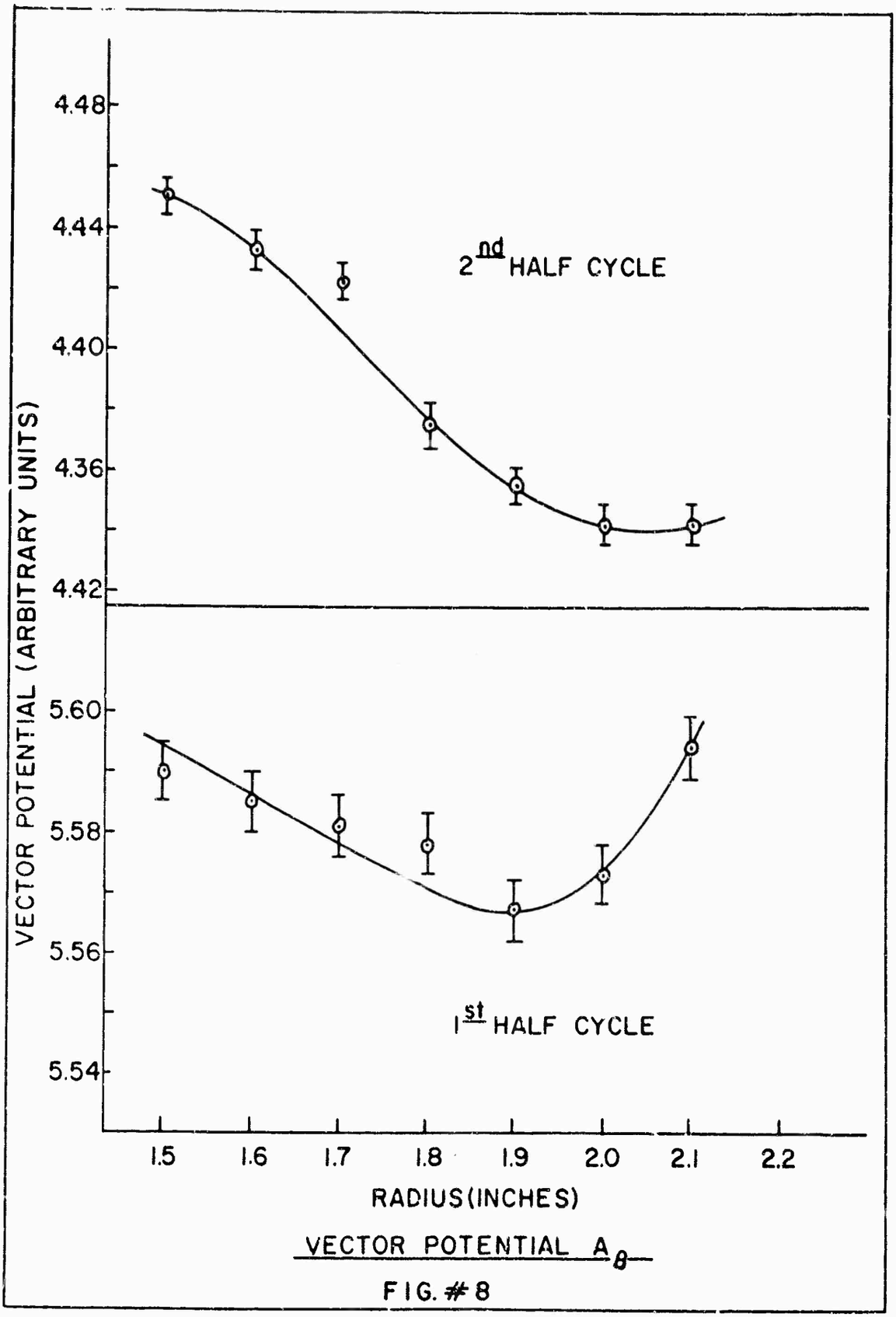

VECTOR POTENTIAL A_θ

FIG. # 8

The densitometer consists of a Derbyshire lathe cross-head (for the x-y motion), modified to hold the Polaroid film, and a microscope. The cross-head and microscope were rigidly attached to a one inch thick steel plate.

Operation as a densitometer is carried out by connecting a 931A photomultiplier tube to the microscope eyepiece. The field of view could be changed by placing appropriate apertures in the plane of the cross-hairs. Aperture sizes ranged from .001" to.005" dia. With a sufficiently small aperture the accuracy of the device is determined by the cross-head and the trace width on the film. With the Derbyshire cross-head co-ordinates could be measured to within ± .0005". Since this is a fixed number it is obvious that the error associated with an amplitude measurement depends on the amplitude, ie., the larger the amplitude the smaller the percentage error. A second complication arises because of electrical noise on the signal which lasts for approximately 25% of the first quarter cycle. This noise, and width of the trace, though very small for most purposes, was still large enough to make the error at the start of the signal larger than the 0.1% we discussed previously. Nevertheless, we still measured A_θ (λ) at different instants of time during the first quarter period.

The accuracy of these measurements was only 0.75-1.0% but served to show that nothing drastic was happening to A_θ during this time.

Because of the extreme difficulties involved in measuring the magnetic field at times other than at the peaks, no further attempts were made to improve the accuracy.

The azimuthal variation of the betatron guide field at the equilibrium orbit radius in the "untrimmed" condition is shown in Fig.#2. The corrected field variation is also shown on the same plot. The corrections were made by adding copper shims to the flux concentrator disc that is nearest to the coil mid-plane. The shims are placed at those azimuths where the field is too large. Filing then permits finer field adjustments to be made. (Fig.#5). The amplitude of the first four harmonics of the corrected field were computed and are listed below.

Harmonic #	Amplitude
1	0.48%
2	0.22%
3	0.48%
4	0.21%

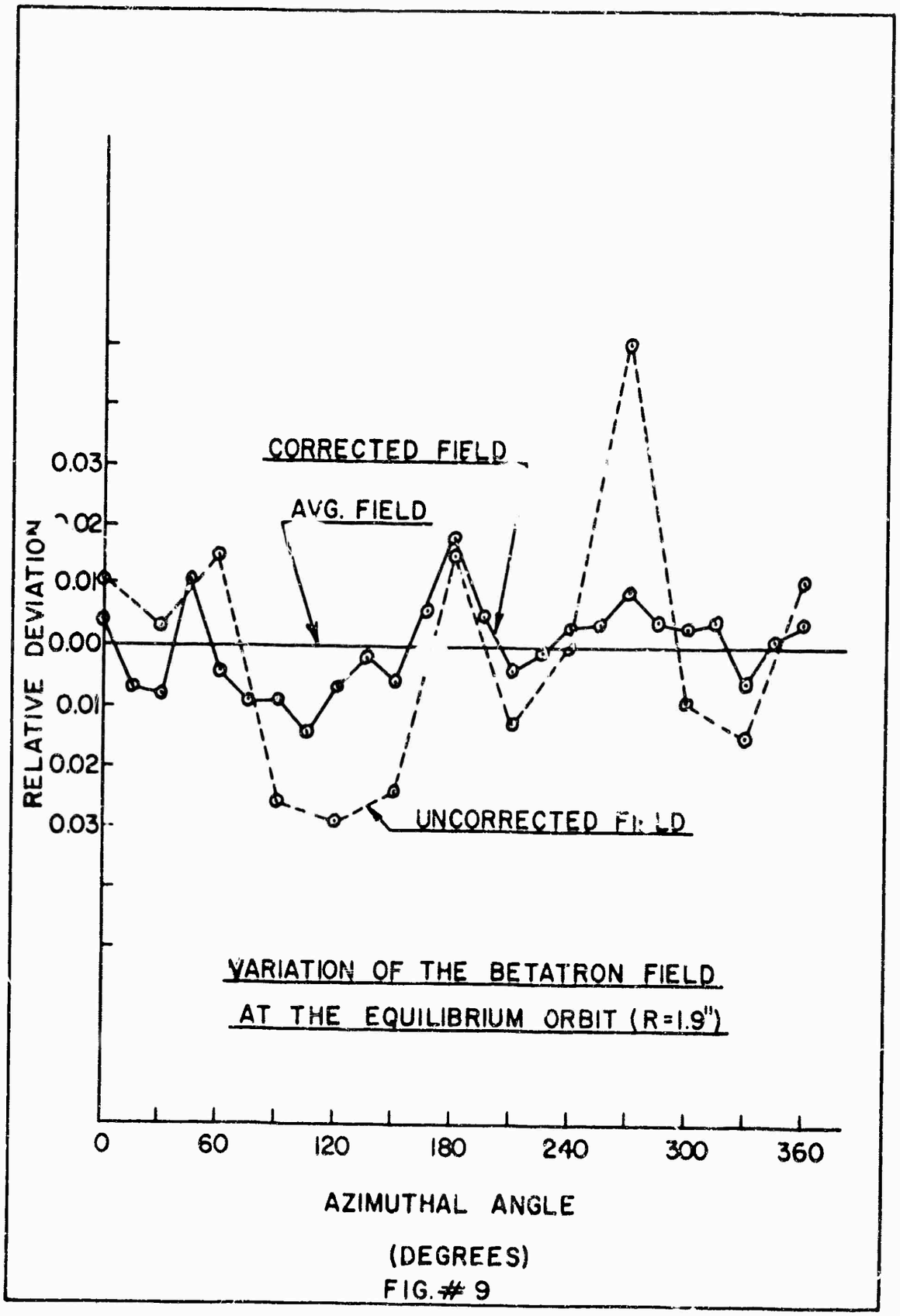

VARIATION OF THE BETATRON FIELD
AT THE EQUILIBRIUM ORBIT (R=1.9")

FIG.# 9

If we insert these values into the equation for the particle displacement from the equilibrium orbit in a betatron field (eq#3.23) we find that the maximum amplitude of oscillation will be $\approx$ 0.02". Allowing a factor of five to include the effects of the B_θ windings[21] the maximum amplitude becomes $\approx$ 0.10" which is well within the limits of the vector potential well (see Fig.#8).

All the magnetic field measurements just described were performed under the same experimental conditions that were used for experiments with plasma save one. All of the measurements were made without the B_θ windings in place. The presence of the extra copper, for the B_θ field, that is required for runaway production leads one to suspect that the field configuration with the B_θ coils in place may be quite different from the one without them.

A second field-coil together with flux concentrators was constructed in order to answer questions such as this one while experiments were being conducted in the first coil. The only difference between the two systems was in the design of the flux-concentrators. The separation between successive discs in each flux concentrator was increased from 0.010" in the first set, to 0.030" in the new set. The gap in each disc was increased to .030",

the mylar insulation between the discs removed, and the entire space between the discs filled with epoxy to improve the bond.

A betatron field in the mid-plane of the field coil was obtained with a flux concentrator separation just slightly greater than that in the experimental coil (approximately 0.1"). The vector potential in the mid-plane and 1/8" above and below the mid-plane of the field coil is shown in Fig.#10. The equilibrium orbit is again at a radius of 1.9 inches. The vector potential well in this case is slightly deeper than in Fig.#8, because the "n" value is smaller (close to zero, but not equal to zero).

The effect of the B_θ coils on the betatron field shape was determined by placing on the single turn coil holder, a system of coils that duplicated the coils used to generate the B_θ field. In addition a type "c" network indentical to the network used to drive the coils was placed across the dummy system. The resulting vector-potential agreed with the vector potential without the coils within the accuracy of our measurements.

Thus we can conclude that the presence of the B_θ coil does not seriously affect the betatron field shape, at least not the azimuthally averaged value.

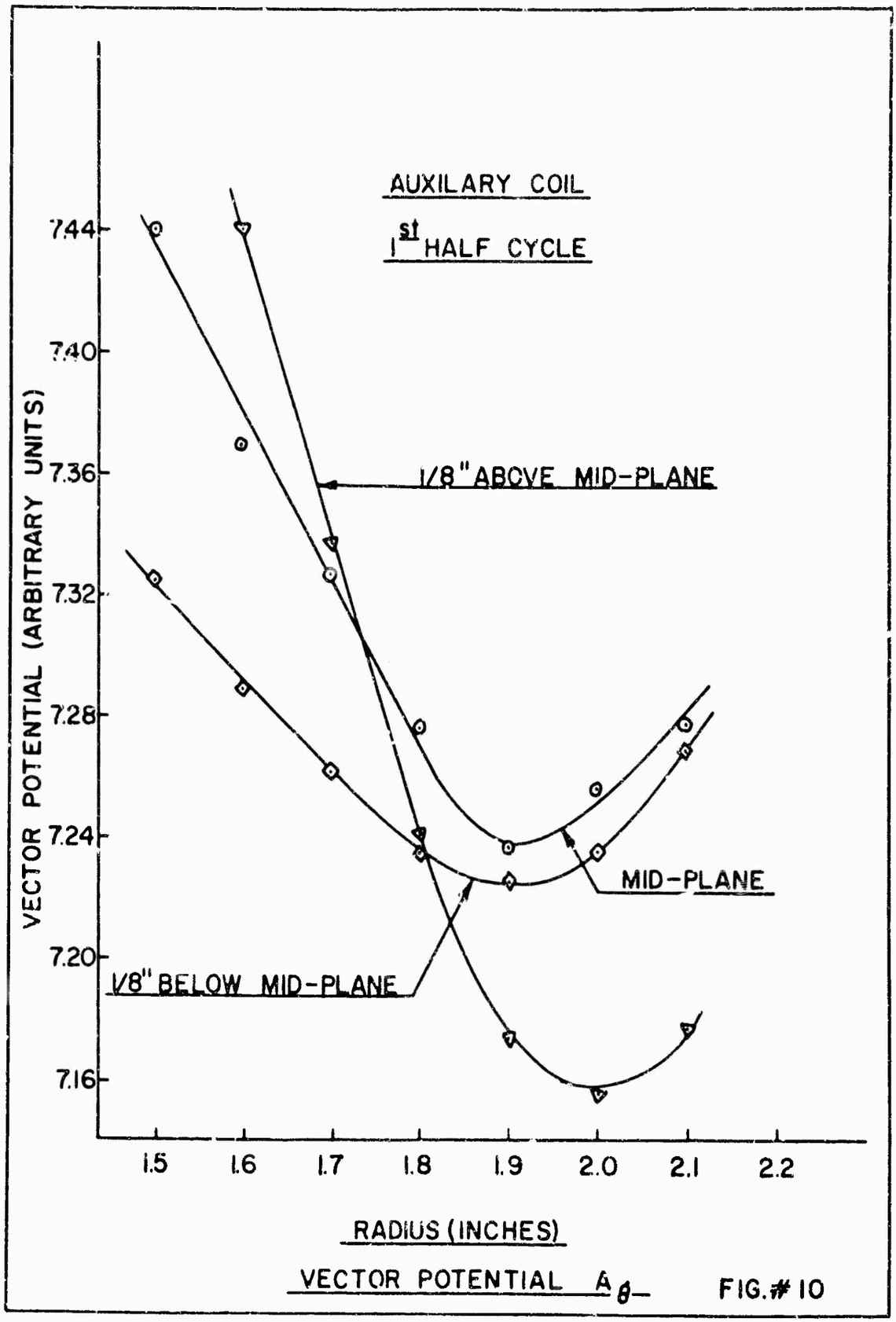
AUXILARY COIL
1st HALF CYCLE
7.44
7.40
7.36
7.32
7.28
7.24
7.20
7.16
VECTOR POTENTIAL (ARBITRARY UNITS)
1/8" ABOVE MID-PLANE
MID-PLANE
1/8" BELOW MID-PLANE
1.5
1.6
1.7
1.8
1.9
2.0
2.1
2.2
RADIUS (INCHES)
VECTOR POTENTIAL A_θ

FIG.# 10

4.10 Summary

In the preceeding paragraphs we have described in detail the entire process of constructing the magnetic guide field for a low inductance plasma betatron, using flux concentrators. The techniques used to make precise pulsed magnetic field measurements in the betatron coil were also described. In the final few sections we have presented experimental data that show that the magnetic field distribution does indeed satisfy the betatron conditions for both equilibrium and stability.

V ADDITIONAL APPARATUS AND PLASMA GENERATION

5.1 The B_θ Field

The B_θ magnetic field was generated by the discharge of a low impedance transmission line through the toroidal windings wound on the vacuum chamber. The line, shown in Fig.#11, which is designated as a Type "C" (24-26) network, is formed by the parallel connection of "n" individual L_m-C_m elements each of which is resonant at an odd harmonic of the fundamental frequency of the first section. This type of network has the advantage that it incorporates constructively the internal inductance present in all high voltage capacitors. This feature makes the line very easy to build.

The design parameters for the Type "c" drive were determined primarily from the requirement that the B_θ field remain essentially constant during several half cycles of the betatron field. Preliminary experiments on runaway generation with a faster B_θ drive ($\tau/2 \approx$ 25 μ sec) system indicated the magnitude of the B_θ field that was necessary for x-ray production. These considerations led to the following specifications for the type C-network.

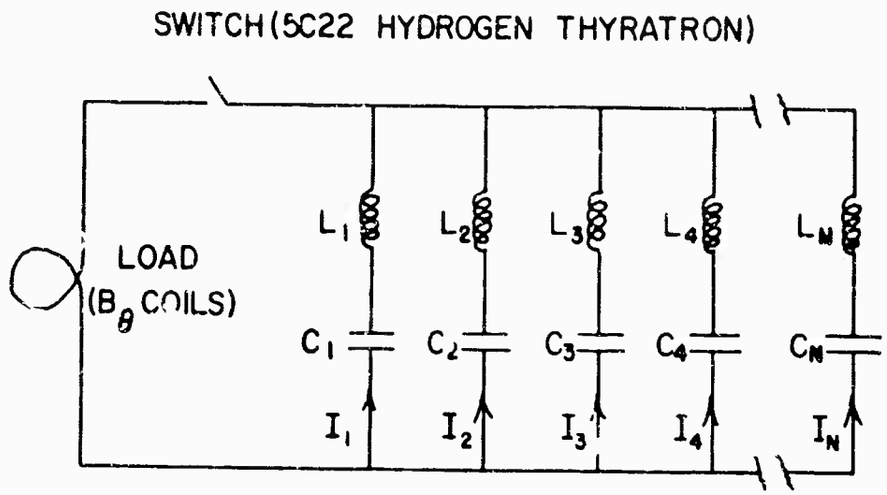

TYPE "C" NETWORK

FIG. #11

peak current	=	5000 amp.
current wave form	=	trapezoidal
rise time	=	10 μ sec
decay time	=	10 μ sec
pulse duration	=	100 μ sec
characteristic impedance Z_o	=	.286 Ω

The design synthesis is based upon Guilleman's technique of the Fourier analysis of the desired continuous wave train from an ideal short-circuited lossless transmission line, ie., the current through the load is given by

$$I(t) = I_o \sum_{n=1}^{\infty} b_n \sin\left(\frac{n\pi t}{\tau}\right) \qquad 5.1$$

where $$b_n = \frac{2}{\tau}\int_0^{\tau} \frac{I(t)}{I_o} \sin\left(\frac{n\pi t}{\tau}\right) dt \qquad 5.2$$

I_o = peak current

b_n = Fourier coefficient of the n^{th} section

τ = pulse length in seconds.

The inductive and capacitive values of each section are determined by the desired characteristic impedance Z_o and τ , namely

$$\left(\frac{L_n}{C_n}\right)^{1/2} = Z_o/b_n$$

$$\left(L_n C_n\right)^{-1/2} = n\pi/\tau \qquad 5.3$$

The calculated values of the b_n , C_n and L_n parameters for a four section line with the current and waveform that was specified earlier are presented in Table #2.

Table # 2

Calculated Values

Section	b	L (uh)	C (uf)	fr(kc)
1	1.252	7.3	140	4.9
3	.364	8.3	13.5	14.7
5	.163	11.1	3.62	24.5
7	.067	19.5	1.07	34.3

Measured values

Section	L (uh)	C (uf)	fr(kc)
1	7.3	140	4.95
3	8.2	14.5	14.7
5	11.2	3.51	25.5
7	20	1.06	34.8

Because of the low frequencies involved, the series inductances L_m were generally quite larger than the internal inductance of the capacitors C_m. The additional inductance was achieved by winding #18 copper wire on 1"-O.D. poly vinyl chloride tubing until the measured resonant frequency of each section agreed with the calculated frequency. The sections were then joined together with RG-8U coaxial cable, and switched into the B_θ solenoid with a 5C22 hydrogen thyration. The magnitude of B_θ vs the line charging voltage is shown in Fig.12.

5.2 The Vacuum System

The acceleration chamber was a pyrex glass torus with major and minor diameter of 3.8" and 5/8" respectively. A single radial port was used both to pump out the chamber and to provide easy access to the chamber interior. The chamber was connected to two two inch oil diffusion pumps placed in series. With the second diffusion pump blanked off the base pressure of the system was 10^{-8} mm Hg measured at the pump. The base pressure at the acceleration chamber was 5×10^{-6} mm Hg. No provision to bake the system was made because the small clearances between the vacuum chamber and the flux concentrators would allow too much heat transfer to the flux concentrators. A variable leak connected to the vacuum system between the diffusion pumps and acceleration chamber was used to admit the experimental gas and control the background pressure. The initial neutral pressure was varied between .5-2 Torr. (Argon and Krypton).

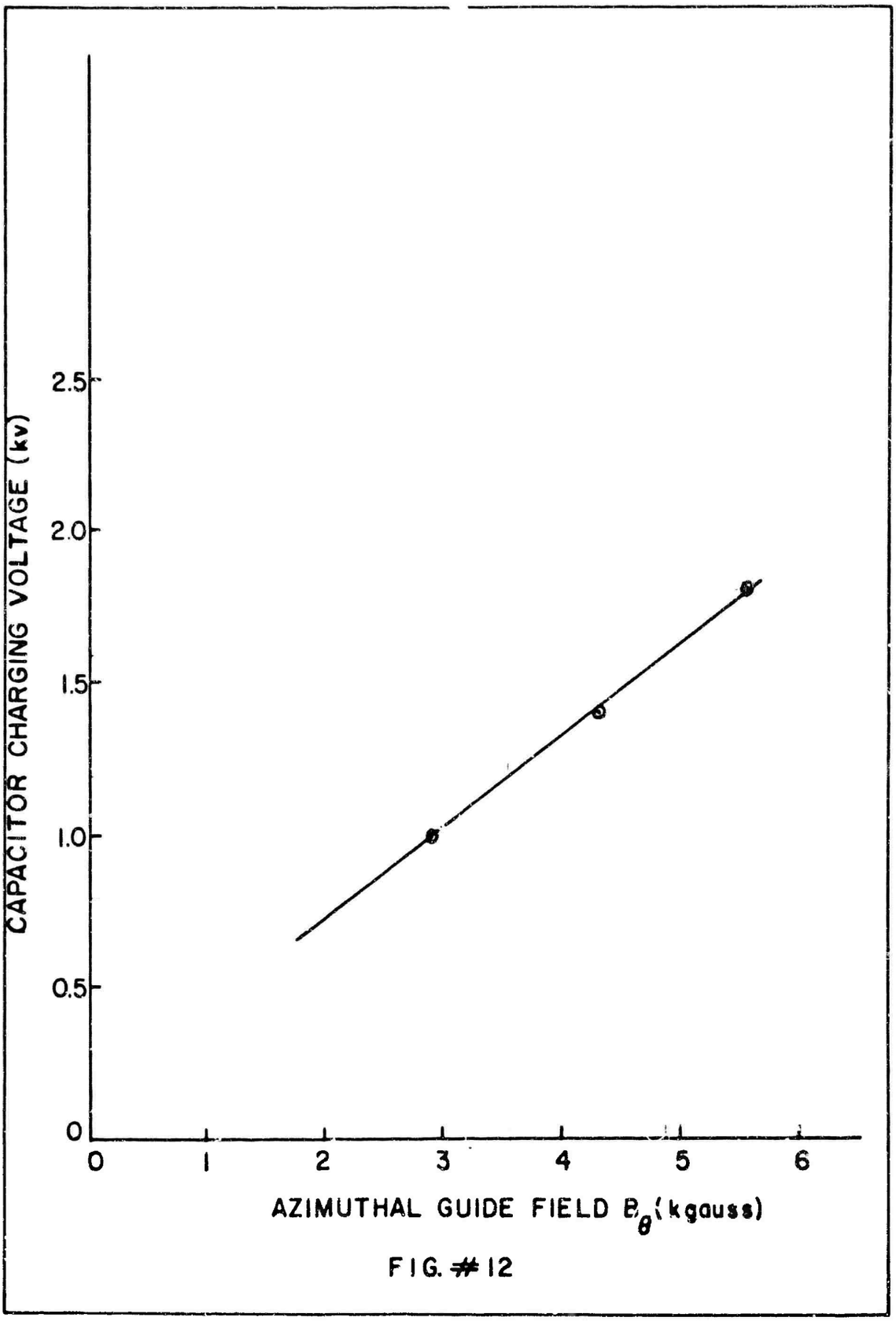
CAPACITOR CHARGING VOLTAGE (kv)
2.5
2.0
1.5
1.0
0.5
0
0
1
2
3
4
5
6
AZIMUTHAL GUIDE FIELD B_θ (kgauss)

FIG. # 12

BLANK PAGE

5.3 Plasma Generation

Considerations of maximum beam current leads to an upper bound on the electron density that can be present in the vacuum chamber just prior to the application of the betatron field. The maximum beam current in a plasma betatron has been calculated by Schmidt[4], for the case of zero azimuthal magnetic field. Since the beam is diamagnetic the position of the equilibrium orbit will be shifted radially inward from the single particle position. If N is the number of electrons per unit length of stream and A_ϕ the vector potential due to the betatron field the maximum beam current $i = N\beta v_0$ is determined from[4]

$$\nu\lambda = \left[\frac{\left|\frac{\partial A_\phi}{\partial r}\right|}{B_z} \right]_{r=r_0'} \qquad 5.4$$

where $\nu = N e^2/m$, r_0' is the position of the new equilibrium orbit, and λ is related to the self inductance of the beam via. $\lambda = L/2\pi\lambda$. Using values of $\frac{\partial A_\phi}{\partial \lambda}$ determined from the shape of the vector potential on the 1st and 2nd half cycles (Fig.#8) we find that the maximum possible beam current on the first half cycle is about 70 amp. and about 300 amp. on the second. Thus, the

initial electron density should be on the order of 10^{10}-10^{11} per cm^3.

In order to keep neutral gas scattering losses to a minimum the backround neutral pressure should be as low as possible. This means that we should have $p_o < 10^{-3}$ mm Hg. At these backround pressures the mean free path l for an ionizing collision is much greater than the vacuum chamber dimensions (d). When $l \gg d$ breakdown is most easily accomplished by means of electron multipaction[27]. This process makes use of the secondary emission properties of the walls of the vacuum vessel. Briefly the breakdown process proceeds as follows. An R-F electric field is applied between the walls of the vacuum chamber as sketched below (care must be taken so that walls with good secondary emission properties are used).

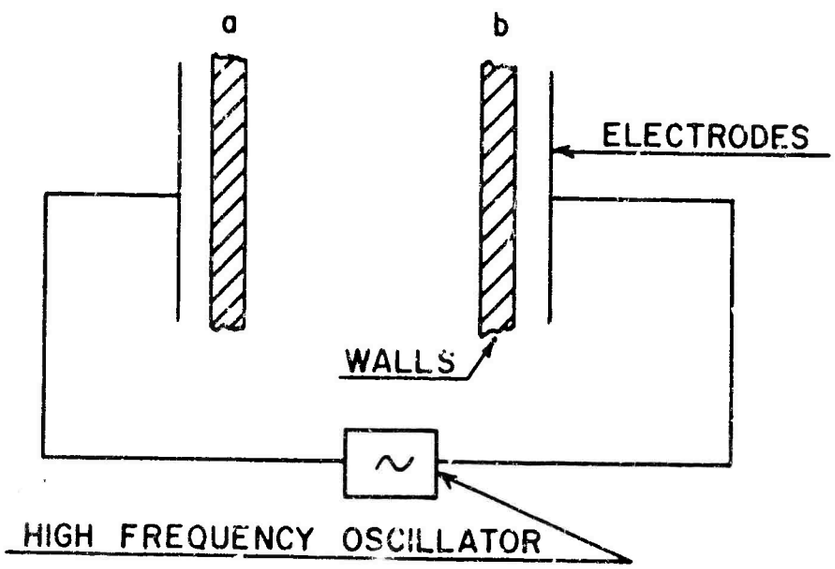

(One can also place the electrodes inside the vacuum chamber. For this case the electrodes must be good secondary emitters). We start by assuming that there is a free electron near "a". The initial polarity is chosen so that the electron is accelerated toward "b". The frequency of the R-F field is determined by the requirement that the electric field change sign when the electron reaches "b". Then if the electron has gained sufficient energy to generate more than one secondary at "b", the electrons at "b" will be accelerated toward "a". In this manner we can build up a cloud of electrons oscillating between the vacuum chamber walls. Some of the electrons make ionizing collisions and thus a discharge is gradually built up. The process of electron multipaction takes place whenever the mean free path is greater than the vacuum chamber dimensions and the frequency and amplitude of the R-F field satisfy the conditions just described. In fact in some cyclotrons electron multipaction can prevent the build up of the R-F Dee voltage because of the additional oscillator loading at resonance. This is overcome by making the R-F voltage build up sufficiently rapidly so that the resonance region is swept through quickly, or by applying a d.c. bias voltage to the electrodes which destroys the resonance.

An elementary calculation of the resonance

conditions proceeds as follows; we assume that the R-F electric field is given by $E_o \sin \omega t$. The equation of motion for an electron in this field is

$$\frac{dv}{dt} = \frac{q}{m} E_o \sin \omega t$$

thus

$$v = -\frac{q E_o}{m \omega} \cos \omega t + A \qquad 5.5$$

If we take v=o at t=o, then $A = q E_o / m\omega$. Integrating a second time we get

$$x = \frac{q E_o}{m \omega} \left(t - \frac{1}{\omega} \sin \omega t \right) + B$$

Similarly we take x =o at t=o, then B=0. Hence the velocity "v" and displacement "x" are given by

$$v = \frac{q E_o}{m \omega} \left(1 - \cos \omega t \right)$$

$$x = \frac{q E_o}{m \omega} \left(t - \frac{1}{\omega} \sin \omega t \right) \qquad 5.6$$

The resonance conditions are obtained by requiring that the electric field change sign at x=d, this means that when x=d, we must have $\omega t = \pi$. The electron energy Wo at x=d must be large enough so that the secondary

electron emission coefficient γ is greater than unity (γ is the number of secondaries released per primary). Substituting into (5.6) we find that resonance occurs when ω satisfies the pair of equations

$$W_0 = \frac{2q^2 E_0}{m \omega_r^2}$$

$$d = \frac{\pi q E_0}{m \omega_r^2} \qquad 5.7$$

Solving for ω_r we get

$$\omega_r = \frac{\pi}{\sqrt{2}} \frac{W_0^{1/2}}{m^{1/2} d} \qquad 5.8$$

For pyrex glass $W_0 \approx 100$ volts for good secondary emission. Then with d=1 cm we find that

$$f_r = \omega_r / 2\pi \approx 150 \text{ m c}$$

A high frequency quadrupole electric field, was used to preionize the gas within the vacuum chamber. To minimize the effects of the quadrupole field during betatron acceleration, the quadrupole electrodes were designed so that the position of the R-F potential minimum is close to the position of the equilibrium orbit in the betatron field. (This calculation is described in appendix #3).

The quadrupole electrodes and acceleration chamber are shown in Fig.#13. The quadrupole wires were brought out through the gap in the median plane of the field coil and connected to a two wire transmission line of variable length. The transmission line was shorted at the far end so that it could also be used to couple power from the oscillator. The quadrupole electric field has no effect on the runaway behavior since the x-ray emission time with the quadrupole electric field turned off 1×10^{-6} sec before the application of the betatron field is the same as it is when the electric field is run continuously.

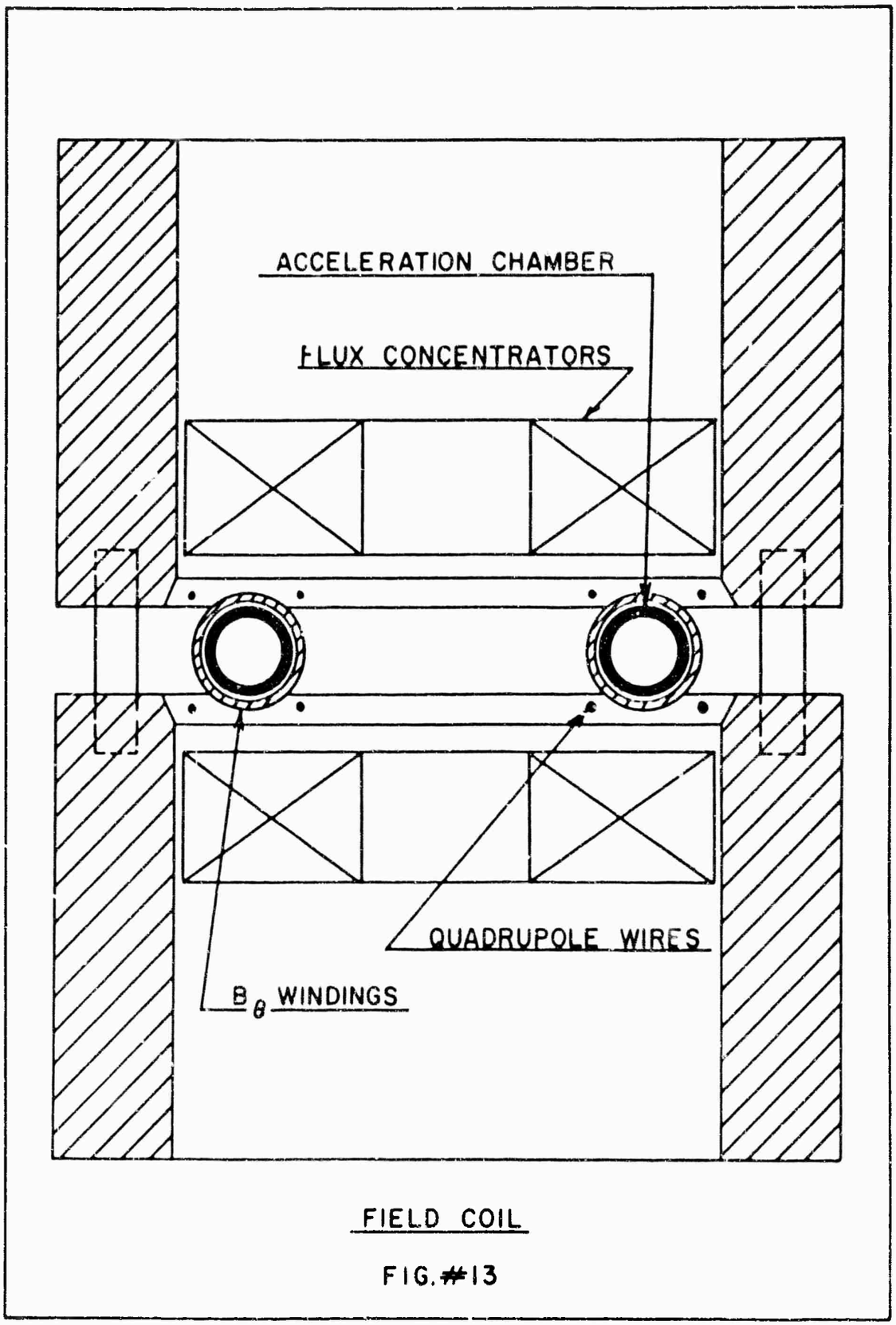

FIELD COIL

FIG. #13

BLANK PAGE

VI DIAGNOSTICS

6.1 Electron Density

Electron density measurements in the R-F generated plasma are difficult because conventional diagnostic techniques such as Langmiur probes, double Langmuir probes or microwaves (cavity techniques excepted) cannot be used effectively at the electron densities and temperatures in the discharge. Absence of a reference electrode prevents the use of the single Langmuir probe. Attempts to measure the density with double probe technique of Johnson and Malter were frustrated because the radius of the space charge sheaths turned out to be larger than any convenient probe separation. At the low electron densities present in the discharge ($\approx 10^{10}/cm^3$) the required microwave wave length is much greater than the dimensions of the plasma so that phase shift measurements are impossible.

In recent years Dattner and others[46] have generated new interest in the dipole resonances first studied by Tonks. Briefly if one places a plasma in an oscillating electric field, a resonance takes place when the frequency of the field ω is related to the plasma frequency via the equation

$$\omega = \frac{1}{k^{1/2}}\,\omega_p = \frac{1}{k^{1/2}}\left(\frac{n_e e^2}{m \epsilon_0}\right)^{1/2} \qquad 6.1$$

where k is a constant that depends on the plasma geometry. (k=1 for plane, k=2 for cylindrical and k=3 for spherical). There are other resonances present but the one just mentioned is the strongest. Thus by observing the frequency at which resonance occurs one can determine the electron density, at least in principle. The only requirement on the frequency is that the wave length should be greater than the dimensions of the plasma.

An experiment was set up to see if the Tonks-Dattner resonance could be observed in the R-F exdited plasma. Plasma was generated by applying R-F voltage at 120 mc. to a vacuum chamber and quadrupole system identical to the system used in the field coil. A strip line was placed across one half of the vacuum chamber as sketched below.

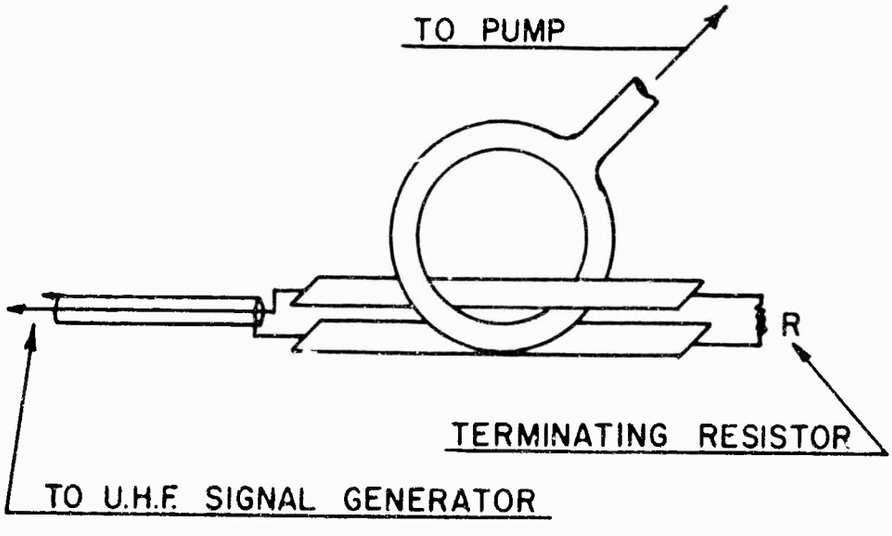

The strip line was then connected to a signal generator whose frequency could be varied between 500 and 1000 mc. The experiment proceeded as follows. At a given frequency the line was tuned to give a low standing wave ratio, (V.S.W.R.) typically 1.05 with no plasma in the discharge vessel. A plasma was then generated and the V.S.W.R. remeasured. We would expect to see a dramatic change in the V.S.W.R. as the frequency of the R-F field went through the plasma resonant frequency. The frequency was varied from 500-1000 mc. in steps of 20 mc. No change in the V.S.W.R. indicative of a plasma resonance was observed. Since the discharge could not be run continuously (because of vacuum chamber heating) it is possible that there was enough variation in the electron density between discharges to mask out the effects of the plasma resonance. It is also possible that the frequency steps were too wide. If the "Q" of the resonance was greater than 50 then the band width $\Delta f = f/Q$ would be less than the frequency steps used.

In another experiment the frequency was varied continuously from 500-1000 mc. and the reflected power from the strip line was recorded on a chart recorder. No significant change in the reflected power was observed between the plasma and no plasma conditions.

In the former experiment the transmission system is not "flat" over the frequency range 500-1000 mc. There are many resonances present without a plasma in the vacuum chamber. Under these circumstances it is quite possible that a system resonance could completely overcome any effect of a plasma resonance. Thus the next step was to shut off the quadrupole electric field and look for resonances during the plasma decay. Efficient detection was accomplished by terminating the strip line with the characteristic impedence of the cable, and measuring the power reflected from the plasma column back toward the signal generator. A directional coupler was inserted between the plasma column and generator with a 20 db pickoff to a crystal detector. Approximately 10-15db attenuation was used between the directional coupler and the U.H.F. generator for isolation. The 120 mc. breakdown oscillator generates large D.C. level signal in the crystal. The oscilloscope, used to monitor the reflected power, was adjusted so that the D.C. signal from the reflected U.H.F. signal is on screen. Then the signal induced by the quadrupole electric field (q.e.f.) will cause the D.C. level of the trace to move off screen. Off resonance, or with no plasma, a step response is seen as the q.e.f. is turned off. The output changes from the negative D.C. level of both the q.e.f. and the U.H.F. to the less negative value of just

the U.H.F. At the resonance a pulse appears relative to the U.H.F. level with no plasma (in the positive direction). Initial experiments were performed in argon at high pressures, typically 100 microns, in order to make detection of the resonance easier. Figure #14 illustrates a typical curve of electron density versus time during the afterglow. The argon pressure was held constant at 100 microns and the time of resonance was measured at frequency increments. The electron density was calculated from the frequency relation for a dipole resonance

$$\omega_r^2 = \frac{n_e q^2}{2m\varepsilon_0} \qquad 6.2$$

with corrections made for the glass vacuum chamber walls. Results show a decay to a fixed value (not=0) of electron density which is believed to be that maintained by the U.H.F. The initial decay was evaluated in terms of the volume recombination coefficient (∂). If the particle loss is due to volume recombination only then the temporal behavior of the density is given by

$$\frac{1}{n_e} - \frac{1}{n_{e0}} = \partial t \qquad 6.3$$

where n_{e0} is the initial electron density. If we

extrapolate the density data in Fig.#14 to zero time we find that $n_{e_o} \approx 7.5 \times 10^{9}$ electrons /cm^3. The first four points result in ∂ values of 9.19×10^{-7}, 9.43×10^{-7} and 9.34×10^{-7} cm^3/sec respectively. The difference between the ∂ values obtained here and the value of $6.7 \pm 0.5 \times 10^{-7}$ cm^3/sec reported recently (28) for argon is probably due to diffusional losses.

At the neutral pressure used in this experiment the space charge sheaths surrounding Langmiur probes are small enough so that I-V characteristics can be interpreted without a great deal of error. Thus the density during the quadrupole electric field discharge was determined with double Langmuir probes and compared with that obtained via the resonance technique. The ion (hence electron) density was obtained from the well known relation $i_s = A n_i q \bar{v} / 4$ where i_s is the saturated ion current, A is the effective probe area, ($\bar{v}$) is the ion thermal velocity (the ion temperature is assumed to be the same as that of the neutral gas). The electron density obtained this way is about a factor of ten higher than that obtained with the resonance technique. As the neutral gas pressure is lowered the electron temperature increases and the density probably decreases thus making double probe data impossible to interpret and furthermore,

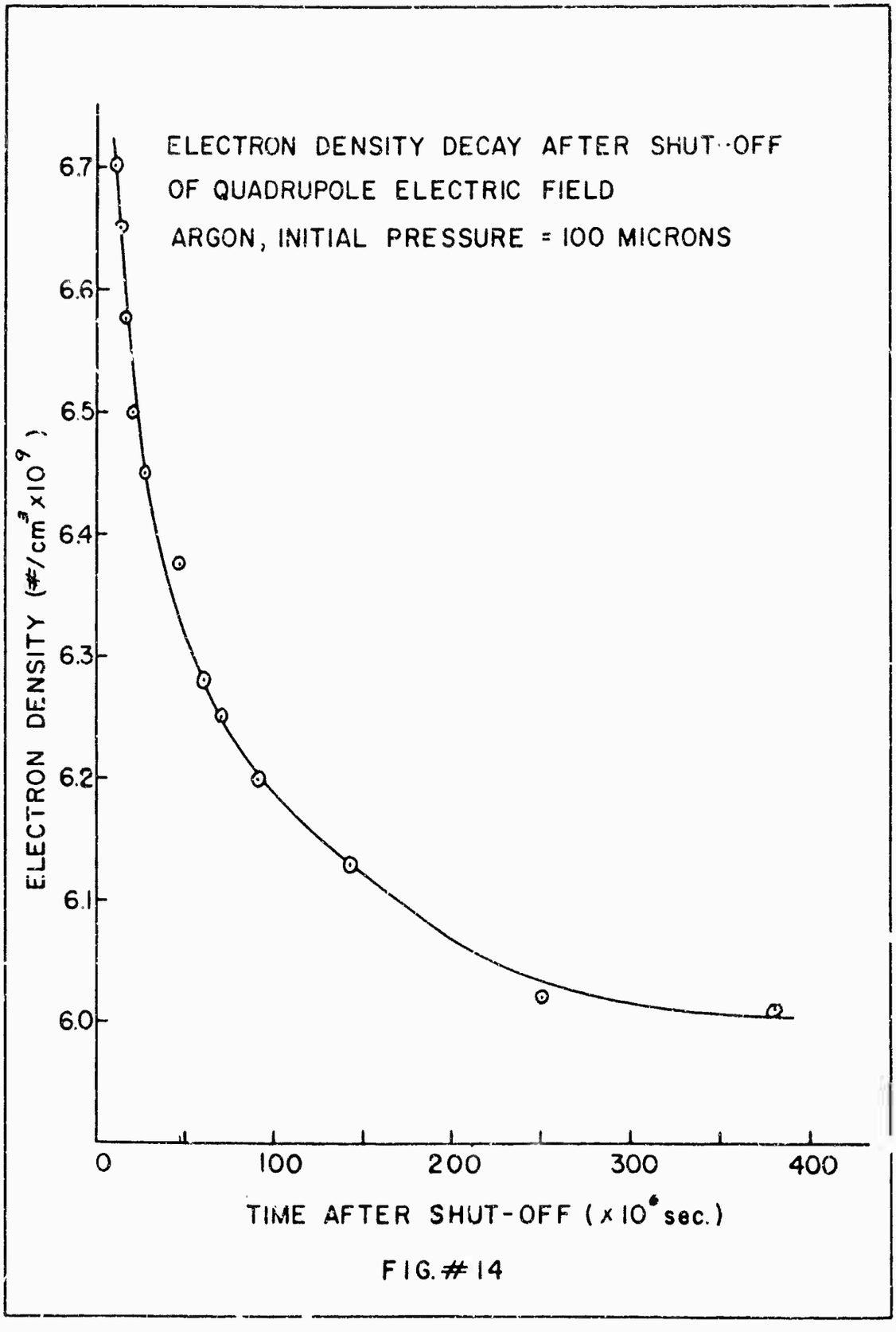
ELECTRON DENSITY DECAY AFTER SHUT-OFF
OF QUADRUPOLE ELECTRIC FIELD
ARGON, INITIAL PRESSURE = 100 MICRONS
ELECTRON DENSITY (#/cm³ x10⁹)
6.7
6.6
6.5
6.4
6.3
6.2
6.1
6.0
0
100
200
300
400
TIME AFTER SHUT-OFF (x 10⁶ sec.)

FIG. # 14

BLANK PAGE

the resonance becomes more difficult to find for reasons that are so far unexplained. Because of the large difference between the two density results at high neutral pressure, no extensive investigations were carried out at lower pressures.

An attempt was made to measure the electron density spectroscopically using the method of Inglis and Teller.[29,30] If one examines the broadening of individual lines of a series such as the Balmer series, one finds that the higher members of the series are broadened more than the lower members. Since the higher members of the series are also closer together than the lower members, one eventually reaches a point where the broadening of the lines is comparable to the spacing between them, and at this point the lines in the series merge together and are no longer visible as distinct lines. This process manifests itself in the spectrum as a depression of the series limit and is equivalent to saying that the perturbation of the energy levels due to the Stark effect becomes comparable to the energy difference between two adjacent levels. By equating these two energy terms one can solve for the principle quantum number n_m of the upper level of the last distinct line of the series. The ion density is then given by

$$\log_{10} n_i = 23.26 - 7.5 \log_{10} n_m \qquad 6.4$$

This method has been used sucessfully to determine the ion density in a decaying hydrogen plasma[31] at relatively high ion densities ($10^{15}/cm^3$). At low electron densities ($10^{9}/cm^3$) the upper quantum number n_m of the last line of the series is very large ($\approx$ 90) therefore a spectroscope with large dispersion is required. After the betatron field is turned on the electron (and ion) density increases, the discharge "blooms". It is quite possible that the electron density may reach a value of $10^{12}/cm^3$ during this discharge. At this density $n_m \approx 20$ and hence may be observable without resorting to sophisticated experimental apparatus. Although all of our experiments were done with argon and krypton, helium was used to test this method because of its simpler spectral structure. The spectral lines of interest were from the series $n\,^1D_2 \rightarrow 2\,^1P_1$ (series limit-3679.7 A°). This series was chosen because of its close resemblence to that of Hydrogen[32], especially at high values of the principle quantum number. The discharge was viewed with a Hilger Medium Quartz Spectrograph (for this experiment a glass

prism was used). The spectrum was recorded on Kodak Type F Spectroscopic plates and developed in Acufine to improve the speed.[33] The experiment proceeded as follows. A plasma was generated using the high frequency quadrupole electric field. The spectroscope shutter was opened manually just prior to the application of the betatron and B_θ magnetic fields, and closed again as soon as possible after the discharge. Although the shutter is open for a period of time considerably longer than the duration of the betatron field, the maximum light intensity occurs during this time. When the spectrum obtained this way is compared with the spectrum from the R -F excited plasma alone, we find additional lines which we believe are due to additional excitation during the pulsed discharge. If the electron density is in the region 10^{10} -10^{12}/cm^3 the last distinct line of the series will be in the wave length region between 3757.1 and 3679.1 A^o. We observe what appears to be Nitrogen band structure in this wave length region which makes interpretation of the series limit impossible. Spectra were again taken after the R-F discharge had been run for some time, but the results were the same. In order to make the discharge spectroscopically clean it is necessary to run the discharge with the B_3 and B_θ fields, for extended periods of time.

Since this pulse cleaning would have required extensive revision of the electronic controls this was not pursued.

In the preceeding paragraphs we have discussed several attempts to measure the electron density in the R-F excited plasma. The reasons for not obtaining a satisfactory result for the electron density with the various techniques were also discussed. So far no mention has been made of still another experimental parameter from which at least a lower bound on the electron density can be obtained; namely the induced current in the acceleration chamber. The induced current, i measured with the Rogowsky coil wrapped around the vacuum chamber, is related to the electron density via the relation

$$\frac{i}{A} = n_e q \langle v_e \rangle + n_i q \langle v_i \rangle \qquad 6.5$$

were A is the vacuum chamber cross-sectional area and $\langle v_e \rangle$ and $\langle v_i \rangle$ are suitably averaged velocities. Since the electrons are much more mobile than the ions we can assume that they carry all the current; then we have

$$\frac{i}{A} = n_e q \langle v_e \rangle \qquad 6.6$$

If we let $\langle v_e \rangle = C$; the velocity of light, we obtain a lower bound on the electron density (assuming n_e is uniform over the entire cross-section). Since the maximum x-ray yield occurs for peak values of conduction currents in the vicinity of 100 amperes we find that with i=100 amp, the electron density is greater than $10/cm^3$. As we will see in section #6.3 the runaway current only makes up a small fraction of the total induced current, therefore we should put $\langle v_e \rangle < c$. Since the azimuthal velocity of the bulk of the electrons is very uncertain we will assume that $\langle v_e \rangle \approx 1/10\, c$. With this assumption the electron density during the acceleration cycle is in the neighborhood of $10^{11}/cm^3$. This is the value of electron density that we will use in all future discussions. This assumption may not be as bad as it seems at first because collective electronic processes usually involve the plasma frequency ω_p which depends on $n_e^{1/2}$.

The possibility of measuring the electron density during the acceleration cycle using double Langmuir probes will be discussed in section #6.6.

6.2 Electron Temperature

The electron temperature in the R-F excited plasma was determined from the i-v characteristic of the double probe date. The measured T_e was approximately 20 e.v. at an initial argon pressure of 5×10^{-4} mm Hg. This temperature seems to be much too large and could result from either the poor sampling of the electron population or from the interpenetration of the probe sheaths. Therefore we have assumed that the initial electron temperature is $\approx$ 10 e.v. and that it is also 10 e.v. at the start of each of the successive half cycles of the betatron field.

6.3 The Runaway Current

The runaway current is a very important piece of data in this experiment. With a knowledge of the runaway current we can determine the total number of runaways, therefore the beam plasma frequency, and the relative efficiency of runaway production. The Rogowsky coil that is wrapped around the vacuum chamber measures the total current that is flowing through the chamber. This current is composed of two parts; a conduction current (resistive) and a runaway current (inductive). One hopes in an experiment such as this, that the runaway current will indicate its presence by a sudden dip in the total current when x-ray emission starts (ie, the energetic runaway electrons generate x-rays at the vacuum chamber wall). This will certainly be true if the runaway current is a substantial fraction of the total current. Unfortunately the runaway current in this experiment has been too small to be detected easily by means of the Rogowsky coil, (the minimum current we can detect is $\approx$ 10 amp.). Therefore we have had to obtain the numerical value of the runaway current from x-ray data. One important step in this procedure is the measurement of the azimuthal variation of the x-ray emission. Fig.#15-18 show the scintillator pulse height versus peak conduction current for four different azimuthal positions of the detector.

The position of the collimating lens was chosen so that the scintillator would view only one quadrant of the acceleration chamber at a time. Because of the considerable variation in the scintillator pulse height from discharge to discharge, no attempt was made to plot the x-ray signal verses the measured peak current, but instead all the scintillator signals that corresponded to currents within a 10 ampere interval were plotted on the same ordinate (at the center of the interval).

The variation in scintillator signal from discharge to discharge does not necessarily mean that the number of runaway electrons is fluctuating by the same amount. A limited number of experiments were performed with two counters, each one viewing a different position of the acceleration chamber. Again there was variation in the signals from each counter, but there was no correlation between the pulse heights, ie., if one counter had a large signal there might have been zero signal on the other and vice-versa. Because of this type of variation in the x-ray output from different positions of the vacuum chamber, we will assume that the average scintillator signal at any position will be representative of the x-ray flux from that position. As we can see from Figs.#15-18 the x-ray emission varies about a factor of two around the vacuum

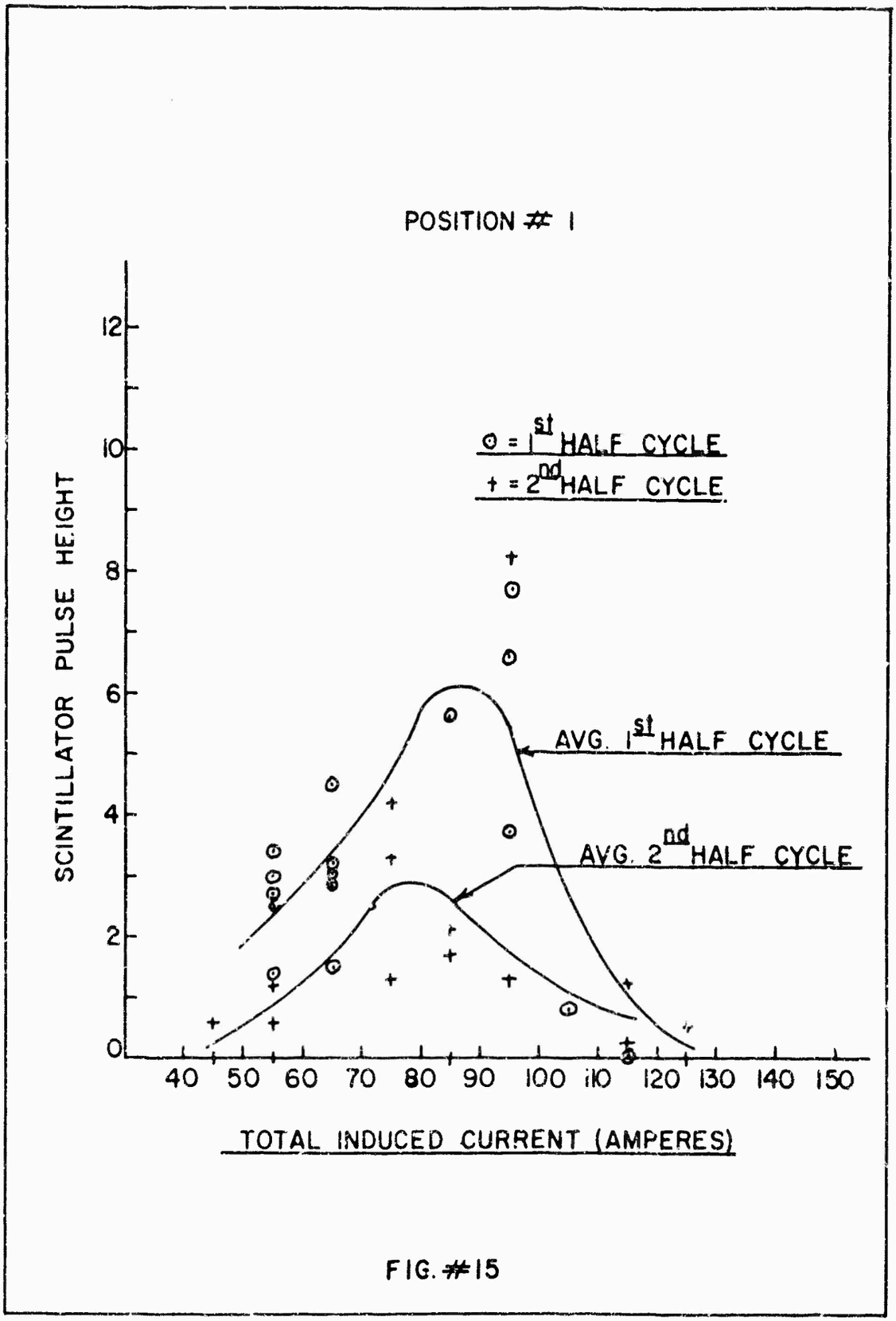
POSITION # 1
SCINTILLATOR PULSE HEIGHT
0
2
4
6
8
10
12
⊙ = 1st HALF CYCLE
+ = 2nd HALF CYCLE
AVG. 1st HALF CYCLE
AVG. 2nd HALF CYCLE
40 50 60 70 80 90 100 110 120 130 140 150
TOTAL INDUCED CURRENT (AMPERES)

FIG. #15

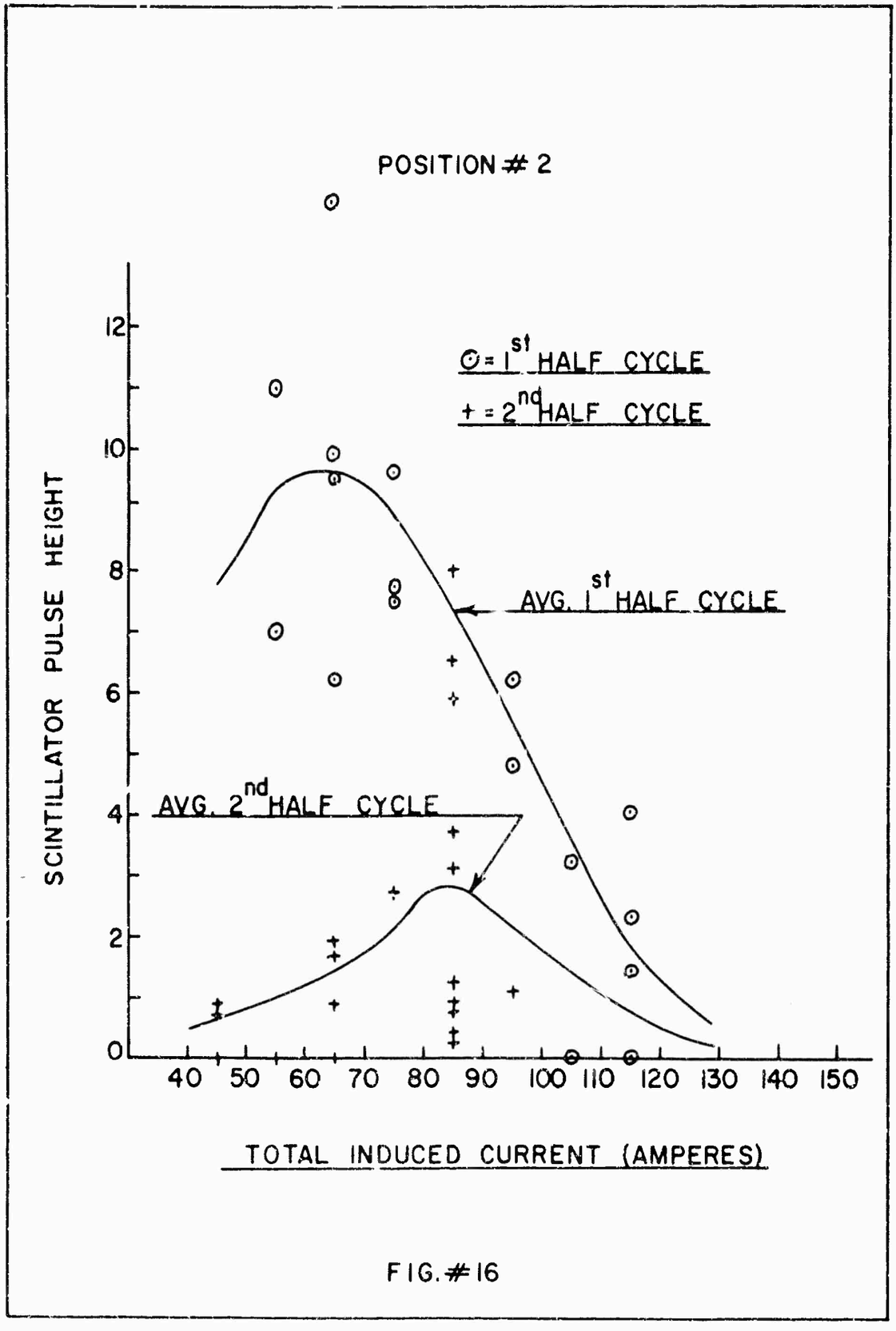
POSITION # 2
⊙ = 1st HALF CYCLE
+ = 2nd HALF CYCLE
AVG. 1st HALF CYCLE
AVG. 2nd HALF CYCLE
SCINTILLATOR PULSE HEIGHT
0
2
4
6
8
10
12
40 50 60 70 80 90 100 110 120 130 140 150
TOTAL INDUCED CURRENT (AMPERES)

FIG. # 16

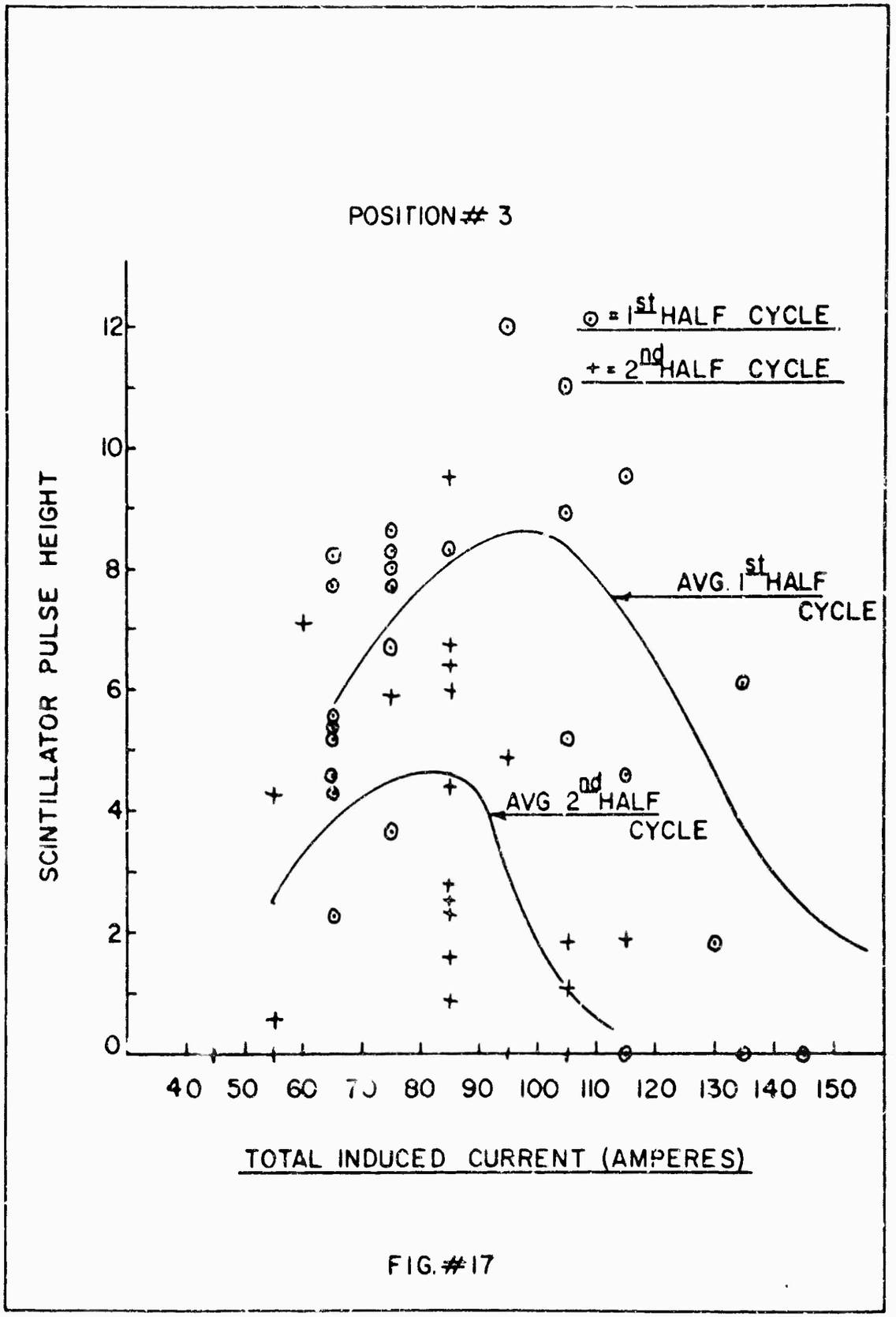
POSITION # 3
⊙ = 1st HALF CYCLE
+ = 2nd HALF CYCLE
AVG. 1st HALF CYCLE
AVG 2nd HALF CYCLE
SCINTILLATOR PULSE HEIGHT
0
2
4
6
8
10
12
40 50 60 70 80 90 100 110 120 130 140 150
TOTAL INDUCED CURRENT (AMPERES)

FIG. #17

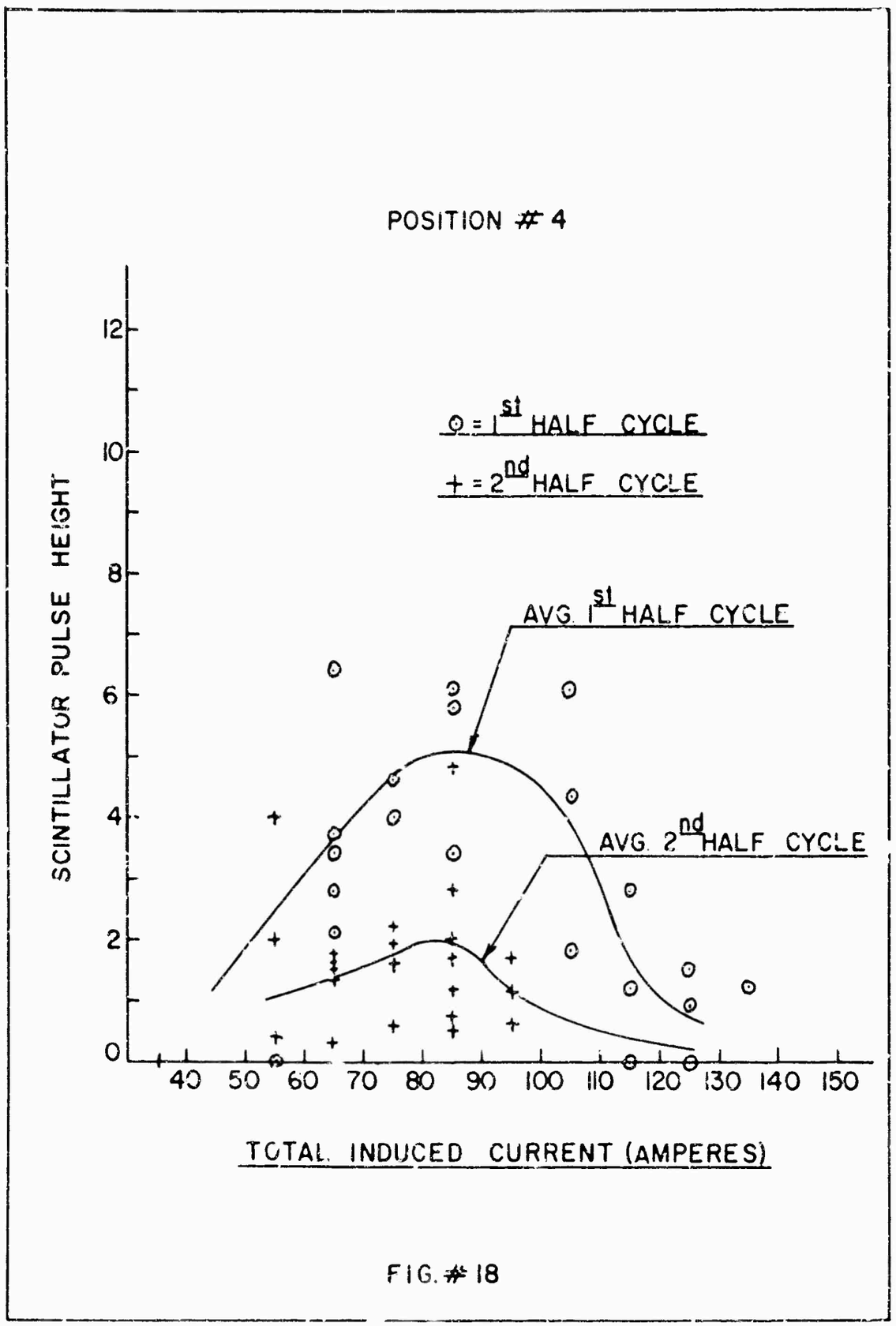
POSITION # 4
⊙ = 1st HALF CYCLE
+ = 2nd HALF CYCLE
AVG. 1st HALF CYCLE
AVG. 2nd HALF CYCLE
SCINTILLATOR PULSE HEIGHT
0
2
4
6
8
10
12
40
50
60
70
80
90
100
110
120
130
140
150
TOTAL INDUCED CURRENT (AMPERES)

FIG. # 18

chamber. Since there is no azimuth at which x-ray emission is extremely pronounced we will assume that it is uniform. Then the number of photons N that correspond to a scintillator pulse height (Ph) is given by

$$N = (Ph)\,\psi_o^{-1}\,\varepsilon^{-1}\,G^{-1} \qquad (7)$$

where ψ_0 is the counter response (pulse height for a single photon of a given energy), ε is the counter efficiency and G is a geometry factor (essentially the solid angle subtended by the scintillating crystal).

The counter efficiency ε was determined with a calibrated radio-active source (N_a^{22}, 100-101 uc,2/26/63). The counting rate versus pulse height for two different source to counter distances is shown in Fig.#19. Since the 1.28 mev x-ray peak occurs at a pulse height of 1.4 volts, the counter response ψ_0 =0.41 v/375kev photon(the scintillating crystal was thallium activated sodium iodide whose response to photons is linear with energy).

We observe that the counting rate for the 1.28 mev line for the two different source to counter distances does not behave as $1/r^2$. The ratio of the counting rates is approximately 3 whereas it should be 4 if the $1/r^2$ law were followed. We believe that this discrepancy is due to a too low discriminator level in the pulse height analyzer.

Since this error will be small compared to other errors that will be made in determining the runaway current we will neglect it.

The counter efficiency ϵ is defined as the ratio of the counting rate to the rate at which x-rays are incident on the scintillating crystal. The number of x-rays from the Na_a^{22} source that are incident on the crystal is

$$N_i = \frac{(\pi D^2/4)}{4\pi x^2} I_0 \exp\left[-0.69\, t/\tau_{1/2}\right] \qquad 6.8$$

where D is the diameter of the crystal (1.75"), x is the crystal to source distance (6"), I_0 is the original source streng . (100-101 u c), $\tau_{1/2}$ is the half life of the source (2.6 years for Na_a^{22}) and t is the time at which the calibration is performed. If we insert these numbers into equation #6.8 we find that

$$N_i = \frac{(1.75)^2}{16\,(6)^2} \times 10^2 \times 3.7 \times 10^{10} \times 10^{-6}\, e^{-\frac{1.58}{8.76}}$$

$$N_i = 1.3 \times 10^4$$

Since only 25.8% of the incident γ -rays are stopped in the crystal

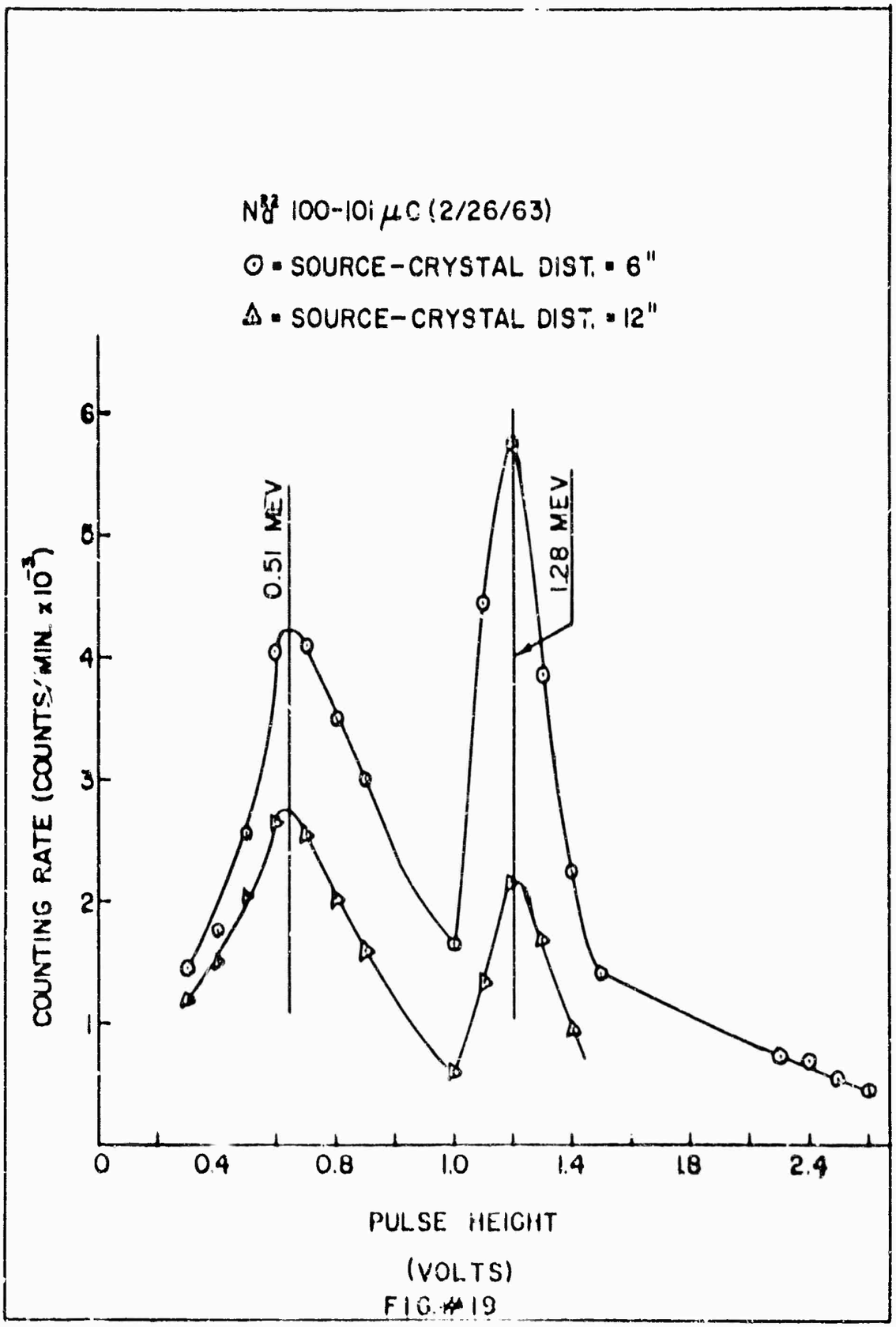
Na^{22} 100-101 μC (2/26/63)
⊙ = SOURCE-CRYSTAL DIST. = 6"
△ = SOURCE-CRYSTAL DIST. = 12"
0.51 MEV
1.28 MEV
COUNTING RATE (COUNTS/MIN. x 10^{-3})
6
4
2
0
0.4
0.8
1.0
1.4
1.8
2.4
PULSE HEIGHT
(VOLTS)
FIG. #19

BLANK PAGE

$$N_\lambda = 3.36 \times 10^{3} \text{ } \gamma \text{ rays/sec at 1.28 mev}$$

from Fig.#19 the counting rate at 1.28 mev(pulse height of 1.4 volts) is 5600 counts/min or 93 counts/sec, therefore the counter efficiency is

$$\varepsilon = \frac{93}{3.36 \times 10^{3}} = 2.77 \times 10^{-2}$$

The geometrical factor G is just the fractional solid angle subtended by the crystal.

$$G = \frac{\pi D^2/4}{4\pi R^2} \qquad 6.9$$

where R is now the distance from the crystal to the vacuum chamber (a more elaborate calculation, which takes the finite size of the acceleration chamber into account changes the G value from eq.6.9 by only 5%). Thus

$$G = \frac{(1.75)^2}{16\ (17.26)^2} = 6.4 \times 10^{-4}$$

Finally for a pulse height of 50 volts (375 kev photons) the number of x-rays generated at the vacuum

chamber wall is

$$N = (50)(.41)^{-1}(2.71\times10^{-2})^{-1}(6.4\times10^{-4})^{-1}$$

$$N = 0.7\times10^{7} \quad \text{photons}$$

Now all we need do to obtain the number of runaway electrons that correspond to N photons, is to determine the efficiency of x-ray production by the electrons.

The long succession of gradually improving theories of bremsstrahlung has dealt almost exclusively with the thin target case. Here one calculates the radiation expected from a collimated beam of mono-energetic electrons while passing through a target which is so thin that the electrons lose no appreciable energy by ionization, suffer no significant elastic deflections, and suffer only one radiative collision. The thick target case, although far less adequately covered by theory because of its complexity, is nevertheless the usual laboratory situation. In this experiment we will assume that the x-radiations detected with the scintillation counter are produced via thick target bremsstrahlung.

The average bremsstrahlung energy emitted in an element of path length ds is[34]

$$(dT)_{RAD} = \left(\frac{dT}{ds}\right)_{RAD} ds = \frac{\left(\frac{dT}{ds}\right)_{RAD}}{\left(\frac{dT}{ds}\right)_{ION.} + \left(\frac{dT}{ds}\right)_{RAD.}} dT \qquad 6.10$$

where $\left(\frac{dT}{ds}\right)_{RAD.}$ is the energy lost per cm via bremsstrahlung and $\left(\frac{dT}{ds}\right)_{ION.}$ is the energy lost per cm via ionization. The average energy I radiated by an electron of initial energy T in being stopped is

$$I = \int_0^T \frac{(dT/ds)_{RAD.}}{\left(\frac{dT}{ds}\right)_{ION.} + \left(\frac{dT}{ds}\right)_{RAD.}} dT \qquad 6.11$$

Integration using the theoretical values of radiative and ionization losses is valid only over the portion of the path for which the electrons velocity is large compared with the velocity of the atomic electrons. In most cases, the integration must be performed graphically because of the complicated form of $\left(\frac{dT}{ds}\right)_{ION.}$ and $\left(\frac{dT}{ds}\right)_{RAD.}$.

The spectral distribution of thick target bremsstrahlung from non-relativistic electrons[34] can be thought of as the sum of the contributions from a number of thin target cases of various electron energies as

shown in Fig. #20

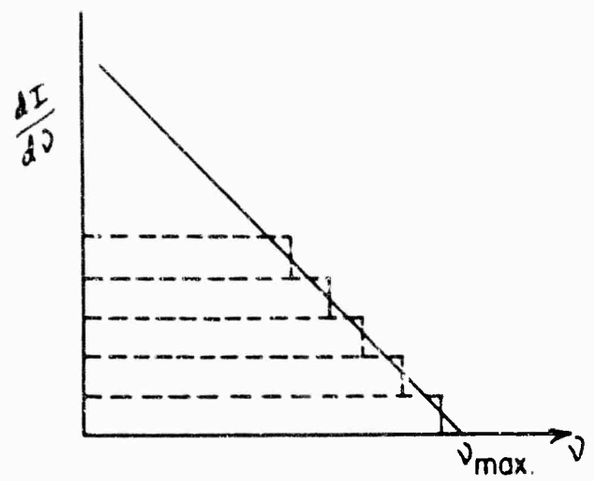

FIG.# 20

The total energy per frequency interval $dI/d\nu$ is proportional to $Z\ (\nu_{max.} - \nu\ )$, ie,

$$dI = \text{CONST.}\ Z\ (\nu_{MAX.} - \nu)\, d\nu \qquad 6.12$$

If eq. 6.12 is integrated over all frequencies from $\nu=0$ to $\nu_{MAX} = T/h$(h=Planck's constant), we find for the total bremsstrahlung energy I, in mev per incident electron

$$I = k Z E^2 \qquad 6.13$$

No simple dependence of the x-ray intensity in any given direction on Z and E is found experimentally.[34] The total bremsstrahlung integrated over all angles is found to be proportional to Z, within the accuracy of measurement, and also to be proportional to E^2 within $\pm$ 10 percent, in agreement with eq. 6.13.

The numerical value of the constant k is known only approximately, the values ranging between 0.3 and 1.1×10^{-3} $(mev)^{-1}$. Following Evans[34] we will assume that

$$I = 0.7 \times 10^{-3} Z E^2 \qquad 6.14$$

(I and E in mev). Thus the fraction of the incident electrons energy which is converted to bremsstrahlung in a thick target is approximately

$$\frac{I}{E} = 0.7 \times 10^{-3} Z E$$

For glass (S_i O_2), the effective Z is 10. Therefore 375 kev electrons lose 0.26% of their energy via bremsstrahlung. Finally, the number of runaway electrons that correspond to the flux of 7×10^7 photons is

$$N_e = \frac{.7 \times 10^7}{2.6 \times 10^{-3}} = .27 \times 10^{10}$$

The runaway current is (typical)

$$i = \frac{.27\times10^{10}\times1.6\times10^{-19}}{2\pi\,(1.9\times2.54)\times10^{-2}} \times 2.7\times10^{8}$$

$$i = 0.36 \text{ AMP.}$$

As we have just seen the total runaway current is quite small. This result is consistant with our Rogowsky coil measurements. One can obtain greater sensitivity with the Rogowsky coil if one measures di/dt instead of the current i. This was not done in the first place because the di/dt signals become very difficult to interpret as soon as the current waveform has some high frequency structure on it. A further complication arises because of the noise signal that is generated by the B_z and B_θ fields. In our situation the signals generated by this pickup was approximately 30 times greater than the signal from the plasma current. The pickup from the B_z and B_θ fields is easier to eliminate if all the signals are integrated.

Although there were only two stray magnetic fields present, three distinct signals had to be removed from the Rogowsky coil circuit, ie., the signals from B_z and B_θ, and the signal from the current that was induced in the B_θ coil driving circuit by the time varying

B_z field. The latter signal, which should have been proportional to B_z, was distorted by the large capacity (140 uf) present in the Type "C" network. The effect of this signal was eliminated by placing in series with the B_θ coils, a back-winding which linked flux from B_z. Signals from pick-up loops that linked flux from B_z and B_θ separately, were integrated and fed in parallel into one channel of a Tektronix Type Z differential preamplifier. Each integrating network had in addition to the usual integrating resistor R, a small variable resistor in series with R, so that the attenuation could be varied by a small amount. The integrated signal from the Rogowsky coil was then applied to the other channel of the preamp. and the difference taken. The amount of flux linking the two auxillary coils was changed until the effects of B_z and B_θ on the difference signal was almost completely eliminated. Changing the integration time constant with the variable resistor helped to make the cancellation better. The cancellation cannot be made complete because the pick-up loops are not the same electrically and therefore introduce some distortion. In this manner the signals from the stray fields were reduced so that plasma currents as small as 10 amp. could be detected.

As we have just seen typical runaway currents were of the order of one amp. therefore too small to be observed on the Rogowsky coil current trace. Since the plasma current turned out to be a fairly smooth function of time any small kink in the current would be magnified on the di/dt signal. Rather than going through the complicated process of eliminating pick-up, the Rogowsky coil signal was differentiated electronically and then displayed on the C.R.O. screen. The Type Z amplifier was plugged into a portable preamp. power supply. The output from the Type Z , (the plasma current), was then differentiated with a Tektronix Type "O" operational amplifier. Displaying di/dt instead of i also failed to reveal the runaway current. Since the peak x-ray emission occurs at plasma conduction currents of 80-100 amperes. the failure to observe a runaway current of only one amp. is not surprising.

6.4 X-Ray Measurements

The most extensively studied parameter in this experiment has been "t_x" the x-ray emission time. "t_x" is defined as the time delay between the start of the betatron acceleration cycle (ie, when B_3 goes through zero) and the on-set of x-ray emission. It is important that this quantity be measured accurately so that the effects of varying the other experimental parameters can be determined. The x-ray detector (Na-I crystal, RCA 6810-A photo-multiplier) was designed with enough gain so that the start of the scintillator pulse could be made unambiguous. Thus a good measurement of "t_x" now only required that the zeroes of the betatron field be measured accurately. All the difficulties associated with measuring the zeroes of an integrated $d\phi_3/dt$ signal or with measuring the positions of the maxima on a $d\phi_3/dt$ signal are eliminated if one uses a peaking strip probe[35] placed in the fringing field to measure the zeroes of B_3. The peaking probe consists of a few turns of copper wound on a short length of Mo-permalloy wire. The Mo-permalloy wire saturates at only few orsteds of total field. Thus if the peak time varying fields are large a very precise measurement of the zero of the total field can be made.

The output pulse from the peaking strip probe

used for these measurements has a full width at half maximum of $\approx$ 0.05 μ sec so that the position of the peak could be determined to within $\approx \pm$ 0.02 μ sec. The scintillator signal was extrapolated back to zero and its displacement from the peaking strip maximum was measured on a photograph of the CRO trace with a calibrated steel scale and magnifying glass. A typical scintillator and peaking strip signal is shown in Fig.#21. The total error associated with measuring "t_π" is believed to be approximately $\pm$ 0.03 μ sec.

Since the peaking probe measures the zero of the total field care must be taken to make sure the stray field from the B_θ coils does not have any effect on the probe. The position of the peaking strip pulse relative to the start of the oscilloscope trace was measured with $B_\theta \approx 5000$ gauss and $B_\theta = 0$ using the measuring techniques just described. The peak betatron field was varied over all of the values used for x-ray measurements. No systematic differences between the B_θ =5k gauss and B_θ =0 conditions was observed. Thus we conclude that the B_θ field has no effect on the peaking strip signal, within the accuracy of our measurements.

UPPER TRACE = TOTAL INDUCED CURRENT 110 amp/cm
SWEEP = 2×10^{-6} sec./cm. BRIGHT PORTION INDICATES DURATION OF LOWER TRACE.

LOWER TRACE = PEAKING STRIP SIGNAL AND SCINTILLATOR SIGNAL.
SWEEP = 5×10^{-7} sec./cm

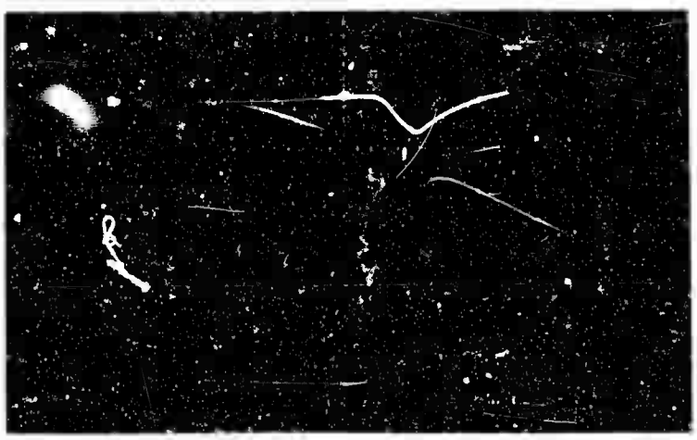

TIME ⟶

PEAKING STRIP SCINTILLATOR

TYPICAL SIGNALS

FIG. #21

6.5 X-Ray Absorption Measurements

The x-ray energies indicated in Figs.#27-33 were obtained from the value of the betatron magnetic field at the orbit at "t_x", the time x-ray emission begins, via the relation

$$T = E - m_0c^2 = (p^2c^2 + m_0^2c^4)^{1/2} - m_0^2c^2 \qquad 6.15$$

$$T = \left[(3B_0\rho \sin \omega t_x)^2 + m_0^2c^4\right]^{1/2} - m_0c^2 \qquad 6.16$$

where B_0 is the peak field strength at the orbit in kilo-gauss, ρ is the orbit radius in cm, and ω is the frequency of the betatron field. (the energies T and $m_0 c^2$ in eq.(6.16) are in units of mev). In order to make sure that the x-ray energy does indeed correspond to the electron energy in the betatron field we have made x-ray absorption measurements on both the first and second half cycles. Fig.#22 shows the variation of the scintillator pulse height as a function of absorber thickness on the second half cycle for the conditions indicated. The error flags represent the maximum and minimum of the data points whose average is given by the circles. The slope of the straight line drawn through the points corresponds to a mass absorption coefficient

(μ/ρ) =0.095 cm/gm. The x-ray energy corresponding to this absorption coefficient is 375 kev.[36] With the values of the experimental parameters chosen for these measurements the electron energy in the betatron field at the time the x-ray emission starts is $\approx$ 350 kev.

Since there is considerable variation in the data from the absorption measurements the two energies must be considered to be in agreement.

On the first half cycle of the betatron field interpretation of the absorption data is not as easy as it was for the second half cycle. The scintillator pulse height vs. absorber thickness on the first half cycle is also shown in Fig.#22. The slope of the straight line through the points corresponds to a mass absorption coefficient (μ/ρ) =0.58 cm/gm. The x-ray energy that gives this absorption coefficient is 40 kev. The electron energy determined from t_x and B_o via. eq.#(6.16) is 80 kev, and hence, differs from the absorption measurement energy by a factor of two.

No meaning full error flags can be placed on the 1st half cycle data because of the large fluctuation in the x-ray output from shot to shot. Signals with zero or very small x-ray pulses were observed as often as substantial ones so that the deviations from the average are as large

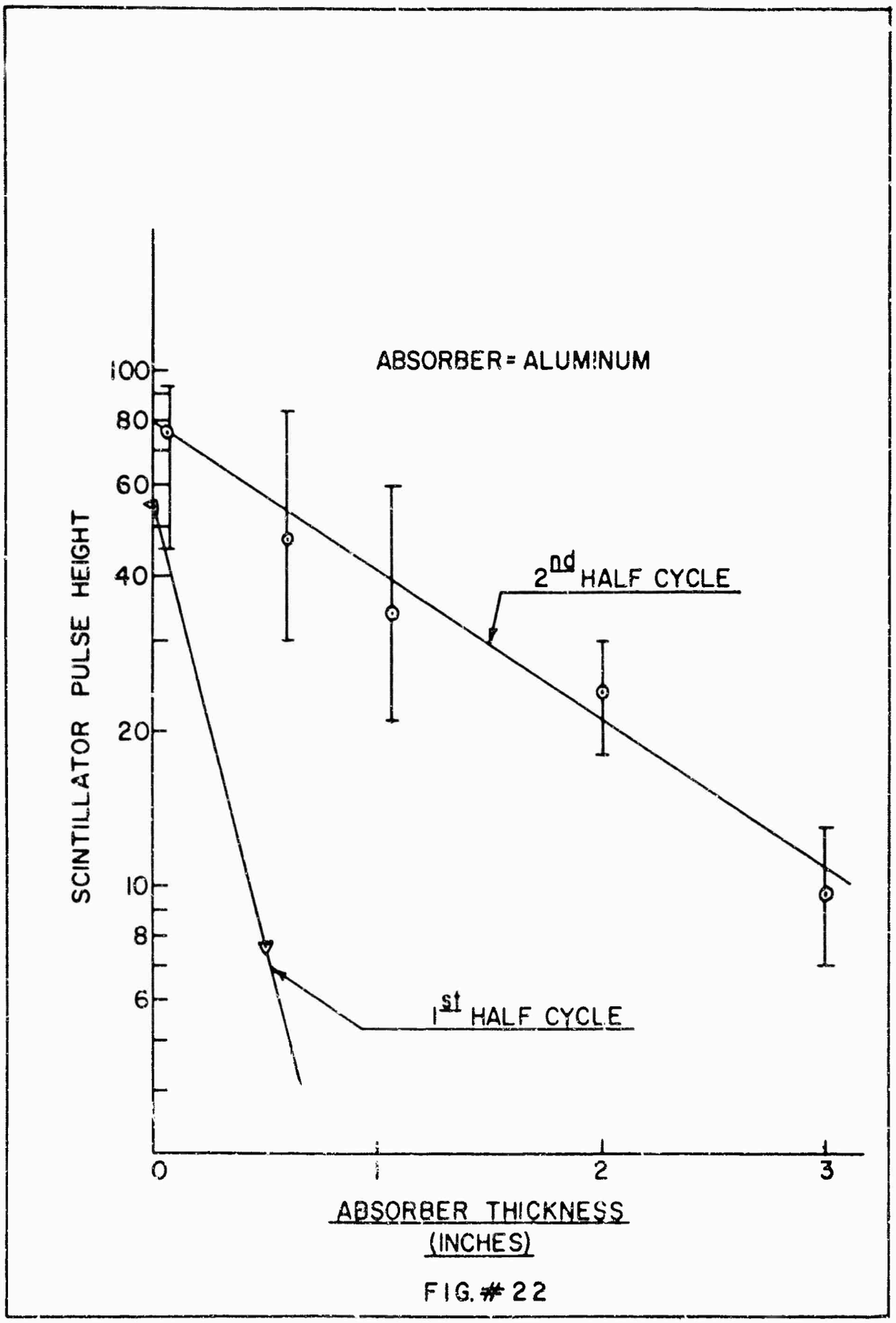
ABSORBER = ALUMINUM
SCINTILLATOR PULSE HEIGHT
100
80
60
40
20
10
8
6
2nd HALF CYCLE
1st HALF CYCLE
0
1
2
3
ABSORBER THICKNESS
(INCHES)

FIG. # 22

as the average. Therefore the measured peak x-ray energy is consistant with the electron energy in the betatron field.

Summary

The measured peak x-ray energy is consistant with the energy the runaway electrons would have attained if they had undergone continuous betatron acceleration during the time "t_{π}". Therefore the runaway electrons were produced by the betatron electric field rather than by the electric field associated with an instability that might have developed during the discharge.

6.6 Electric Field Measurements

Prelimenary measurements were made of the radial and azimuthal electric fields that develop during the acceleration cycle. The fields were determined by inserting into the acceleration chamber two pairs of double probes. The probes were made from 0.025" dia. copper wire separated approximately 0.075"(the Debye length $\lambda_D \approx .003"$). D.C. isolation between the probes and the oscilloscope was accomplished by means of a pulse transformer with a 4:1 turns ratio. A 150 ohm resistor was connected across the pulse transformer secondary so that the primary impedance was $\approx$ 2400 ohms. The Debye length $\lambda_D \ll$ probe separation, and the probe impedance is high, therefore the secondary signal will be just the potential difference between the probes. A typical electric field signal together with the total induced current is shown in Fig.#37. Because of excessive noise generated by the capacitor bank discharge all electric field measurements were made on the 2nd half cycle of the betatron field. Radial electric fields as large as 1000 v/cm have been observed. Peak values of the azimuthal field are very much less than this, typically 50-100 v/cm. It is possible that the azimuthal field probes are in reality measuring a radial electric field because of mechanical mis-alignment, therefore we will focus all of

our attention on the radial field measurements. Data were taken at several radial positions in the acceleration chamber and for both values of $\int$ but for only one value of peak betatron field, B_θ , and ion mass.

The effect of the probe is to decrease the total induced current from the no probe condition. The x-ray emission time was also measured with the probe in place and found to be the same as it was without the probe.

By connecting the primary of the pulse transformer as sketched below it is possible in principle to make ion density measurements during the pulsed discharge.

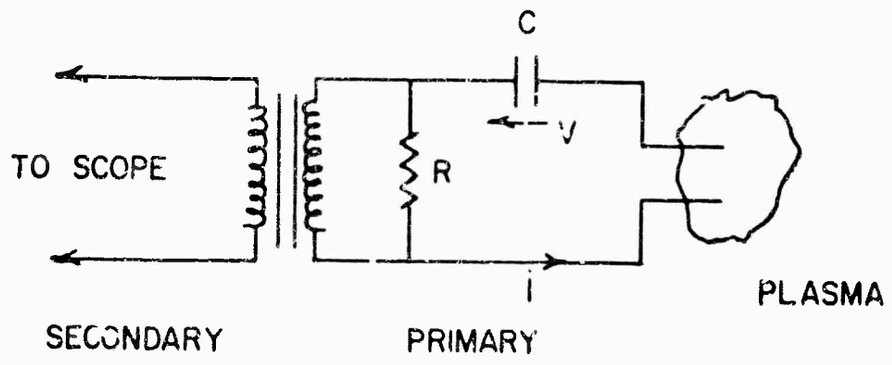

The values of R and C must be chosen so that $RC >> \tau$, the duration of the plasma signal. The value of R must also be chosen so that $Ri \ll V$ the voltage on the capacitor. The maximum value of R that could be conveniently used was $\approx$ 1 ohm. Even with this low value of R no clear interpretation of the data could be made.

VII RESULTS AND ANALYSIS OF X-RAY EMISSION TIME.

The results of the measurements of the x-ray emission time "t_x" are plotted in Figs. #23 to 26. The electron energy in the betatron field at "t_x" is shown in Figs. #27 to 33. The error flags represent the maximum and minimum deviation from the average at each point. On both the first and second half cycles of the betatron field we find that the x-ray emission time decreases as the induction electric field, increases. All the data are presented with B_θ as a parameter. The value of "t_x" at a given E_θ and γ, increases with the magnitude of B_θ until $B_\theta \approx 4000$ gauss and then seems to be independent of B_θ. It is usually the custom with electron betatrons to extract the accelerated electrons when the magnetic field at the orbit has reached its peak value. This is usually done by distorting the magnetic field shape. The resulting large amplitude betatron oscillations then cause the electrons to move away from their equilibrium orbit and strike a target. In this experiment no external means are used to disrupt the electron acceleration. The energetic electrons strike the vacuum chamber because of internal processes rather than from some externally applied disturbance. There is no x-ray emission for times between the start of the cycle and "t_x". The x-ray emission begins at "t_x" and is most

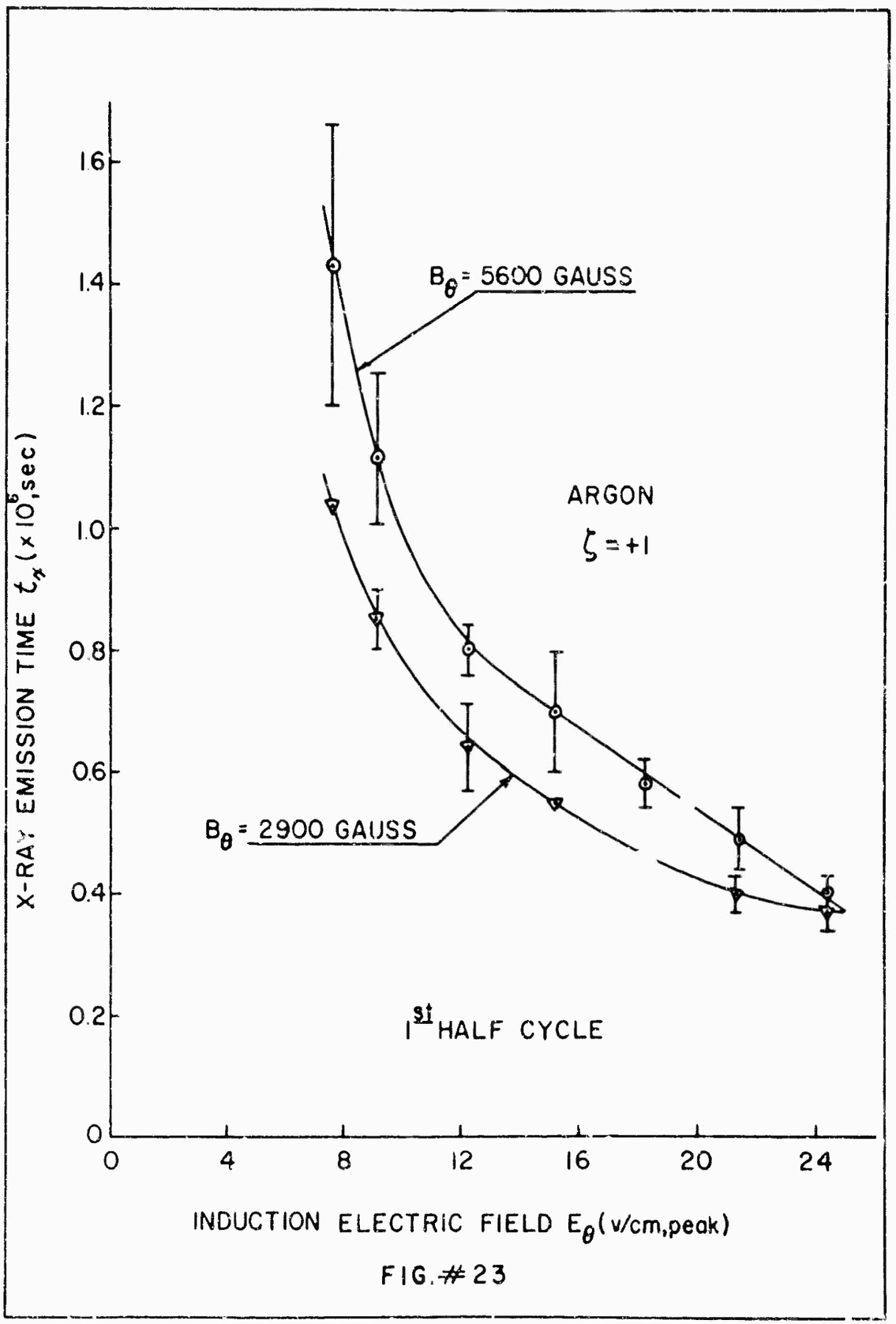
X-RAY EMISSION TIME t_x ($\times 10^6$ sec)
1.6
1.4
1.2
1.0
0.8
0.6
0.4
0.2
0
B_θ = 5600 GAUSS
ARGON
$\zeta = +1$
B_θ = 2900 GAUSS
1st HALF CYCLE
0
4
8
12
16
20
24
INDUCTION ELECTRIC FIELD E_θ (v/cm, peak)

FIG. # 23

BLANK PAGE

the resonance becomes more difficult to find for reasons that are so far unexplained. Because of the large difference between the two density results at high neutral pressure, no extensive investigations were carried out at lower pressures.

An attempt was made to measure the electron density spectroscopically using the method of Inglis and Teller.[29,30] If one examines the broadening of individual lines of a series such as the Balmer series, one finds that the higher members of the series are broadened more than the lower members. Since the higher members of the series are also closer together than the lower members, one eventually reaches a point where the broadening of the lines is comparable to the spacing between them, and at this point the lines in the series merge together and are no longer visible as distinct lines. This process manifests itself in the spectrum as a depression of the series limit and is equivalent to saying that the perturbation of the energy levels due to the Stark effect becomes comparable to the energy difference between two adjacent levels. By equating these two energy terms one can solve for the principle quantum number n_m of the upper level of the last distinct line of the series. The ion density is then given by

$$\log_{10} n_i = 23.26 - 7.5 \log_{10} n_m \qquad 6.4$$

This method has been used sucessfully to determine the ion density in a decaying hydrogen plasma[31] at relatively high ion densities ($10^{15}/cm^3$). At low electron densities ($10^{9}/cm^3$) the upper quantum number n_m of the last line of the series is very large ($\approx$ 90) therefore a spectroscope with large dispersion is required. After the betatron field is turned on the electron (and ion) density increases, the discharge "blooms". It is quite possible that the electron density may reach a value of $10^{12}/cm^3$ during this discharge. At this density $n_m \approx 20$ and hence may be observable without resorting to sophisticated experimental apparatus. Although all of our experiments were done with argon and krypton, helium was used to test this method because of its simpler spectral structure. The spectral lines of interest were from the series $n\,^1D_2 \rightarrow 2\,^1P_1$ (series limit-3679.7 A°). This series was chosen because of its close resemblence to that of Hydrogen,[32] especially at high values of the principle quantum number. The discharge was viewed with a Hilger Medium Quartz Spectrograph (for this experiment a glass

prism was used). The spectrum was recorded on Kodak Type F Spectroscopic plates and developed in Acufine to improve the speed.[33] The experiment proceeded as follows. A plasma was generated using the high frequency quadrupole electric field. The spectroscope shutter was opened manually just prior to the application of the betatron and B_θ magnetic fields, and closed again as soon as possible after the discharge. Although the shutter is open for a period of time considerably longer than the duration of the betatron field, the maximum light intensity occurs during this time. When the spectrum obtained this way is compared with the spectrum from the R -F excited plasma alone, we find additional lines which we believe are due to additional excitation during the pulsed discharge. If the electron density is in the region 10^{10} -$10^{12}/cm^3$ the last distinct line of the series will be in the wave length region between 3757.1 and 3679.1 A°. We observe what appears to be Nitrogen band structure in this wave length region which makes interpretation of the series limit impossible. Spectra were again taken after the R-F discharge had been run for some time, but the results were the same. In order to make the discharge spectroscopically clean it is necessary to run the discharge with the B_3 and B_θ fields, for extended periods of time.

Since this pulse cleaning would have required extensive revision of the electronic controls this was not pursued.

In the preceeding paragraphs we have discussed several attempts to measure the electron density in the R-F excited plasma. The reasons for not obtaining a satisfactory result for the electron density with the various techniques were also discussed. So far no mention has been made of still another experimental parameter from which at least a lower bound on the electron density can be obtained; namely the induced current in the acceleration chamber. The induced current, i measured with the Rogowsky coil wrapped around the vacuum chamber, is related to the electron density via the relation

$$\frac{i}{A} = n_e q \langle v_e \rangle + n_i q \langle v_i \rangle \qquad 6.5$$

were A is the vacuum chamber cross-sectional area and $\langle v_e \rangle$ and $\langle v_i \rangle$ are suitably averaged velocities. Since the electrons are much more mobile than the ions we can assume that they carry all the current; then we have

$$\frac{i}{A} = n_e q \langle v_e \rangle \qquad 6.6$$

If we let $\langle v_e \rangle = C$; the velocity of light, we obtain a lower bound on the electron density (assuming n_e is uniform over the entire cross-section). Since the maximum x-ray yield occurs for peak values of conduction currents in the vicinity of 100 amperes we find that with i=100 amp, the electron density is greater than $10^{10}/cm^3$. As we will see in section #<u>6.3</u> the runaway current only makes up a small fraction of the total induced current, therefore we should put $\langle v_e \rangle < c$. Since the azimuthal velocity of the bulk of the electrons is very uncertain we will assume that $\langle v_e \rangle \approx \frac{1}{10} c$. With this assumption the electron density during the acceleration cycle is in the neighborhood of $10^{11}/cm^3$. This is the value of electron density that we will use in all future discussions. This assumption may not be as bad as it seems at first because collective electronic processes usually involve the plasma frequency ω_p which depends on $n_e^{1/2}$.

The possibility of measuring the electron density during the acceleration cycle using double Langmuir probes will be discussed in section #<u>6.6</u>.

6.2 Electron Temperature

The electron tempe

plasma was determined from t

double probe date. The meas

20 e.v. at an initial argon

This temperature seems to be

result from either the poor

population or from the inter

sheaths. Therefore we have

electron temperature is $\approx$

10 e.v at the start of each o

of the betatron field.

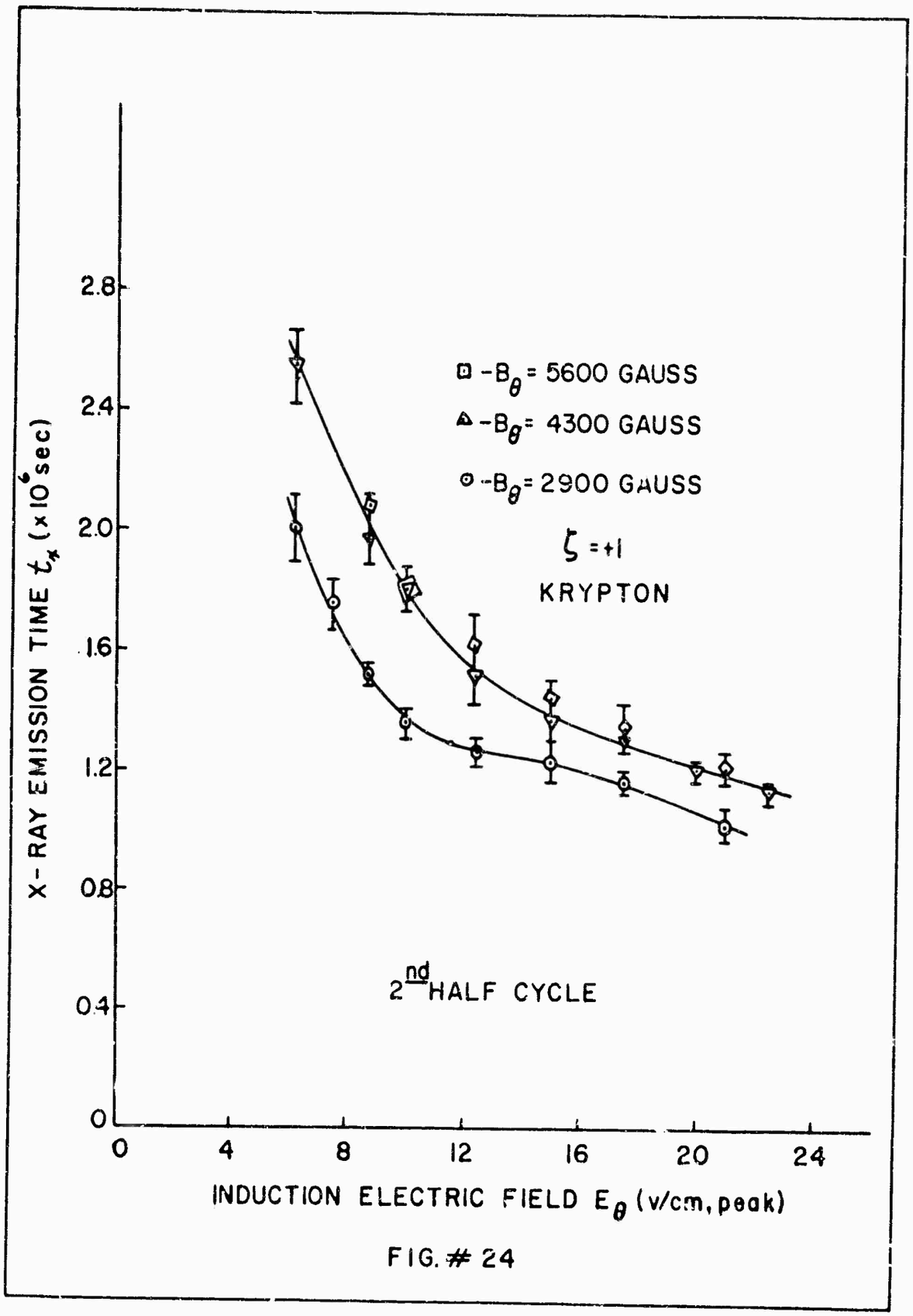
X-RAY EMISSION TIME t_x (x10^{6}sec)
2.8
2.4
2.0
1.6
1.2
0.8
0.4
0
0
4
8
12
16
20
24
INDUCTION ELECTRIC FIELD E_θ (v/cm, peak)
$-B_\theta$ = 5600 GAUSS
$-B_\theta$ = 4300 GAUSS
$-B_\theta$ = 2900 GAUSS
ζ = +1
KRYPTON
2nd HALF CYCLE

FIG. # 24

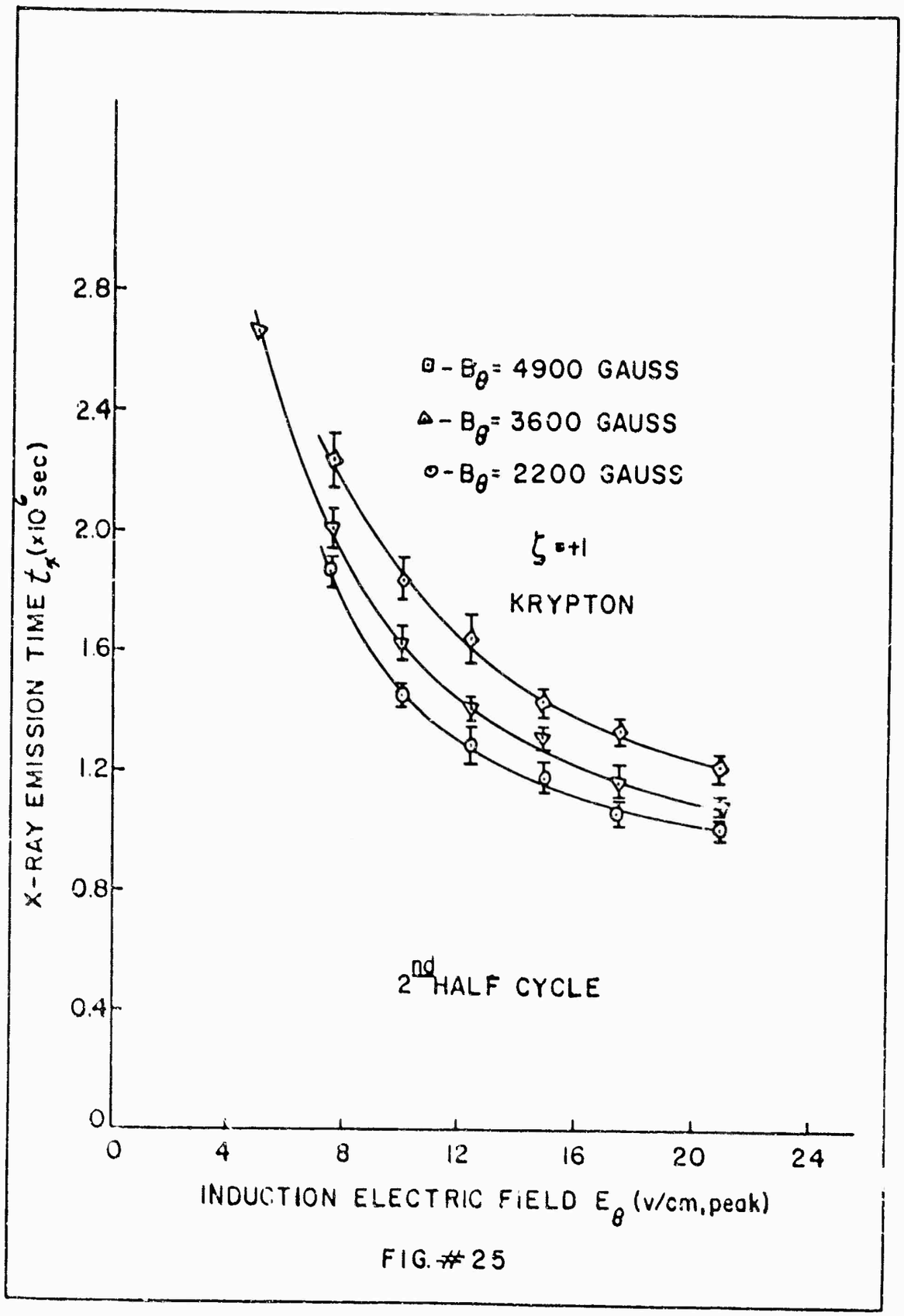
X-RAY EMISSION TIME t_x ($\times 10^{-6}$ sec)
2.8
2.4
2.0
1.6
1.2
0.8
0.4
0
0
4
8
12
16
20
24
INDUCTION ELECTRIC FIELD E_θ (v/cm, peak)
□ - B_θ = 4900 GAUSS
△ - B_θ = 3600 GAUSS
○ - B_θ = 2200 GAUSS
ζ = +1
KRYPTON
2nd HALF CYCLE

FIG. # 25

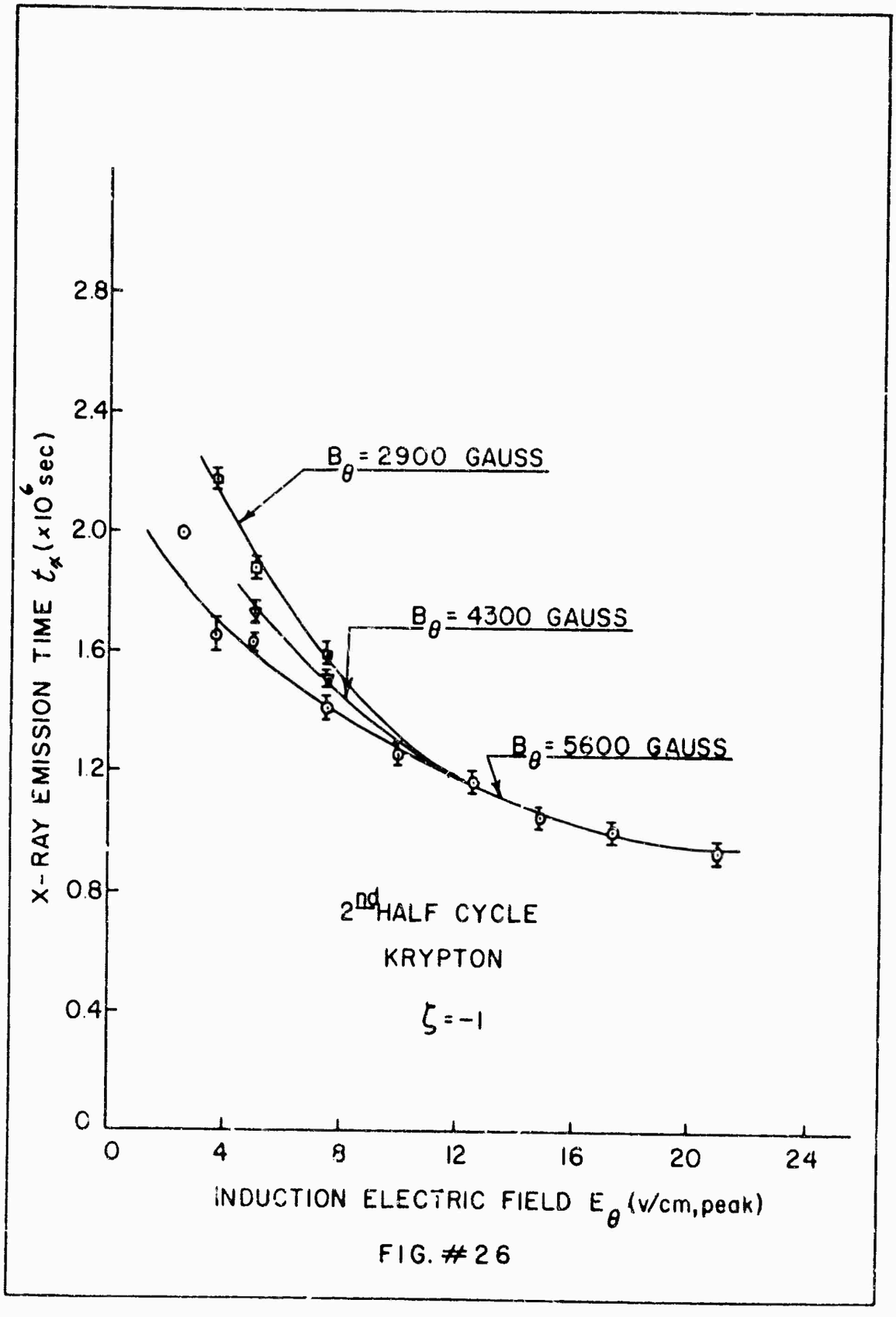
X-RAY EMISSION TIME t_x (x10^6 sec)
2.8
2.4
2.0
1.6
1.2
0.8
0.4
0
B_θ = 2900 GAUSS
B_θ = 4300 GAUSS
B_θ = 5600 GAUSS
2nd HALF CYCLE
KRYPTON
$\zeta = -1$
0
4
8
12
16
20
24
INDUCTION ELECTRIC FIELD E_θ (v/cm, peak)

FIG. #26

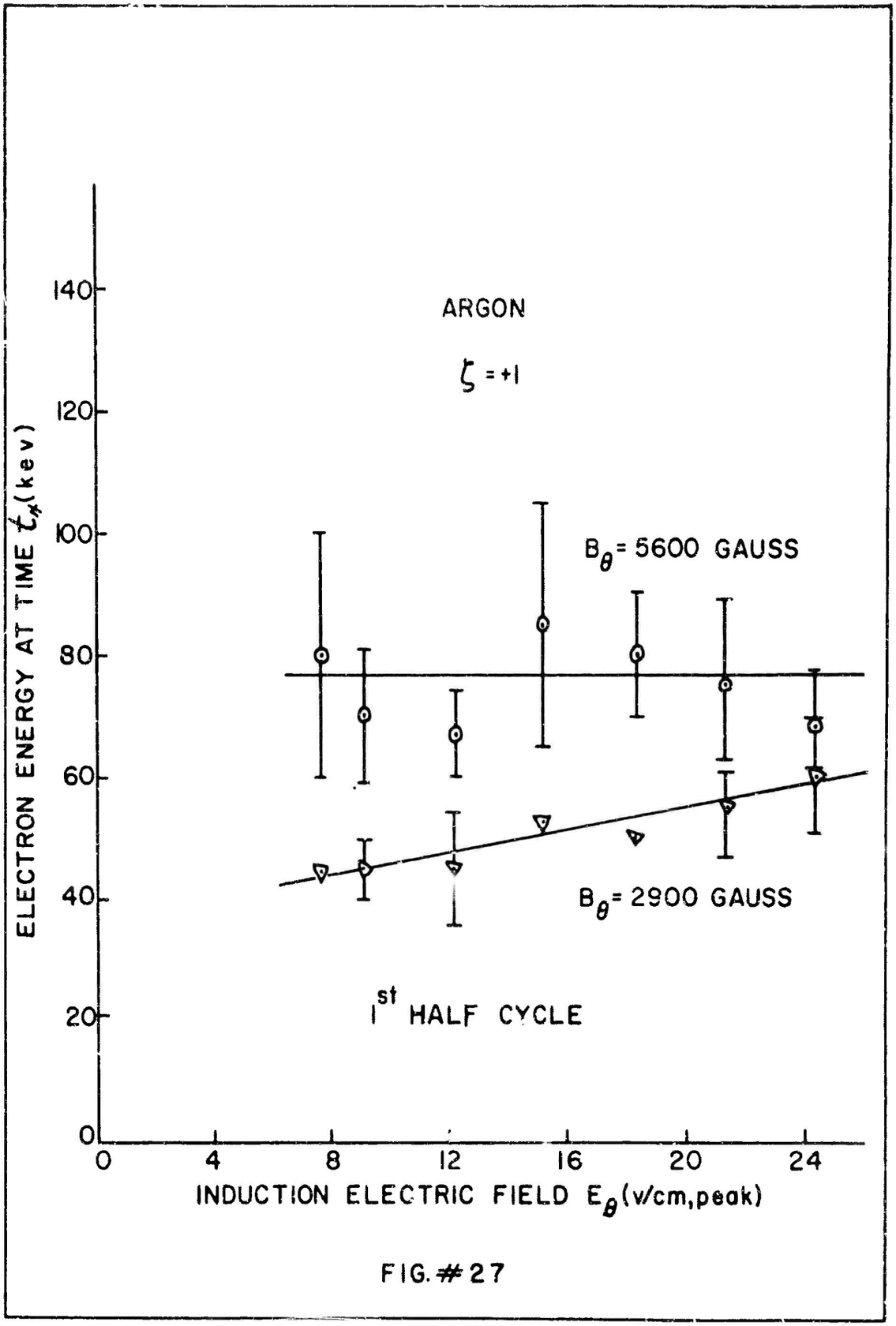
ARGON
ζ = +1
B_θ = 5600 GAUSS
B_θ = 2900 GAUSS
1st HALF CYCLE
ELECTRON ENERGY AT TIME t_x (kev)
INDUCTION ELECTRIC FIELD E_θ (v/cm, peak)
0
20
40
60
80
100
120
140
0
4
8
12
16
20
24

FIG. # 27

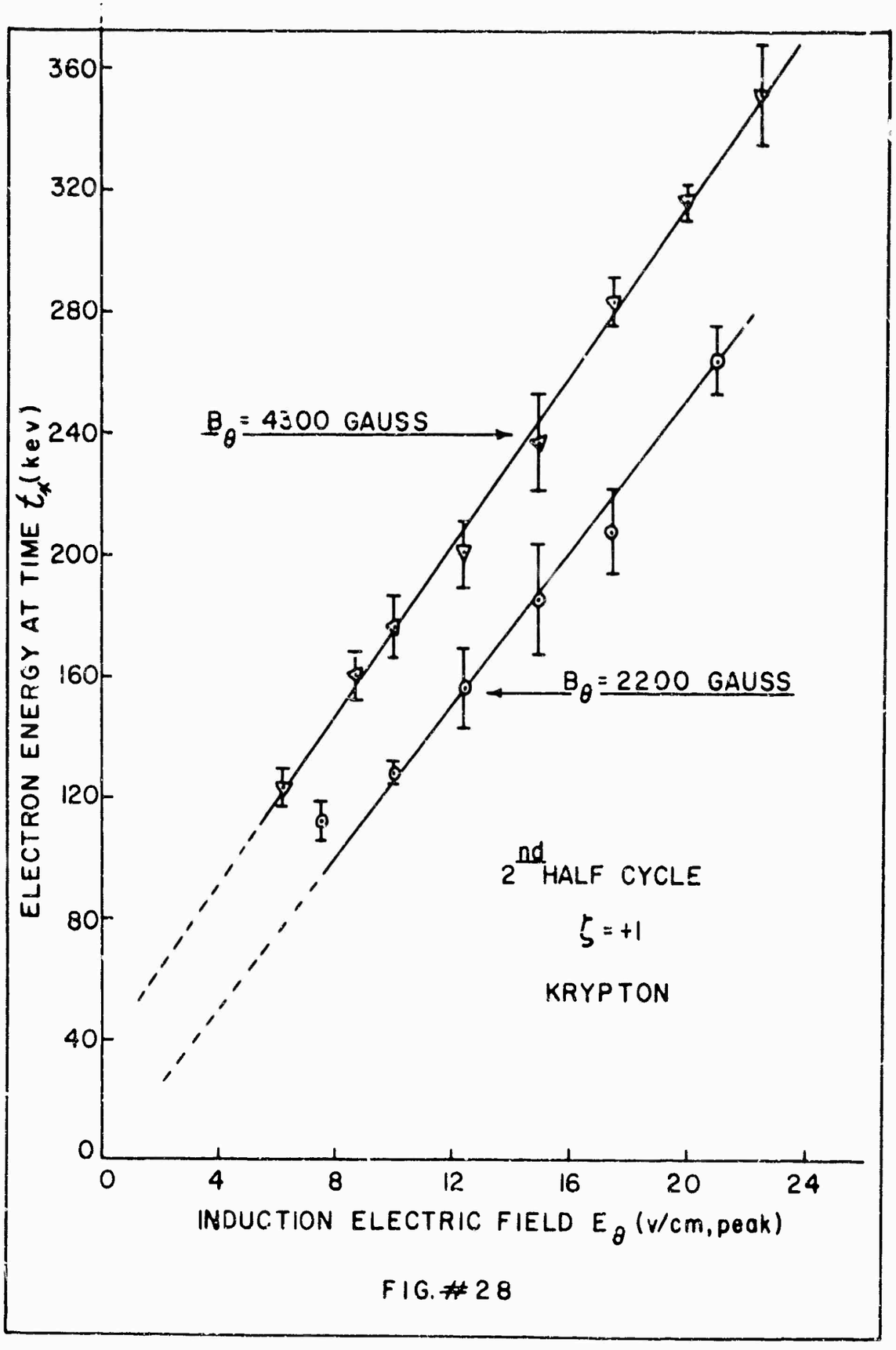
360
320
280
240
200
160
120
80
40
0
ELECTRON ENERGY AT TIME t_x (kev)
B_θ = 4300 GAUSS
B_θ = 2200 GAUSS
2nd HALF CYCLE
ζ = +1
KRYPTON
0
4
8
12
16
20
24
INDUCTION ELECTRIC FIELD E_θ (v/cm, peak)

FIG. # 28

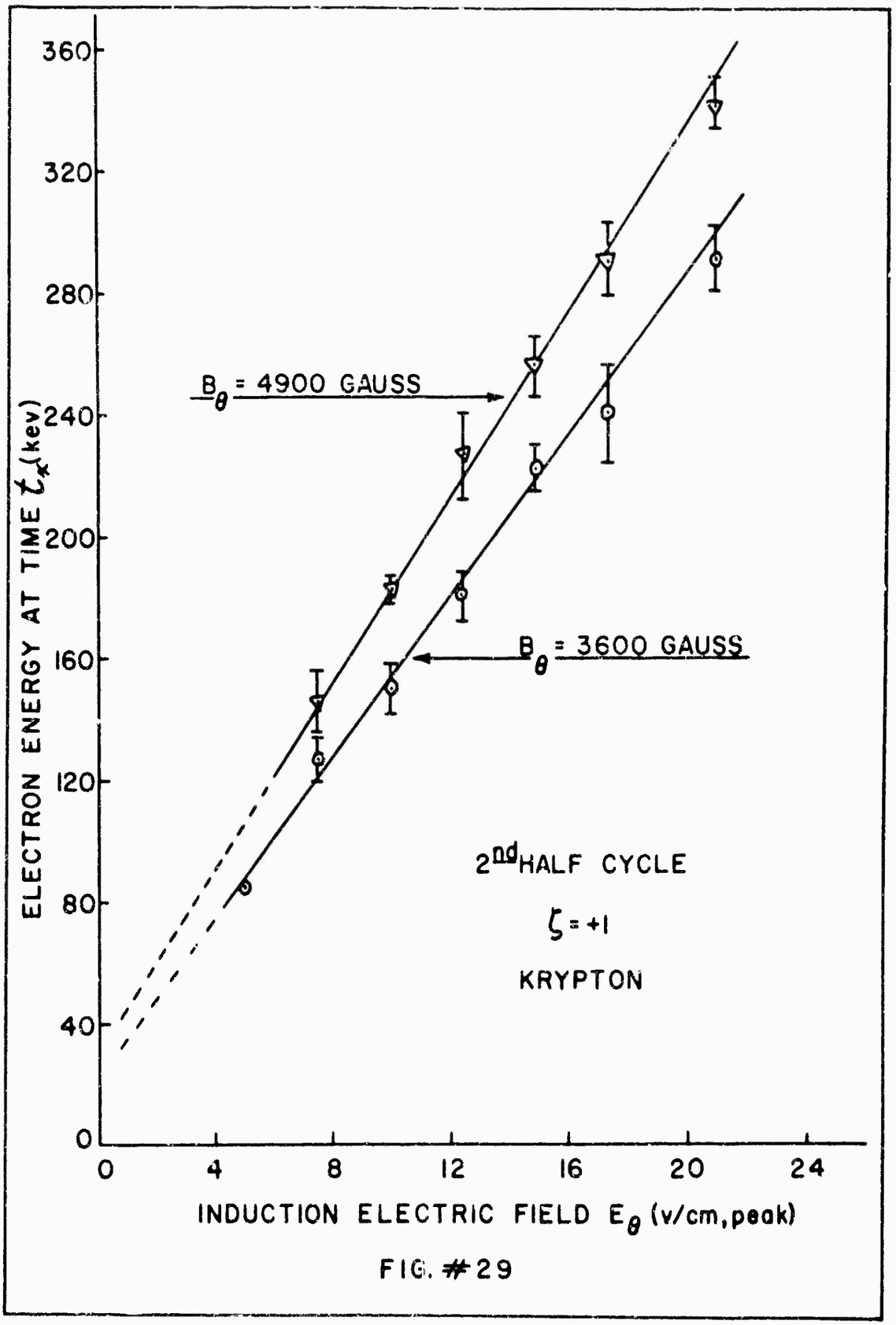
360
320
280
240
200
160
120
80
40
0
0
4
8
12
16
20
24
ELECTRON ENERGY AT TIME ζ_x (kev)
INDUCTION ELECTRIC FIELD E_θ (v/cm, peak)
B_θ = 4900 GAUSS
B_θ = 3600 GAUSS
2nd HALF CYCLE
ζ = +1
KRYPTON

FIG. #29

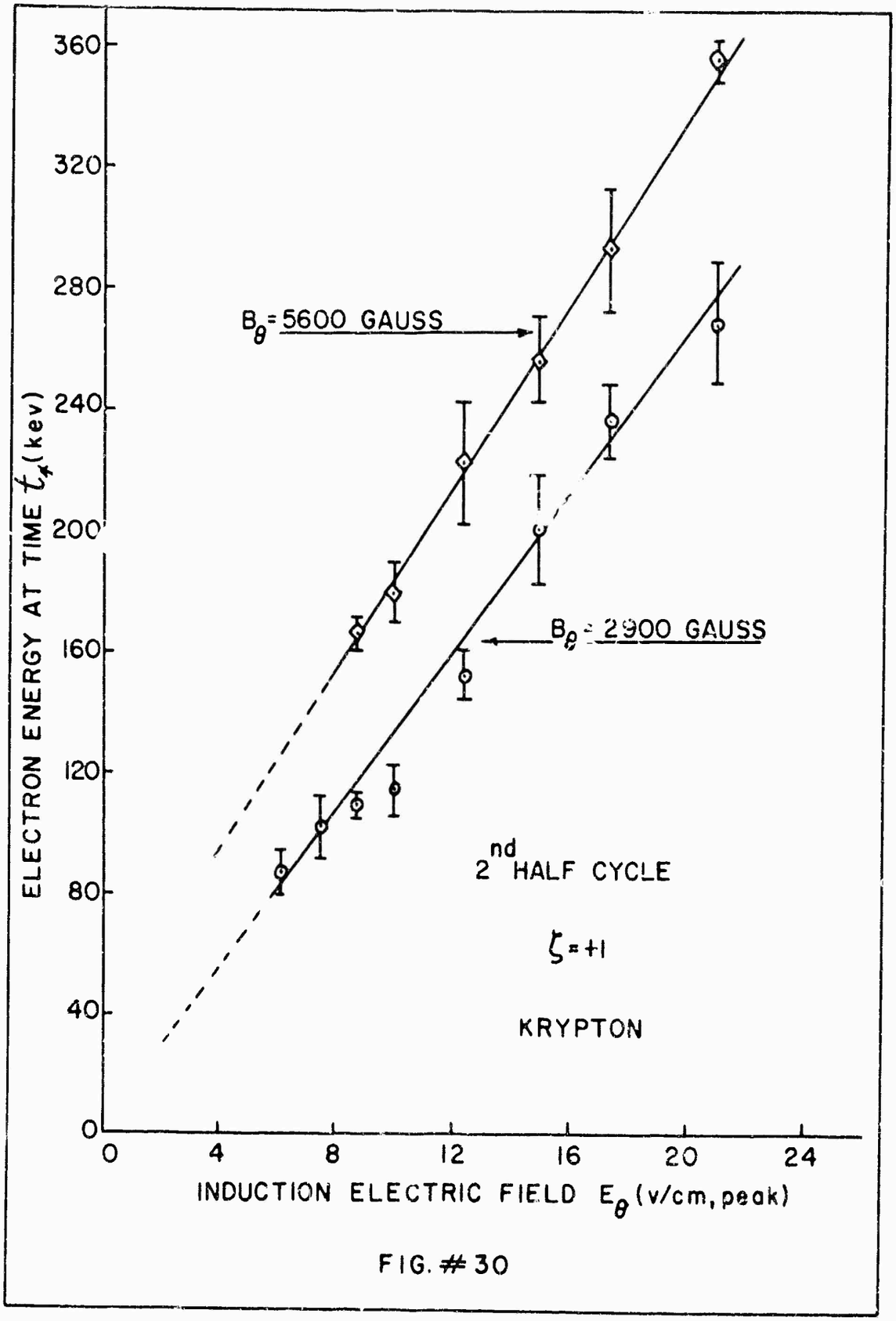
360
320
280
240
200
160
120
80
40
0
0
4
8
12
16
20
24
ELECTRON ENERGY AT TIME t_4 (kev)
INDUCTION ELECTRIC FIELD E_θ (v/cm, peak)
B_θ = 5600 GAUSS
B_θ = 2900 GAUSS
2nd HALF CYCLE
$\zeta = +1$
KRYPTON

FIG. # 30

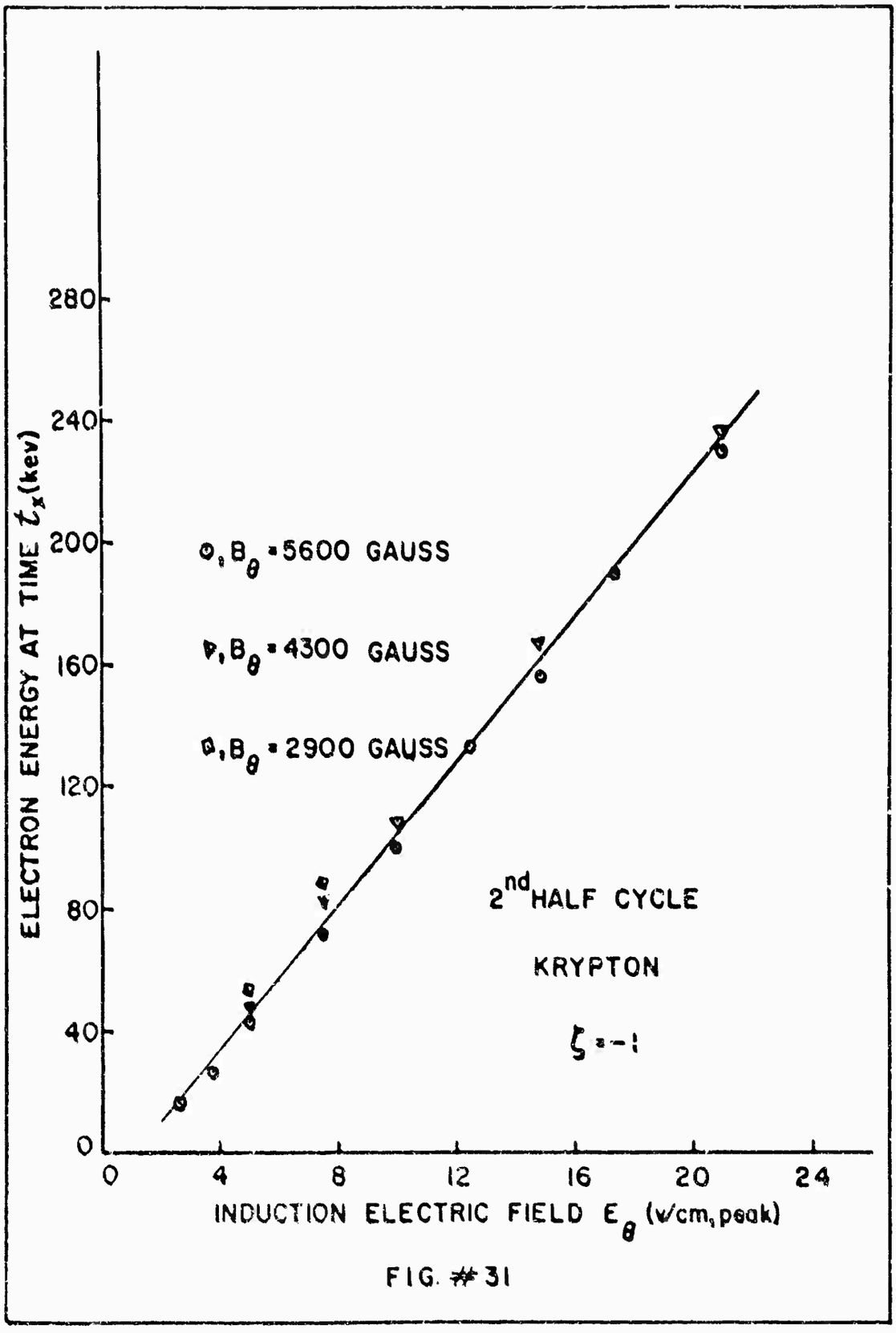
ELECTRON ENERGY AT TIME t_x(kev)
280
240
200
160
120
80
40
0
0
4
8
12
16
20
24
INDUCTION ELECTRIC FIELD E_θ (v/cm, peak)
○, B_θ = 5600 GAUSS
▷, B_θ = 4300 GAUSS
□, B_θ = 2900 GAUSS
2nd HALF CYCLE
KRYPTON
$\zeta = -1$

FIG. #31

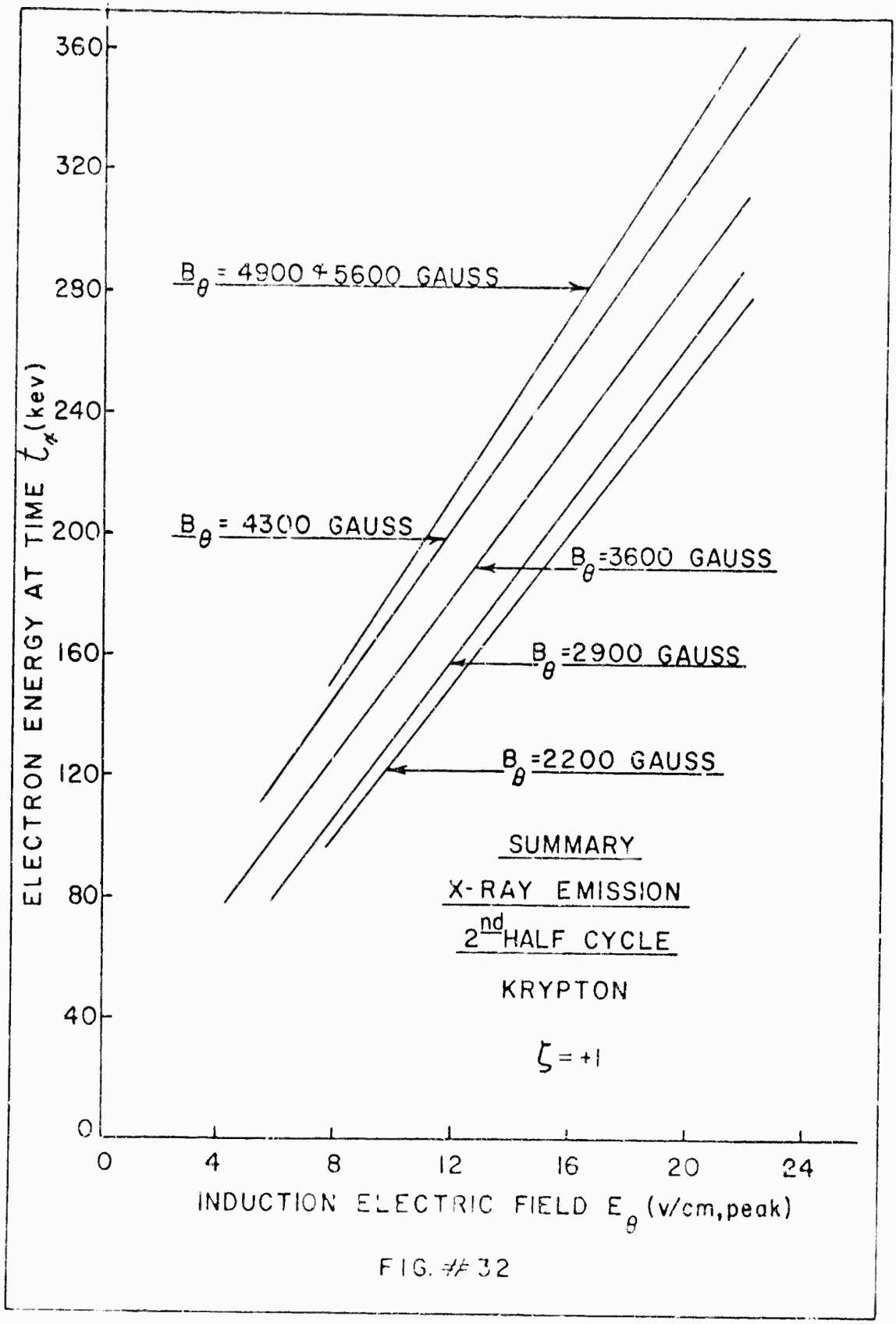
360
320
280
240
200
160
120
80
40
0
ELECTRON ENERGY AT TIME t_x (kev)
B_θ = 4900 & 5600 GAUSS
B_θ = 4300 GAUSS
B_θ =3600 GAUSS
B_θ =2900 GAUSS
B_θ =2200 GAUSS
SUMMARY
X-RAY EMISSION
2nd HALF CYCLE
KRYPTON
$\zeta = +1$
0
4
8
12
16
20
24
INDUCTION ELECTRIC FIELD E_θ (v/cm, peak)

FIG. #32

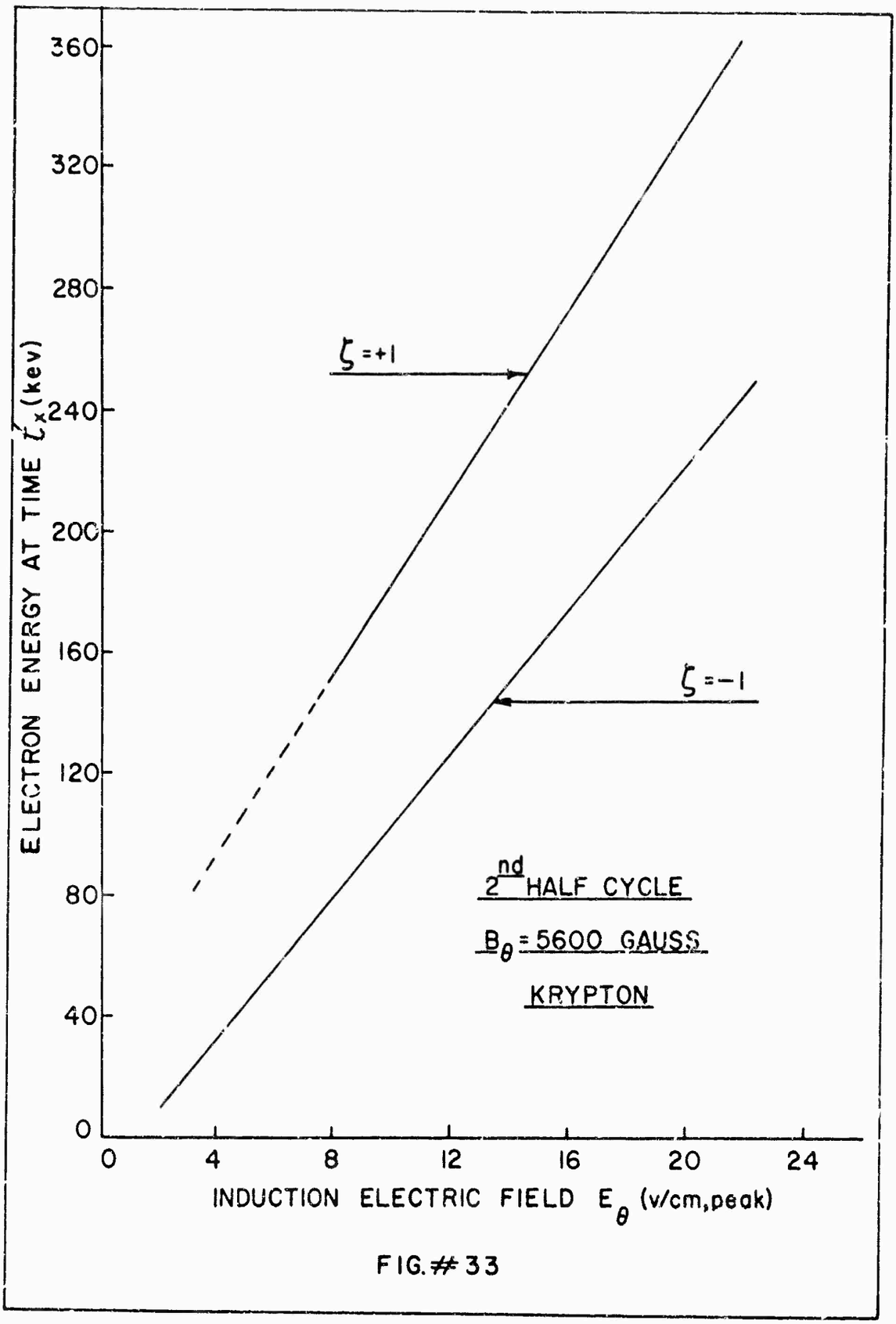
360
320
280
240
200
160
120
80
40
0
ELECTRON ENERGY AT TIME t'_x (kev)
$\zeta = +1$
$\zeta = -1$
2^{nd} HALF CYCLE
$B_\theta = 5600$ GAUSS
KRYPTON
0
4
8
12
16
20
24
INDUCTION ELECTRIC FIELD E_θ (v/cm, peak)

FIG. # 33

intense there (Fig.#34). Subsequent x-ray emission lasts for times as long as 2 μ sec after "t_x", indicating that x-rays corresponding to the peak energy of the machine are probably generated.

As we can see from the experimental data there is a considerable difference in the x-ray emission time, and hence the electron energy, for the two orientations of B_θ relative to E_θ.

In the suceeding paragraphs we present several models to represent the processes taking place during the acceleration cycle. The experimental data are then analyzed in terms of these models with the hope of gaining some insight into the processes that take place during the acceleration cycle; the processes that are responsible for the x-ray emission and those that lead to different results for the two directions of B_θ.

The simplest process that can lead to premature x-ray emission comes from the diamagnetic properties of the beam. As we have discussed earlier (section #5.3) G. Schmidt has calculated the maximum beam current that a betatron field can hold without collapsing. Application of the Schmidt formula to the vector potential shown in Fig.#8 yields a maximum beam current of approximately 70 amperes on the 1st half cycle and 300 amp. on the second. This calculation was done for a plasma betatron

without an azimuthal magnetic field. Just how the formula should be modified to take into account the additional field is not clear. However we observe no change in "t_{γ}" as the peak induced current is varied from zero to over several hundred amperes. The quantity that does change as the induced current is varied is the x-ray emission intensity and therefore the runaway current. (Figs.#15 to 18)

The observation of the large fluctuating electric fields that develop during the discharge leads one to construct the following model for the interaction between the runaway electrons and the background plasma through which they move. Sudden application of the betatron electric field causes some of the plasma electrons to runaway. The electrons are accelerated to high velocity very rapidly and hence move through the background plasma without collisions. When the runaway current reaches a critical value there is an interaction between the runaways and the plasma. We assume that some sort of wave is generated. The runaway electrons then give energy to the wave, move across the B_θ field and strike the vacuum chamber walls. This model fails to account for the difference in "t_{γ}" that exists between the two values of δ ($\delta = \vec{E}_\theta \cdot \vec{B}_\theta / |E_\theta B_\theta|$). Moreover since the x-ray emission times are comparable with the times that are

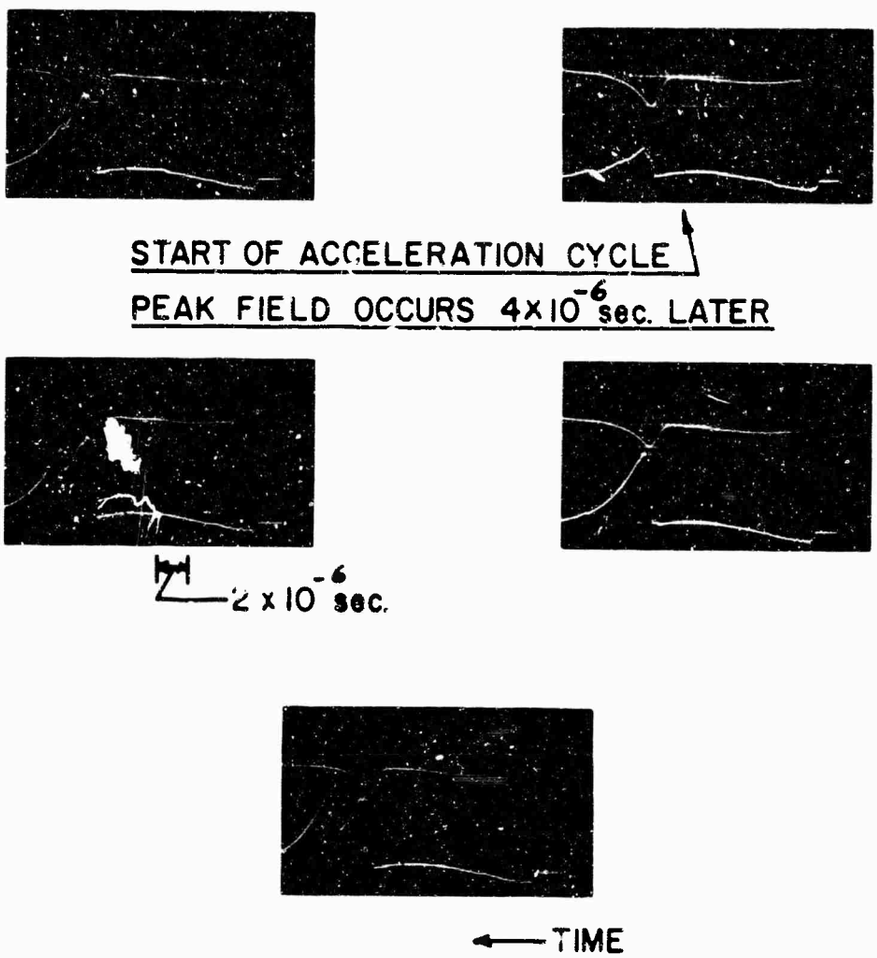

SCINTILLATOR SIGNALS SHOWING SUDDEN ONSET AND DURATION OF X-RAY EMISSION

FIG. #34

associated with ionic processes ($\omega = 2\pi / t_x \times \omega_{pi}$

$\omega_{p_i} = \left(\frac{n_i q^2}{m_i \epsilon_0}\right)^{1/2}$, $\omega \approx \omega_{c_i} = \frac{q B_\theta}{m_i}$),

we would expect "t_x" to also depend on the ion mass. The x-ray emission time is essentially the same for both argon and krypton while there is a factor of two difference in the ion masses. The insensitivity of the experimental data to the ion mass leads us to conclude that the x-ray emission time depends on electronic processes only.

As we have just mentioned the times associated with the onset of x-ray emission are comparable to the ion plasma period and ion cyclotron period and consequently are several orders of magnitude larger than the values of the same quantities for the electrons. Thus we can also conclude that collective electronic process are not responsible for the disruption of the betatron acceleration, however they may be responsible for the number of runaways that are generated. In the following paragraphs we assume that the runaway electrons are moving through the backround plasma as single particles. We then analyze the single particle motion more carefully than was done in sections 3.1-3.3 .

Using a single-particle model in the guiding center approximation Meservey and Goldberg [37] have made calculations of the shape and position of particle surfaces

(locus of guiding-centers) for runaway electrons in a figure-eight stellarator with fixed rotational transform and uniform axial plasma current density. This work was prompted by the experiments of Bernstein et al[38]; who reported on the energy and the time at which runaway electrons reach the aperature limiter in the stellarator for the case when the accelerating electric field $\vec{E}$ is parallel to $\vec{B}$ (σ = + 1) as well as for the anti-parallel case (σ =-1). Their experimental results agree qualitatively with ours, ie, as the magnetic field is increased with $\vec{E}$ held constant, the x-ray emission begins at later times. Similarly the peak x-ray energy and emission time is greater for σ = + 1 than it is for σ = -1. Meservey and Goldberg have also made measurements which qualitatively confirm the prediction of their simple theory, namely that, in a machine whose figure eight twist is negative "runaway" surfaces drift toward the center of curvature (inside) of the stellarator loop for accelerating field $\vec{E}$ parallel to the confining field $\vec{B}$ (σ = + 1) and toward the outside for $\vec{E}$ anti parallel to $\vec{B}$. The motions are reversed for a machine with positive twist and with no machine transform the asymmetry disappears, and the particle surfaces move toward the outside for both parallel and anti parallel cases . These results have led us to consider a similar type calculation for our

situation. In section #3.3 we studied the motion of a single electron in the combined betatron and azimuthal magnetic fields. We found that in the limit $B_\theta/B_z >> 1$ the motion in the transverse plane (x, z) was composed of two elementary motions, a rapid motion with frequency ω_2 close to the cyclotron frequency superimposed on a slow elliptic motion with $\omega_1 \approx \frac{\omega_0^2}{\omega_c}\left[n(1-n)\right]^{1/2}$. The slow elliptic motion is just the locus of the guiding center and hence traces out the particle surfaces and leads to a rotational transform. This analysis was done under the assumption of zero plasma current. If we assume that in addition to the runaway electrons there is a uniform plasma current flowing, the equations of motion (3.24) are modified to

$$\ddot{x} + \left[\omega_0^2(1-n) + \Omega^2\right]x = \omega_c \dot{z}$$

$$\ddot{z} + \left[\omega_0^2 n + \Omega^2\right] z = -\omega_c \dot{x} \qquad 7.1$$

where $\Omega^2 = \frac{e}{m} R_0 \omega_0 \left(\frac{\mu_0 i}{2\pi R^2}\right) = \frac{e}{m} R_0 \omega_0 \mu_0 J/2$ and J is the current density. (These equations with $\omega_c = 0$ agree with those derived by Rogers[39]). Again if we assume that x and z vary as $e^{i\omega t}$ we find that in the limit $B_\theta/B_z >> 1$ the motion in the (x, z) plane is the same as that discussed above but with the fast and slow frequencies now given by

$$\omega_1^2 = \frac{\omega_0^2}{\omega_c^2}\left[\Omega^2 + \omega_0^2 n(1-n)\right]$$

$$\omega_2^2 = \omega_c^2\left[1 + \frac{\Omega^2}{\omega_c^2} + \frac{\omega_0^4}{\omega_c^4} n(1-n)\right] \quad 7.2$$

By inspection we can see that the electron motion is independent of the direction of the azimuthal magnetic field (excluding the usual Larmor precession). Thus the presence of the rotational transform and the finite plasma current density does not seem to be responsible for the difference between the parallel and antiparallel situations in our experiment.

So far in our discussion no mention has been made of the effects of the stray magnetic fields that are generated by the helical windings used to generate the azimuthal guide field. In principle the currents used to generate the B_θ field should lie in a plane that is orthogonal to the "θ"-direction. The finite pitch of the B_θ windings causes a component of current to flow in the "θ"-direction thereby generating magnetic fields in the "r" and "z' directions. In the following section we will discuss the effects these pertubbing fields have on the electron motion.

A uniform transverse field in the "z" direction is the simplest perturbing field one can have. Let " B' " be the value of the perturbation field. Then the equations of motion become

$$\ddot{x} + \omega_0^2\left(1-n-\frac{B'}{B_0}\right)x = -R_0\,\omega_0^2\,\frac{B'}{B_0} + \omega_c\,\dot{z}$$

$$\ddot{z} + \omega_0^2\, n\, z = -\omega_c\,\dot{x} \qquad 7.3$$

where B_0 is the value of the betatron field at the orbit radius (R_0) and terms containing (B'/B_0)^2 have also been dropped. If we put

$$x = x' - \frac{R_0\,(B'/B_0)}{1-n-B'/B_0} \qquad 7.4$$

the equations take on the familiar form

$$\ddot{x}' + \omega_0^2\left(1-n-\frac{B'}{B_0}\right)x' = \omega_c\,\dot{z}$$

$$\ddot{z} + \omega_0^2\, n\, z = -\omega_c\,\dot{x}' \qquad 7.5$$

the effect of the transverse field B' is to displace the position of the equilibrium orbit by an amount given by

$$\delta x = x' - x = \frac{R_0\,(B'/B_0)}{1-n-B'/B_0} \qquad 7.6$$

Since B_0 starts from zero we can see that even small values of B' could shift the position of the equilibrium orbit outside of the acceleration chamber. We recall that

the equations of motion (7.3) with $B' = 0$ are only valid for times greater than t_ν. Similarly equations (7.3) should only be valid for $t > t_\nu$. Thus t_ν is the most logical time to evaluate δ_n. Refering back to section #3.4 we find that $t_\nu = 7 \times 10^{-8}$ sec with $B_\theta = 5$ k gauss, $B_z = 1$ k gauss (peak field at orbit) and $\Omega = 0.39 \times 10^6$. Therefore the field at the orbit is $B_o \approx B_z \Omega t_\nu = 28$ gauss. If we assume that $B' = 5$ gauss, the displacement of the equilibrium orbit will be approximately 2 cm, and therefore it will lie outside of the acceleration chamber. Since B_o varies with time so will the position of the equilibrium orbit. The velocity with which the orbit position moves can be found by differentiating (7.6) with respect to time.

$$v_{\delta n} = \frac{d(\delta n)}{dt} \approx \frac{n_o}{1-n} \frac{B'}{B_z} \frac{d}{dt}\left[\sin \Omega t\right]^{-1} \qquad 7.7$$

$$v_{\delta n} \approx \frac{n_o}{1-n} \frac{B'}{B_z} \frac{1}{\Omega t^2} \qquad 7.8$$

If we evaluate $v_{\delta n}$ for the conditions given above we find that $v_{\delta n} \approx 2 \times 10^9$ cm/sec, therefore under these conditions the equilibrium orbit will be located within the vacuum chamber before the electrons have traveled very far.

One may argue that the value of $B' = 5$ gauss

chosen for the calculation in the preceeding paragraph is entirely too small since it is only 1/10% of the value of the azimuthal guide field. This question can be answered by actually measuring in detail the magnetic field distribution produced by the B_z coils. The purpose of the preceeding paragraphs was to show the asymmetric particle behavior with respect to the direction of B_θ and not to do a detailed calculation of the single particle orbits. The effect of reversing the direction of B_θ can be seen by examining (7.6). If we reverse the direction of B_θ relative to E_θ, the value of the perturbing field changes sign, causing the position of the equilibrium orbit to lie radially inward from R_0 instead of at a radius $R > R_0$ (or vice-versa). If the direction of E_θ as well as the direction of B_θ i reversed, thereby preserving the value of γ, the position of the equilibrium orbit does not change as can be seen from (7.5) (Both B' and B_0 change sign, preserving the sign of the ratio B'/B_0. The fact that the right hand side changes sign does not introduce as asymmetry). This effect has also been observed experimentally, ie, the x-ray emission time "t_γ" does not change if both E_θ and B_0 are reversed.

The fact that a small transverse field can lead to a large displacement of the equilibrium orbit by

equation 7.6 still causes concern. It is possible that there will be no electrons available for capture into a stable betatron orbit at the time the position of the equilibrium orbit returns to the interior of the vacuum chamber. This will certainly be true if the initial displacement is large enough. In section #6.5 we have shown, via. absorption measurements, that the peak x-ray energy agrees with the energy that the electrons should have at "t_π ", if they have undergone continuous betatron acceleration. To make sure that a betatron field is necessary to produce runaway electrons in this device we removed the flux concentrators and searched for x-rays originating from the vacuum chamber. Experiments were carried out under experimental conditions which lead to runaway electron currents when B_z was shaped to satisfy the betatron condition; the maximum values of the parameters were B_z =7.5 k gauss, (B_θ)=7$\frac{1}{2}$gauss, and E_θ =55 v/cm. No x-rays were detected under these conditions. In an attempt to generate a more uniform B_θ field, a coil support form was constructed. The coils instead of being placed directly on the vacuum chamber were then located approximately 1/4" away from the flux concentrators. The x-ray emission under these circumstances was greatly reduced from that with the coils directly on the vacuum chamber. The presence of the extra metal so

close to the flux concentrators distorts the betatron field and hence to a decrease in the runaway current. Thus from this experiment and from the x-ray absorption measurement we can conclude that a betatron field is necessary for runaway production in this experiment.

Because of the method of producing the B_θ field, a transverse field in considerable excess of 1/10% of the main field might easily be present. This would then, as we have discussed before, place the equilibrium orbit far outside the vacuum chamber and thus prevent betatron acceleration. But we have shown experimentally that betatron acceleration has in fact taken place, thereby casting suspicion on the model for the perturbing field that leads to equation (7.6). It is obvious that a better calculation of the perturbing fields is required. The present calculation has value in that the asymmetric behavior with respect to the relative directions of E_θ & B_θ has been revealed.

The considerations of the last few paragraphs lead us to reconsider the model for the x-ray emission proposed at the beginning of this section. We begin this discussion by first calculating the longitudinal electron energy in the combined magnetic fields. The electron kinetic energy in the non-relativistic limit is given by

$$W_\theta = \tfrac{1}{2} m v_\theta^2 = \tfrac{1}{2} m r^2 \dot\theta^2 \qquad 7.9$$

In our linear approximation we have replaced r and $\dot\theta$ with $(r_0 + x)$ and $(\omega + \dot\psi)$ respectively. Since $\dot\psi = -\frac{\omega_0}{r_0} x$, to first order, the electron energy, is,

$$W_\theta = \tfrac{1}{2} m r_0^2 \omega_0^2 \left[1 - \frac{2x^2}{r_0^2} \right]$$

$$W_\theta = W_c \left(1 - \frac{2x^2}{r_0^2} \right), \quad W_0 = \tfrac{1}{2} m r_0^2 \omega_0^2 \qquad 7.10$$

If we put x=b/2, the radius of the acceleration chamber, we find that an electron will hit the vacuum chamber wall if it loses an amount of energy greater than

$$\delta W_\theta = \frac{1}{2} \frac{b^2}{r_0^2} W_0 \qquad 7.11$$

For the present experiment b=0,625" and r_0 =1.9" so that (7.11) reduces to

$$\delta W_\theta = 0.054\, W_0 \qquad 7.12$$

Next we calculate the energy stored in the fluctuating fields that develop during the discharge. The stored energy is given by

$$W_{EM} = \int \left[\frac{(\varepsilon \cdot \vec{E}) \cdot \vec{E}}{2} + \frac{B^2}{2\mu_0} \right] d^3x \qquad 7.13$$

We assume that ε is a scaler and is just ε_0 . Then the stored electric and magnetic energies are equal, thus

$$W_{EM} = \int \varepsilon_0 E^2 d^3x = \varepsilon_0 \langle E^2 \rangle V \qquad 7.14$$

where $\langle E^2 \rangle$ represents the average of E^2 over the plasma volume and V is the plasma volume. The magnitude of the observed electric field is $\approx$ 1000 v/cm and the volume of the vacuum chamber is $\approx$ 60 cm Hence

$$W_{EM} = 8.85 \times 10^{-12} \times 10^{10} \times 60 \times 10^{-6} = 5.3 \times 10^{-6} \quad \text{joules}$$

The electric field measurements were made with B_θ =4500 gauss, E_θ =10 v/cm, and ζ =+1, from Fig.#28 we find that the runaway electrons had a kinetic energy of $\approx$ 170 kev when they hit the vacuum chamber wall. With these experimental parameters the total number of runaway electrons $N_\lambda = 4 \times 10^9$ (Fig.#35). Therefore the total energy given up by the runaway electrons is

$$N_\lambda \delta W_\theta = .054 \times 170 \times 10^3 \times 1.6 \times 10^{-19} \times 4 \times 10^9$$

$$N_\lambda \delta W_\theta = 5.87 \times 10^{-6} \quad \text{joules}$$

Thus it appears that the energy lost by the runaway electrons can be accounted for by the energy stored in the electromagnetic field. The radial electric field measured at four different radial positions is shown in Fig. #37. The fact that at positions 1 and 2 the electric field persists through the current maximum rules out the possibility that the electric field is of a ($L\, di/dt$) origin. Very strong radial fields can develop if there is a radial collapse of the electron stream. In ordinary betatrons the radius of the beam shrinks according to $\rho \propto 1/B_g^{1/2}$ because of adiabatic damping. If a similar type of damping occurs in a plasma betatron large radial fields can develop because the beam will no longer be space-charge neutralized (the ions, since they are considerably less mobile then the electrons, will be left behind. 0.5 ev argon ions will move only 1 mm in 10^{-6} sec). If we examine Fig. #31 we find that the radial electric field does change sign as the probe is moved across the vacuum chamber. This is quite clear for $\gamma = +1$. For $\gamma = -1$ the field seems to be changing sign at x=+.64 cm. For $x > o$ the electric field points radially inward while for $x < o$ the field is radially outward indicating that there is an excess negative charge around x=0. Thus in the next few paragraphs we assume that in addition to the betatron and B fields there is a radial electric field caused by

an excess of electrons around $x = 0$

We assume that the excess electron density is just due to the runaways. Then if $n_r c$ is the charge density, the electric field at $\rho = (x^2 + z^2)^{1/2}$ is given by

$$E_\rho = - \frac{n_r c}{2\varepsilon_0} \rho \qquad 7.15$$

Thus the "x" and "z" equations of motion become

$$\ddot{x} + \omega_0^2 \left(1 - n - \frac{Gc}{m\omega_0^2} \right) x = \omega_c \dot{z} \qquad 7.16$$

$$\ddot{z} + \omega_0^2 \left(n - \frac{Gc}{m\omega_0^2} \right) z = - \omega_c \dot{x} \qquad 7.17$$

where $G = n_r c / 2\varepsilon_0$. By inspection we can see that the radial equation of motion becomes unstable when

$$\frac{Gc}{m\omega_0^2} > (1 - n) \qquad 7.18$$

Hence for stable motion the charge density within the beam must satisfy

$$c n_r < n_{rc} c$$

$$n_{rc} c = 2(1-n) \frac{\varepsilon_0 c}{m} B_0^2 \qquad 7.19$$

and B_0 is the value of the betatron field at the orbit. (This is not correct at $B_0 = B_1$ for at this time, the magnitude of the betatron focusing forces is just equal

to the magnitude of the terms in the expansion of B_θ that were dropped. As we shall see the excess charge density is also zero at this time. Neglecting both these effects will probably not cause too much trouble.) The equations of motion can be uncoupled by differentiating (7.16) with respect to time twice . The resulting "x" equation is then fourth order, i.e.,

$$\frac{d^4x}{dt^4} + \left[\omega_\theta^2 + \omega_c^2\right] \frac{d^2x}{dt^2} + \omega_0^4 n'(1-n')x = 0 \qquad 7.20$$

where $n' = n + \frac{Gc}{m\omega_0^2}$. The slow frequency ω_1 in the $B_\theta/B_0 >> 1$ limit is obtained by neglecting d^4x/dt^4 , ie., ω_1 , is the solution of

$$\frac{d^2x}{dt^2} + \frac{\omega_0^4}{\omega_c^2} n'(1-n')x = 0 \qquad 7.21$$

The fast frequency ω_2 is obtained from the solution of

$$\frac{d^4x}{dt^4} + \left(\omega_\theta^2 + \omega_c^2\right) \frac{d^2x}{dt^2} = 0 \qquad 7.22$$

Equation (7.22) just represents the electron cyclotron motion in the B_θ field while equation (7.21) gives the slow motion about the position of the equilibrium orbit. (Fig.#1). Therefore the temporal behavior of the beam radius will be given by the adiabatic solution of (7.21). Equation (7.21) is of the form

$$\frac{d^2\mu}{dr^2} + k^2(r)\,\mu = 0, \qquad k^2 > 0$$

7.23

(40)

The approximate solution to (7.23) is given by (W.K.B. solution).

$$\mu(r) = A\,k^{-1/2}\,\exp\left[\pm i\int^{r} k\,dr\right] \qquad 7.24$$

where A is an arbitrary constant. Thus the beam radius ρ decreases with time according to

$$\rho \propto 1/B_0 \qquad 7.25$$

In an ordinary betatron the beam shrinks less rapidly since $\rho \propto \frac{1}{B_0^{1/2}}$. Let N_r be the number of runaway electrons, then N_s is the number of electrons captured into stable betatron orbits and hence subject to equation (7.23). Thus the beam density is given by

$$n_v = \frac{N_s}{2\pi^2 R_0\,\rho^2} \qquad 7.26$$

We assume that the beam forms at $t=t_v$ and we also assume that at t_v the beam radius is just the radius of the vacuum chamber. Then the charge density is

$$K = \frac{2N_s e}{\pi^2 R_0 b^2}\left(\frac{B_0^2}{B_1^2} - 1\right) \qquad 7.27$$

where B_i is the value of the betatron field at the orbit at t_r . B_0 increases rapidly with time, therefore for the purposes of this calculation we can neglect unity compared with the ratio. Then since both the charge density given by (7.27) and the critical charge density $n_{bc}e$ given by (7.19) both vary as B_0^2 we have arrived at a condition on N_R the number of runaways. If we put $e n_{bc} = \kappa$ we find that the motion of the runaway electrons becomes unstable for values of N_R that satisfy

$$N_R \geq N_{Rc} = (1-n)\frac{\varepsilon_0}{m}\pi^2 R_0 b^2 B_i^2 \qquad 7.28$$

B_i is given by $B_i \approx B_\theta \Omega t_r$ (section#3.4)
so that (7.28) becomes

$$N_{Rc} = \pi^2 b^2 \frac{\varepsilon_0}{e} R_0 B_\theta \left(\frac{\dot{B}}{B}\right) \qquad 7.29$$

For B_θ =4.3kgauss, b=0.625"

$$N_{Rc} = \frac{8.85\times10^{-12}}{1.6\times10^{-19}} \times 9.85 \times 2.52\times10^{-4} \times 4.85\times10^{-2} \times .43 \times 4.2\times10^{6}$$

or $N_{Rc} = 1.2\times10^{10}$ runaways

Thus 7.29 is in approximate agreement with the experimental results for the number of runaway electrons (Fig.#35). Expression (7.29) gives the correct parametric dependence of N_R with B_θ . Quantitatively the theoretical N_R is too large by a factor of 2-3 for γ =+1. The agreement for γ =-1 is not as good, the experimental

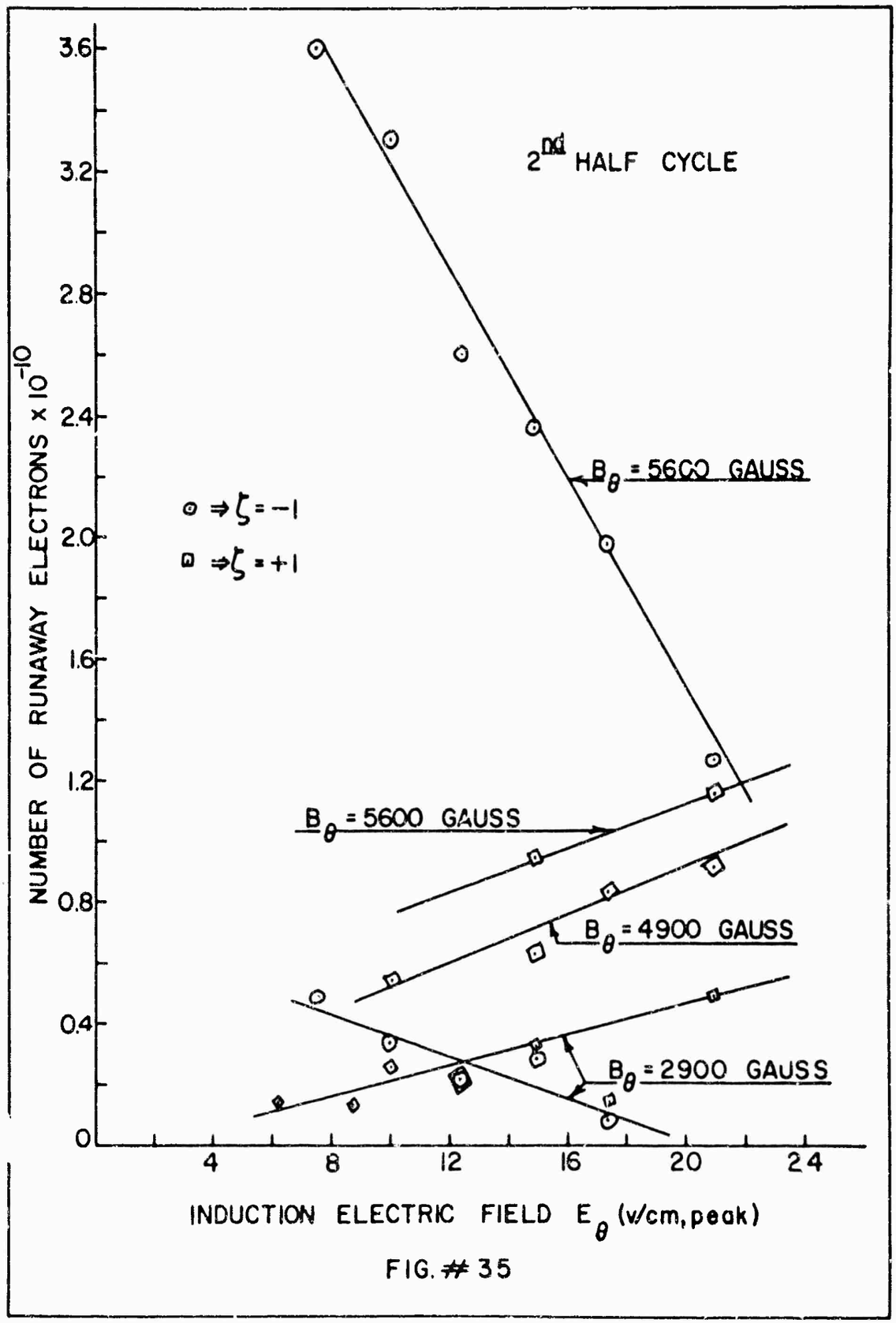
NUMBER OF RUNAWAY ELECTRONS x 10^{-10}
3.6
3.2
2.8
2.4
2.0
1.6
1.2
0.8
0.4
0
4
8
12
16
20
24
INDUCTION ELECTRIC FIELD E_θ (v/cm, peak)
2nd HALF CYCLE
B_θ = 5600 GAUSS
⊙ ⇒ ζ = −1
□ ⇒ ζ = +1
B_θ = 5600 GAUSS
B_θ = 4900 GAUSS
B_θ = 2900 GAUSS

FIG. # 35

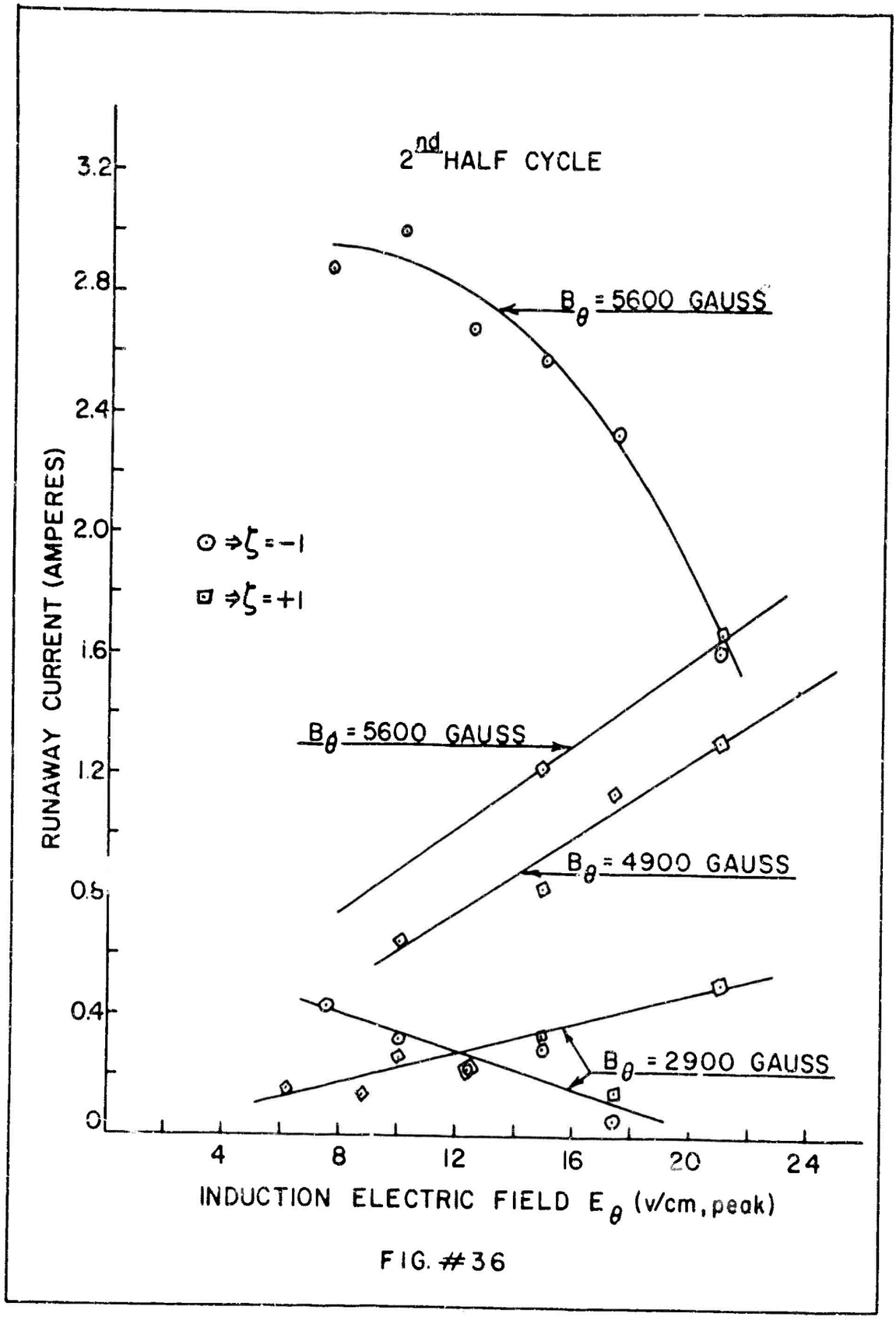
2nd HALF CYCLE
RUNAWAY CURRENT (AMPERES)
3.2
2.8
2.4
2.0
1.6
1.2
0.5
0.4
0
⊙ ⇒ ζ = −1
⊡ ⇒ ζ = +1
B_θ = 5600 GAUSS
B_θ = 5600 GAUSS
B_θ = 4900 GAUSS
B_θ = 2900 GAUSS
4
8
12
16
20
24
INDUCTION ELECTRIC FIELD E_θ (v/cm, peak)

FIG. #36

value is approximately five times larger than that given by (7.29). The dependence of N_R on E_θ is not explained by this calculation.

Harrison[41] in his analysis of the acceleration of electrons in plasmas predicts that electrons should runaway freely when the applied electric field satisfies $E \gg E_c'$ where E_c' is now the maximum value of the fluctuating electric field that exists in the plasma. He claims that E_c' may be of the order of 10^6 v/cm, therefore much larger than the experimentally applied electric fields. Then since $E_\theta \ll E_c'$ only a very small number of electrons should runaway. But we do not observe any fluctuating electric fields(with frequencies within the probe band width) at the start of the acceleration cycle. The electric field begins about 1.5×10^{-6} sec later, therefore we do not believe that Harrison's mechanism[15] responsible for the small number of runaways observed in this experiment.

If the effects of the induced plasma current and the transverse magnetic field are included in the analysis the maximum number of runaway electrons is given by

$$N_R = \pi^2 R_0 \frac{e^2 \varepsilon_0}{m} B_1^2 \left[(1-n) - \frac{B'}{B_0} + \frac{\Omega^2}{\omega_0^2} \right] \quad 7.30$$

When the beam forms, ie, at $t=t_s$ the induced plasma current is zero, then since capture into stable betatron

orbits occurs at t_{ν} , equation (7.30) reduces to

$$N_1 = \pi^2 n_0 b^2 \frac{E_\theta}{m} B_1^2 \left[(1-m) - B'/B_\theta \right] \qquad 7.31$$

Thus we see that a small transverse magnetic field can also cause the number of runaways for $\gamma = +1$ to be different from $\gamma = -1$. Physically, the transverse field reduces the strength of the focusing forces for one orientation and for the opposite case increases it. Therefore the number of runaways will be either less than or greater than the number obtained without the transverse field.

At this point in our discussion it seems that we should review the results of this chapter so that we can decide the direction in which to extend the analysis. We indicated at the beginning of this section that we were attempting to explain a, the difference in x-ray emission time for the two orientations of E_θ relative to B_θ ; and b, the processes that cause the accelerated electrons to move across the B_θ field and strike the walls of the vacuum chamber without any externally applied disturbance. So far we have shown that a small transverse magnetic field arising from the finite pitch of the B_θ coils destroys the symmetry with respect to the direction of B_θ and thus could account for the observed results. The results of this analysis predicted

a displacement of the position of the equilibrium orbit from the $B_\theta = 0$ condition. Thus when the electron motion became unstable the time required to reach the vacuum chamber wall would depend on the orientation of B_θ .

We also found that the self-electric field that arises from the adiabatic collapse of the runaway electron stream tends to reduce the focusing forces that are generated by the betatron magnetic field. Since runaway electrons are captured into stable betatron orbits just after the start of the acceleration cycle, the self-electric field at this time places an upper limit on the number of runaways that can be accelerated. The number of runaways determined from this analysis was found to be in fair agreement with the experimental results.

Thus we have succeeded in explaining a , the observed difference between the two directions of B_θ and b , the reason for the relatively small number of runaways. The processes that are responsible for the disruption of the accelerated beam are still unknown. It also appears that we will have to modify our original assumption that the beam disruption was <u>not</u> caused by electronic processes. As we will discuss shortly the radial electric field rises to its maximum value in $\approx 10^{-7}$ sec, a time that is more consistant with the beam plasma frequency than any of the corresponding ion times. This could then account

for the observed insensitiveness of the x-ray emission time to the ion mass.

As we have just indicated the origin of the very large radial electric field in the acceleration chamber is still unexplained. From Fig.#37 we see that the electric field rises to its full amplitude in approximately 10^{-7} sec. Thus a very rapid collapse of the runaway stream could lead to a beam density considerably in excess of that given by (7.19). The motion of the runaways would then be unstable and they would move across the B_θ field to the walls of the vacuum vessel. Hence there are at least three possible ways for the fast electrons to strike the walls. The electrons can lose longitudinal energy to the electromagnetic field and then move to the walls, they can be lost because of a rapid collapse of the minor beam diameter or, they can lose energy to the electromagnetic field and then move to the walls because of the unstable motion in the resulting electric field.

In the following paragraphs we consider processes whose effect on the runaway motion may fall into one of the catagories just described.

One mechanism which can lead to a collapse of the runaway stream is radiation. The runaway motion in the (x,z) plane can be decomposed into two oscillating electric dipoles, 90° out of phase, one along the "x" axis

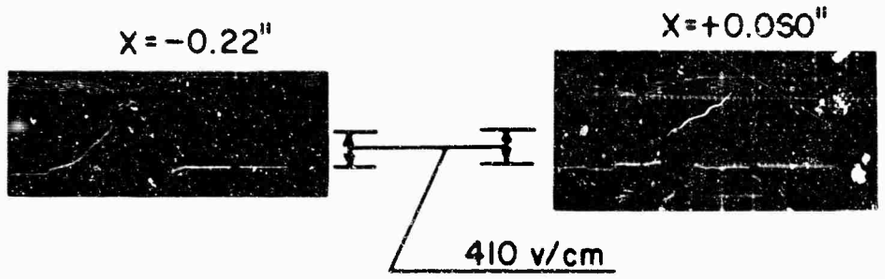

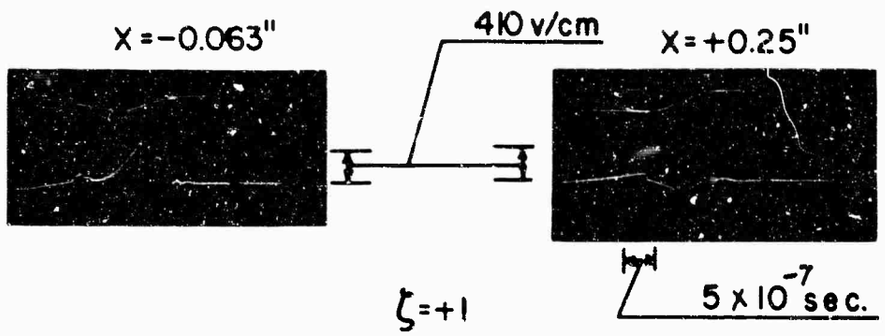

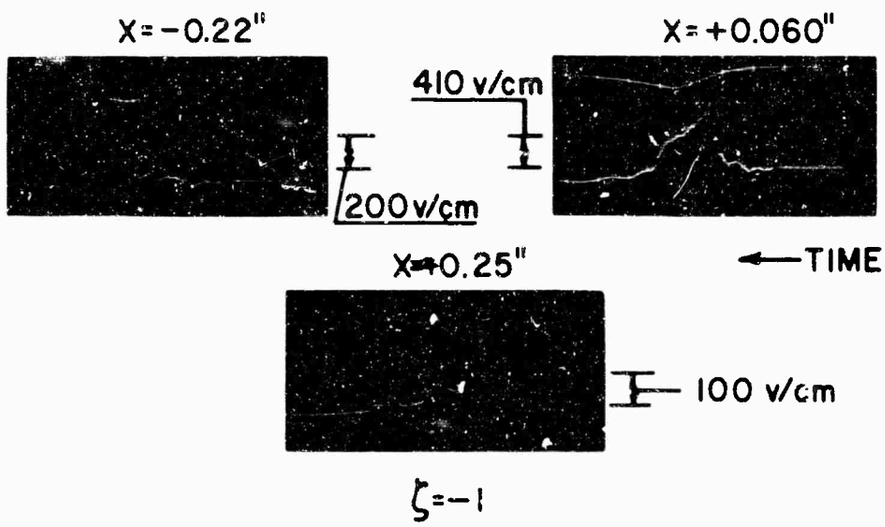

UPPER TRACE = TOTAL INDUCED CURRENT 110 AMP./CM

LOWER TRACE = RADIAL ELECTRIC FIELD E_r

ELECTRIC FIELD MEASUREMENTS

FIG.#37

BLANK PAGE

end the other along the "z" axis. The time required for the beam radius to shrink to $1/e$ of its initial value is given by

$$\tau_R = \frac{1}{2}\,\frac{m^2c^5}{e^4}\,\frac{B_\theta^2}{B_z^4 n(1-n)} \qquad \text{(C.G.S. units)} \qquad 7.32$$

With B_θ =5000 gauss and B_z =200 gauss

$$\tau_R = \frac{6\,(9.1)^3\times10^{-84}\times(5)^5\times10^{50}}{(4.8)^4\times10^{-40}}\times\frac{(5)^2\times10^6}{(2)^4\times10^8}$$

$$\tau_R = 8.2\times10^7 \text{ sec.}$$

Hence τ_R is much too long for the beam collapse to be due to radiation.

We now ask if the magnitude of the observed radial electric field is large enough to cause unstable motion. As we have shown previously the "x" equation of motion is

$$\frac{d^4x}{dt^4} + (\omega_\theta^2+\omega_z^2)\frac{d^2x}{dt^2} + \omega_\theta^4 n'(1-n')x = 0 \qquad 7.20$$

and the "z" equation is obtained by replacing x with z. The slow motion about the B_θ field is given by the solution of (in the $B_\theta/\beta_\theta >> 1$ limit)

$$\ddot{x} + \frac{\omega_\theta^4}{\omega_c^2} n'(1-n') x = 0 \qquad 7.21$$

where the effective field index n' is given by

$$n' = n + \frac{Gc}{m\omega_\theta^2} \quad , \quad G = \frac{n_e e}{2\varepsilon_0}$$

We estimate the value of $Gc/m\omega_\theta^2$ in the following way. We chose an E_θ and ρ and then determine (n_e) from (7.15). With E_θ=1000 v/cm, ρ =.11 cm(evaluated at t= 1 x 10^{-6} sec); we find $n_e = 10^{10}$ electrons /cm.^{3} Then since B =201 gauss at t=10^{-6} sec,

$$\frac{Gc}{m\omega_\theta^2} = \frac{n_e m}{2\varepsilon_0 B_\theta^2} = \frac{10^{16} \times 9.1 \times 10^{-31}}{17.7 \times 10^{-12} \times 4.05 \times 10^{-4}}$$

$$\frac{Gc}{m\omega_\theta^2} = 1.27 \qquad 7.34$$

Therefore since $Gc/m\omega_\theta^2$ =1.27 $> 1-n \approx 0.5$
The electron motion in the (x,z)plane will be unstable. For simplicity we take $n'(1-n') = 1$, then with $\frac{dx}{dt} = 0$ at the time the motion becomes unstable, the solution to (7.21) is

$$x = x_0 \cosh\left[\frac{\omega_\theta^2}{\omega_c} t\right] \qquad 7.35$$

where x_0 is the initial position of the electron. When $x = \frac{\sqrt{2}}{4} b$ the electrons hit the vacuum chamber wall.

If we take $r_0 = b/14.43$ as before, we find that

$$t_w = \frac{\omega_c}{\omega_0^2} \cosh^{-1}\left[\frac{r}{r_0}\right]$$

$$= \frac{mB_\theta}{e B_0^2} \cosh^{-1}[5.1]$$

7.36

$$t_w = \frac{9.1\times10^{-31} \times .43}{1.6\times10^{-19} \times 4.05\times10^{-4}} \times 2.32$$

$$t_w = 1.41\times10^{-8} \text{ SEC.}$$

Thus when the motion becomes unstable the runaway electrons move to the vacuum chamber wall rapidly. The fact that the x-rays do not appear at the peak electric field is not surprising in view of the approximations made, ie, the assumed beam radius, electric field s trength, etc. Much more detailed electric field measurements are required in order to make this last analysis more quantitative.

In the last paragraphs we have shown that radiation damping is much too slow to account for apparent rapid collapse of the runaway stream. We have also shown that the magnitude of the observed radial field is indeed

large enough to cause unstable motion. We have not been able to shed light on the origin of the radial field, ie., does it come from a rapid collapse of the beam minor diameter or is it the result of a longitudinal energy loss?

So far in this analysis no mention has been made of collective plasma effects, with the exception of the self field of the beam. Since we have not been able to understand "t_{π}" on a single particle picture we must now look at the collective modes. In their analysis of the stability of relativistic self-focusing streams Finkelstein and Sturrock[42] have proposed several modes of instability and studied each mode in turn by means of a simple model. The first mode considered is the longitudinal two stream instability. If v_+ and v_- are the velocities of the ion and electron stream respectively and if the velocities are permitted to fluctuate about their equilibrium values as follows,

$$\delta v_{\pm} \propto e^{i(kz-\omega t)} \qquad 7.37$$

the dispersion relation appropriate to infinite plasmas has, in the non-relativistic approximation, the form

$$\frac{\omega_+^2}{(\omega - v_+ k)^2} + \frac{\omega_-^2}{(\omega - v_- k)^2} = 1 \qquad 7.38$$

where ω_+^2 and ω_-^2 are the plasma frequencies for the ions and electrons. The motion is stable for wave numbers which satisfy

$$k > k_c = \left(|v_+ - v_-| \right)^{-1} \left(\omega_+^{2/3} + \omega_-^{2/3} \right)^{3/2} \qquad 7.39$$

The stream we are interested in is non-relativistic therefore ω_+ will be much smaller than ω_- . If the electron stream were relativistic the opposite case could hold since the mass that enters into ω_- is the longitudinal electron mass $m = m_e \gamma^3$, $\gamma = \left[1 - v_-^2/c^2 \right]^{-1/2}$. The electron velocity will also be much greater than that of the ion, therefore, the stability criterion simplifies to

$$k > k_c \approx \frac{\omega_+}{v} = \left(\frac{n_+ e}{m \varepsilon_0} \right)^{1/2} \frac{1}{\lambda_D \omega_0} \qquad 7.40$$

Since $n_+^{1/2} \propto B_0$ and $\omega_0 \propto B_0$, the critical wave number is time independent. If we put $k_c = 2\pi/\lambda_c$ where $\lambda_c = 2\pi \lambda_D$, the critical beam density is $n = 5.8 \times 10^{10}/cm^3$ (evaluated at t=tx). The beam current that corresponds to this density is approximately 400 amp. This is more than two orders of magnitude larger than the observed runaway current. Therefore we can conclude that the two stream instability is not responsible for either the beam disruption or the small amount of runaway current.

Finkelstein and Sturrock also propose several

transverse instabilities that the electron and ion streams will be subject to, however their analysis does not include the strong azimuthal guide field that is present in this experiment. The non-relativistic stream without the B_θ field is subject to the m=0 or sausage type instability. The presence of the strong B_θ field probably removes this instability. Similarly the sinuous or kink instability and the instability due to a displacement of the beams relative to one another will probably be supressed.

The Negative Mass Instability (N.M.I.), as pointed out by Landau,[43] places a much lower limit on the maximum beam current than the two stream instability. A simple explanation of the cause of the instability is the following. Consider an azimuthally uniform distribution of cold particles in a beam. A small perturbation in the beam density will cause a perturbation in the electric potential rotating with the beam. Those particles ahead of the potential bump will be speeded up and those behind it will be slowed down. Those particles that were speeded up move radially outward because of the increased centrifugal force, and vice-versa. The amount of radial motion depends on the magnetic field shape. For weak focusing machines ($0 < n < 1$), the radial motion is large enough to overcompensate the increase in linear velocity so that the angular velocity decreases. Those particles that were

behind the bump are slowed down, move radially inward, and hence increase their angular velocity. The net effect is that the particles move toward the angular position of the potential bump and the perturbation grows. The angular acceleration is opposite to the force so that the particles behave as though they have a negative effective mass. Landau found that the two stream N.M.I. will be suppressed if the longitudinal velocity spread (Δv_z) in the stream satisfies

$$\frac{\Delta v_z}{c} > (\nu g)^{1/2} \qquad 7.41$$

where ν is Budker's parameter, i.e., the number of electrons per length of stream equal to the classical radius of the electron, and g is a geometrical factor. This criterion is most serious at injection time. Therefore if we put $\frac{1}{2} m (\Delta v_z)^2 = \frac{1}{2} m (\Delta v_\theta)^2 = \frac{1}{2} k T_e$ and since $g \approx 4$ the limiting line density ν_c is

$$\nu_c = \left(\frac{k T_e}{m_0 c^2}\right) \frac{1}{g} = \frac{1}{4} \left(\frac{10}{5.1 \times 10^5}\right) \qquad 7.42$$

$$\nu_c = 0.4 \times 10^{-5}$$

The measured ν is greater than ν_c by only an order of magnitude. Since there is considerable uncertainity in T_e and in the measured ν we cannot rule out the N.M.I. as the cause for the low runaway current.

At the beginning of this report we discussed the runaway electron calculations of Field and Fried.[19] Their calculation shows that the runaway current should increase linearly with time until a threshhold current $j = n_e e v_{THERMAL} \left(\frac{m_e}{m_i}\right)^{1/2}$ is reached. The runaways then begin to generate ion-acoustic waves and the runaway current drops to a very low value. Therefore if this were the mechanism for the beam disruption in this experiment, we would expect to see the x-ray emission start a short time after the decrease in the runaway current. In terms of the dimensionless variables $E=E_\theta / n_0 E_c$ and $\tau = \omega_p t$ the runaway current is found to increase linearly with time until

$$\tau \times \tau_1 = \left[125 E^{-1} \ln \left(23 E_\theta / E_c \right) \right]^{1/2} \qquad 7.43$$

ie, when the driving term becomes comparable with the ion-accoustic wave term. The ratio of the measured x-ray emission time to the x-ray emission time computed from eq.(7.43) is plotted in Fig.#38 for two values of B_θ . The plasma density used to evaluate τ_1 , was taken to be the measured runaway density since these are the only electrons that are able to make many complete circuits of the machine without colliding with the vacuum chamber walls. With B_θ =4900 gauss, the calculated x-ray emission time is approximately eight times smaller than the measured time

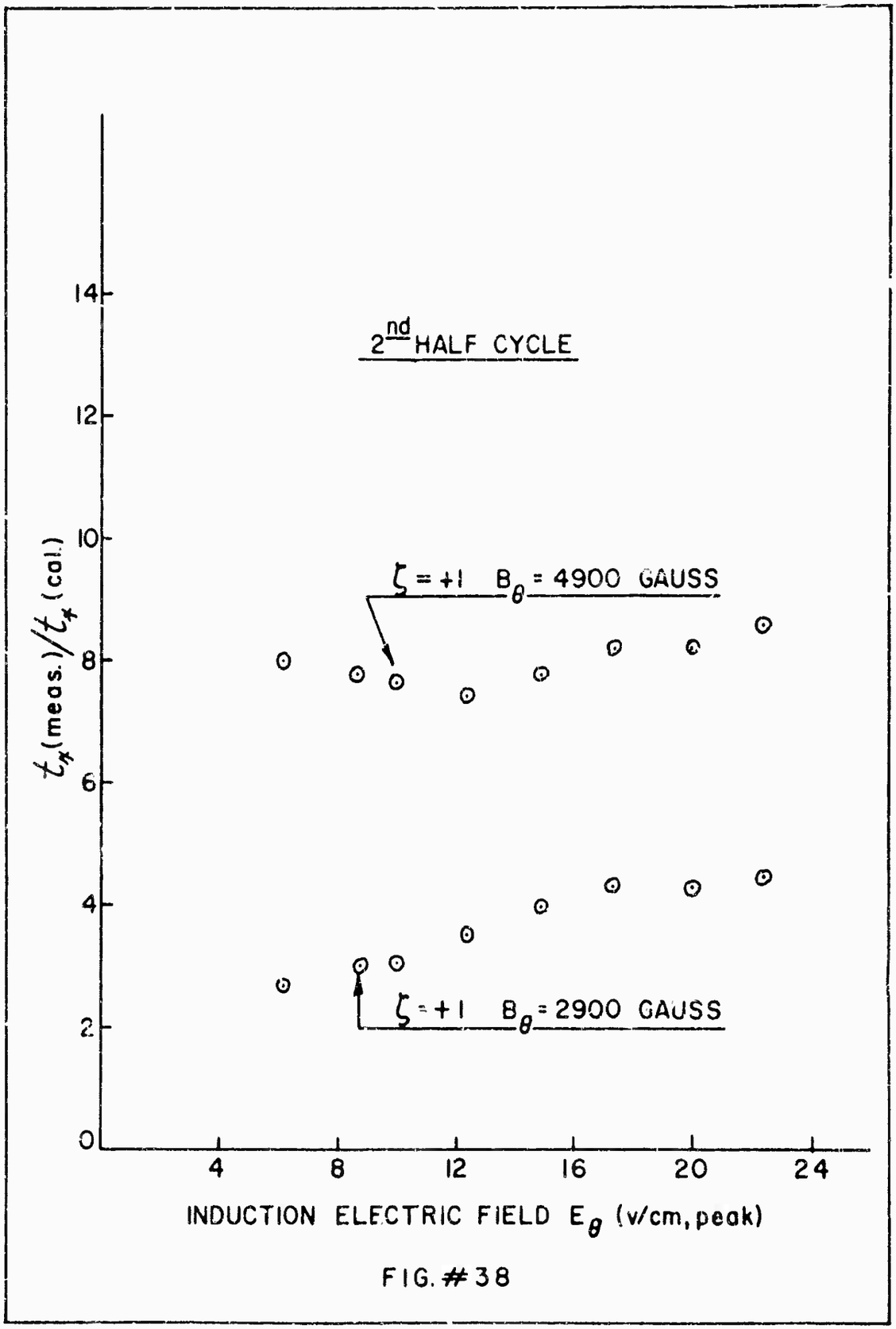
2nd HALF CYCLE
ζ = +1 Bθ = 4900 GAUSS
ζ = +1 Bθ = 2900 GAUSS
τ*(meas.)/τ*(cal.)
0
2
4
6
8
10
12
14
4
8
12
16
20
24
INDUCTION ELECTRIC FIELD Eθ (v/cm, peak)

FIG. #38

BLANK PAGE

and for B_θ =2900 gauss is only about four times smaller. For ζ=-1 the number of runaways increases with increasing electric field. The decrease is large enough to overpower $E^{-1/2}$ and the net result is that t_1, increases with E_θ. This is not observed experimentally (Fig.#23-26) and therefore the comparison for ζ =-1 is not displayed. The electric field measurements show that the equilibrium orbit lies near the outside wall of the acceleration chamber for ζ =-1. Undoubtly the wall plays a role in determining the number of runaways so that the data for this case is suspect. For ζ =+1 the equilibrium orbit lies near the center of the acceleration chamber, hence the effects of the walls will be reduced considerably.

It appears that the mechanism of Field and Fried can explain the beam disruption and subsequent x-ray emission. However equation (7.43) was derived for the case when $E\ell \ll 1$. In this experiment $E\ell \approx 10$ so that (7.43) does not strictly apply. Nevertheless their calculation describes qualitatively the experimental results.

We indicated in the introduction that there are approximately twenty different instabilities that can be generated by an electron beam that is moving through a plasma. The instabilities are usually grouped under two headings, a, those that arise because of Cerenkov excitation, i.e., when $\omega \approx k_n v_n$ and those associated with

the Doppler effect i.e., $\omega \simeq \omega_0 - k_\parallel v_\parallel$. An attractive possibility for this experiment is the occurrence of cyclotron overstability in the electro-static ion cyclotron wave.[44] This ionstability is generated by runaway electrons when the electron energy satisfies

$$W_E >> \left(\frac{m_i}{m_e}\right)(kT_i) \qquad 7.44$$

The x-ray emission time does not change when the ion mass in the experiment is increased by a factor of two. Thus it seems that this cannot be the mechanism responsible for the beam disruption.

In view of the need for more experimental data it does not seem advisable at this time to mention any more of the many possible beam-plasma interactions that could conceivably be responsible for the observed beam disruption.

VIII SUMMARY

We can now summarize the results of this experiment. The asymmetrical behavior with respect to the two directions of B_θ relative to E_θ can be explained by the presence of a small transverse magnetic field arising from the finite pitch of the B_θ coils.

The relatively small number of runaway electrons is probably due to either the Negative Mass Instability or the self electric field of the runaway stream.

The processes that are responsible for the beam disruption are still unknown, however the mechanism of Field and Fried describes qualitatively the x-ray emission time.

IX CONCLUSIONS

In this experiment we have endeavored to make the magnetic guide fields sufficiently homogeneous so that the total number of runaway electrons would not be limited because of magnetic imperfections. The field-coil geometry was chosen to minimize its inductance thus permitting rapid turn on of the betatron guide field. Care was also taken so that neither too much plasma was present at injection nor was its azimuthal distribution extremely non-uniform. In spite of these and other precautions taken the runaway current was only of the order of one ampere in agreement with that found in other plasma betatrons. Examination of the experimental data shows that the maximum beam current determined from the Schmidt criterion could only be reached by raising the value of the accelerating electric field to several thousand volts/cm.

In conclusion it seems that it is impossible to generate large runaway currents in a plasma betatron unless some means can be invented to overcome the effects of the self electric field and or the Negative-Mass-Instability. If these effects can be overcome the electron energy at "t_{χ}" may be sufficiently high to be of interest.

X ACKNOWLEDGEMENTS

The author would like to thank Professor K.C. Rogers for his tireless guidance and advice during this investigation. He would like to express his appreciation to Professor W.H. Bostick who suggested using a pulse transformer to make the electric field measurements, and E. Farber who made a pulse transformer available to us.

The author would also like to thank the many people who have contributed their labor and ideas to this experiment. C.T. Lunghard made most of the measurements described in section #6.1 and also designed a large portion of the electronics. The magnetic measurements in the auxilary field-coil (section #4.9), and the design of the vacuum system was done by I. Mansfield. The difficult job of machining the field-coil to the necessary accuracy was done under the careful supervision of A. Jermakian who was also responsible for the numerical integration in Appendix #1 as well as the method of presentation of the results (Fig.#39). G. Zepko provided valuable assistance with the magnetic field measurements in the experimental field-coil and in addition carried out the numerical integration in Appendix #3.

Last but certainly not least, J. Mezzina transformed the authors horrible sketches into precisely machined designs.

XI APPENDIX #1

In this section we calculate the transient penetration of a magnetic field into a conducting material. For computational ease we consider a semi-infinite half space of material with conductivity σ and permeability μ. The first problem we consider is that of a constant magnetic field applied at t=0. The diffusion of B_z into the conducting half-space is given by a diffusion equation.

$$\frac{\partial^2 B_z}{\partial x^2} - \mu\sigma \frac{\partial B_z}{\partial t} = 0 \qquad 11.1$$

The solution of this equation subject to the condition that

$$B_z(0,t) = 0 \qquad t < 0$$

$$B_z(0,t) = B_0 \qquad t > 0 \qquad 11.2$$

is given by

$$B_z = B_0\left[1 - \operatorname{erf}\left\{\frac{(\mu\sigma)^{1/2}x}{2t^{1/2}}\right\}\right] \qquad 11.3$$

Let us now compute the time (t_p) at which the magnetic field at $x = \left(\frac{2}{\mu\sigma\omega}\right)^{1/2}$ i.e., the skin depth, is equal to $\frac{1}{2}$ the value of the field at the surface.

$$\operatorname{erf}\left[\frac{1}{(2t_p\omega)^{1/2}}\right] = 0.5$$

$$\frac{1}{(2 t_p \omega)^{1/2}} = 0.68$$

Thus with $= .39 \times 10^{6}$ RAD/sec

$$t_p = 1.4 \times 10^{-6} \text{ SEC.}$$

Since the quarter period of the betatron field is only 4μ sec, the step function magnetic field approximation is not a good one. We now solve the diffusion equation with the conditions that

$$B_z(0,t) = 0 \qquad t < 0$$

$$B_z(0,t) = B_0 \sin \omega t \qquad t > 0$$

We have seen that the function

$$B_z(x,t) = B_0 \left[1 - \operatorname{erf} \left\{ \frac{x}{2(\kappa t)^{1/2}} \right\} \right] \qquad 11.3$$

where $\kappa = \frac{1}{\mu \sigma}$, has the property that $B_z(x,0) = 0$ and $B_z(0,t) = B_0$ Thus the function

$$B_z(x,t,t') = g(t') \left[1 - \operatorname{erf} \left\{ \frac{x}{2(\kappa t)^{1/2}} \right\} \right] \qquad 11.4$$

is the function which satisfies the one dimensional diffusion equation and the conditions $B_z(x, o, t') = 0$, $B_z(0, t, t') = g(t')$. Therefore by applying Duhamel's Theorem (45) the solution to the boundry-value problem $B_z(x, o) = 0$, $B_z(0, t) = g(t)$ is given by

$$B_z(x,t) = \frac{\partial}{\partial t}\int_0^t B_z(x, t-t', t')\, dt' \qquad 11.5$$

With $g(t) = B_o \sin \omega t$

$$B_z(x,t) = \frac{\partial}{\partial t}\int_0^t B_o \sin \omega t' \left(\frac{2}{\pi^{1/2}}\right)\int_{\frac{x}{2[k(t-t')]^{1/2}}}^{\infty} e^{-u^2}\, du \qquad 11.6$$

If we carry out the differentiation under the integral sign and let $\chi = \omega t$, $\chi' = \omega t'$, $\delta = 2/(\mu\sigma\omega)^{1/2}$ and $\rho = x/\delta$

the magnetic field is given by

$$B_z(x,\rho) = \frac{B_o \rho}{\pi^{1/2}}\int_0^{\chi} \frac{\sin(\chi-\chi')}{\chi'^{3/2}}\, e^{-\rho^2/\chi'}\, d\chi' \qquad 11.7$$

The integral can be evaluated numerically. This has been done for $\rho = 1$. The result is plotted in Fig. #39 together with the steady state solution

$$B_z(x,\rho) = B_o\, e^{-\rho\sqrt{2}} \sin(\chi - \rho\sqrt{2}) \qquad 11.8$$

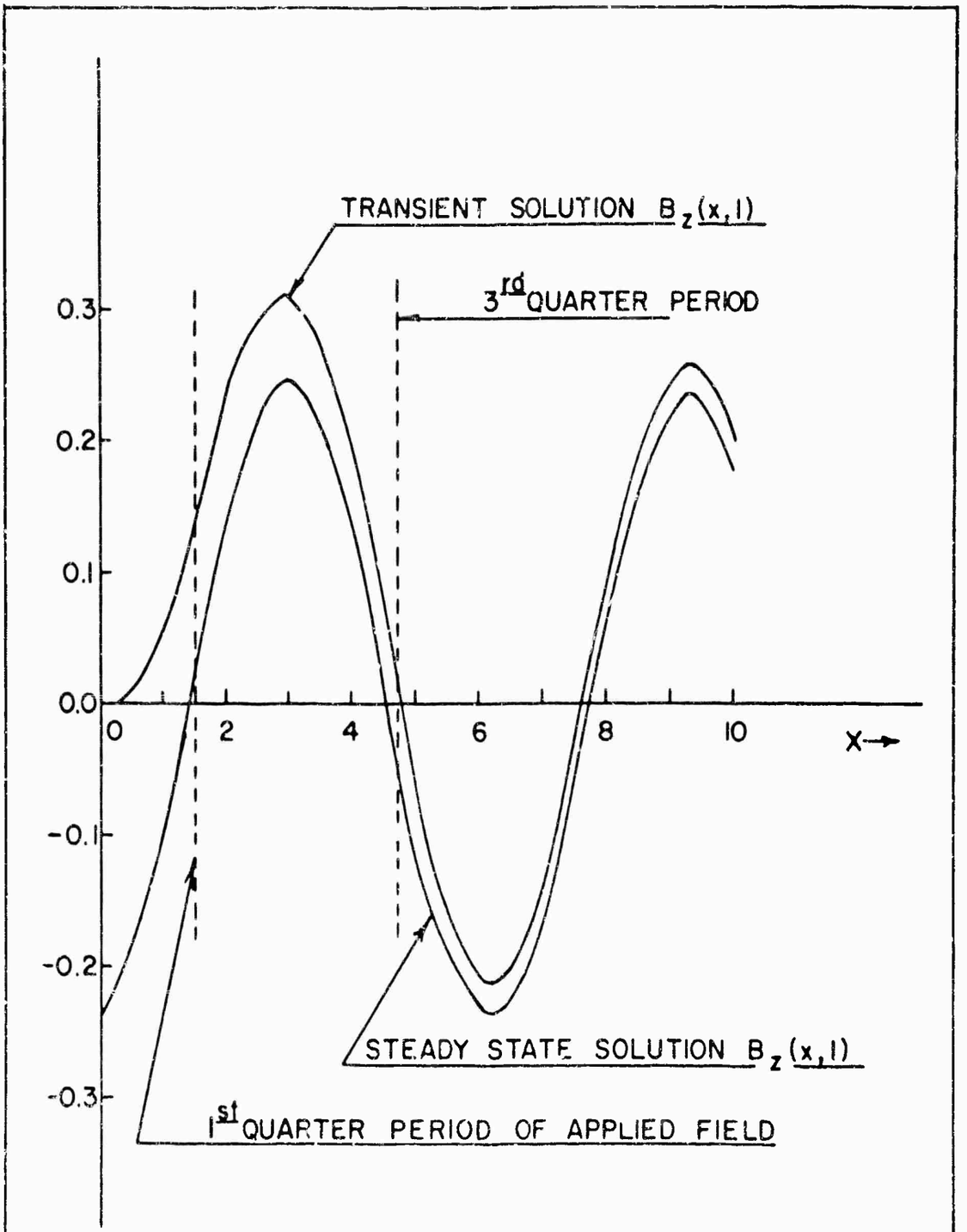

MAGNETIC FIELD IN COPPER AT A DISTANCE OF ONE SKIN DEPTH

FIG. # 39

BLANK PAGE

The $\sqrt{2}$ factor occurs because the most convenient definition for the skin depth in the transient analysis differs by this factor from the usual definition employed in the steady state analysis, *viz.* $(2/\mu\sigma\omega)^{1/2}$. We see from the plot that during the first quarter period of the applied field the penetration is substantially less than is predicted on the basis of the steady state solution. This gives us some confidence that the field shape during this time has a weak time dependence. However by the end of the third quarter period of the applied field the penetration is well described by the steady-state solution. Thus we would expect important differences between the field shapes at the end of the first and third quarter periods, but not between the third and fifth quarter periods. This is in agreement with our measurements (see Fig.#8). These results show that in a coil employing flux concentrators for field shaping, an A.C. steady state method of mapping the field will not give an accurate picture of the transient field shape occuring during the first quarter period following turn "on"; a transient measurement of the field shape must be carried out.

XII APPENDIX #2

In this section we calculate the error in the single turn-coil signal that arises from a lateral shift in the coils. We suppose that the center of the pick-up coil is displaced a distance "a" from the geometric axis of the coil. We would like to know the error in the measured signal that is produced by this displacement.

The voltage induced in the single turn coil is given by

$$V = \oint \vec{E} \cdot d\vec{l} \qquad 12.1$$

where the integration is carried out along the coil. The elemental path of integration is given by

$$dl = \left[r^2 + \left(dr/d\theta \right)^2 \right]^{1/2} d\theta \qquad 12.2$$

Therefore

$$V = \int_0^{2\pi} E_\theta \cos\psi \left[r^2 + \left(dr/d\theta \right)^2 \right]^{1/2} d\theta \qquad 12.3$$

With $\cos\psi = \left[1 - \frac{a^2}{b^2} \sin^2\theta \right]^{1/2}$ and the equation for the displacement circle $r = a\cos\theta + b\left[1 - \frac{a^2}{b^2} \sin^2\theta \right]^{1/2}$ expanded to first order in "a", eq.12.3 becomes

$$V = b \int_0^{2\pi} E_\theta \left[1 - \frac{a}{b} \cos\theta \right] d\theta \qquad 12.4$$

Since $E_\theta = -\frac{\partial A_\theta}{\partial t} = \alpha A_\theta$, $\alpha = CONST.$ we may write for E_θ

$$E_\theta = \alpha A_0 \left[1 + \tfrac{1}{2}(1-n)\left(\frac{x}{\rho_0}\right)^2\right] \qquad 12.5$$

where A_0 is the value of the vector potential at the equilibrium orbit, "n" is the field index and $x = a\cos\theta - \frac{1}{2}\frac{a^2}{\rho_0}\sin^2\theta$. Thus to second order in "a" the induced voltage is

$$V = \alpha\rho_0 A_0 \int_0^{2\pi} \left[1 + \frac{a}{\rho_0}\cos\theta + \frac{1}{2}\frac{a^2}{\rho_0^2}\cos 2\theta + \frac{1}{2}(1-n)\frac{a^2}{\rho_0^2}\cos^2\theta\right] d\theta \qquad 12.6$$

$$V = 2\pi\alpha\rho_0 A_0\left[1 + \frac{1}{4}(1-n)\frac{a^2}{\rho_0^2}\right] \qquad 12.7$$

The signal from the undisplaced loop is $V_0 = 2\pi\alpha\rho_0 A_0$

Hence the fractional error introduced by the shift is

$$\frac{\delta V}{V_0} = \frac{V - V_0}{V_0} = \frac{1}{4}(1-n)\frac{a^2}{\rho_0^2}$$

Typical lateral displacement are $\approx$ 0.005", therefore with ρ_0 =1.9", and n=0

$$\frac{\delta V}{V_0} = \frac{1}{4}\left[\frac{25\times10^{-6}}{3.61}\right] = 1.7\times10^{-6}$$

Thus we see that small lateral displacements of the single turn pick-up coils will not introduce significent errors into the measurement of the radial distribution of the vector potential.

XIII APPENDIX #3

Electr' Quadrupole Coil Design

A four-coil electric quadrupole system has been designed to provide the oscillating R.F. electric field for creation of a low density plasma in the vacuum chamber.

The electric field resulting from four ring charges (of equal absolute magnitudes) in a quadrupole array will vanish along a circular line in the median plane. We want this line to coincide with the location of the minimum in the betatron field vector potential. The expression for the median plane value of the z component of the quadrupole electric field was computed as a function of the radial position ρ measured from the axis of the field coil. The position of the null (ρ_0) was then determined by interpolation. Values were assigned to z_1 and z_2 , the distances of the coils above and below the median plane, and to a_1 , and a_2 the radii of the coils, and E_z was evaluated for various combinations of ρ, a_1, z_1, a_2, z_2 from the expression

$$E_z = \frac{Q}{\pi^2 \varepsilon_0} \left\{ \frac{E(k_1)\, z_1}{\left[(a_1-\rho)^2 + z_1^2\right]\left[(a_1+\rho)^2 + z_1^2\right]^{1/2}} \right.$$

$$\left. + \frac{-E(k_2)\, z_2}{\left[(a_2-\rho)^2 + z_2^2\right]\left[(a_2+\rho)^2 + z_2^2\right]^{1/2}} \right\} \qquad 13.1$$

where $k^2 = \frac{4aρ}{(a+ρ)^2+z^2}$ and E(k) is an elliptic integral of the first kind. The results of the computation are plotted in Fig. #40.

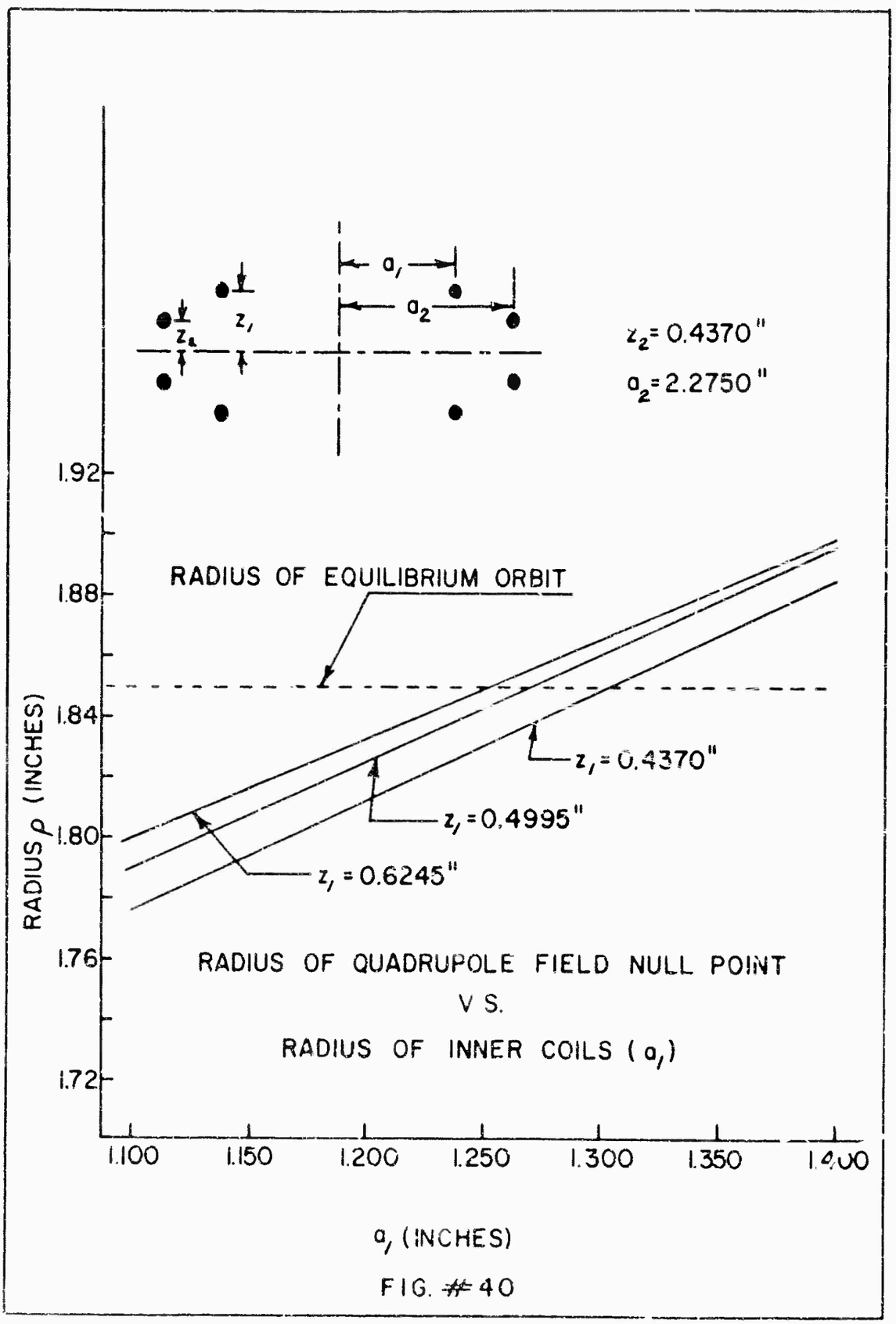
a1
a2
z1
z2
z2 = 0.4370"
a2 = 2.2750"
1.92
1.88
1.84
1.80
1.76
1.72
RADIUS ρ (INCHES)
RADIUS OF EQUILIBRIUM ORBIT
z1 = 0.4370"
z1 = 0.4995"
z1 = 0.6245"
RADIUS OF QUADRUPOLE FIELD NULL POINT
V S.
RADIUS OF INNER COILS (a1)
1.100
1.150
1.200
1.250
1.300
1.350
1.400
a1 (INCHES)

FIG. #40

XIV REFERENCES

1. G.I. Budker, Cern Symposium on High Energy Accelerators and Meson Physics, Vol I, Geneva (1956).

2. W.H. Bennett, Phys. Rev. 45 890 (1934),98,1584 (1955).

3. D. Finkelstein and C. Maisonnier, CERN 59-11 (1959).

4. G. Schmidt, Jour. Nuc. Energy Part C3, 156 (1961).

5. Ya. B. Fainberg, Jour. Nuc. Energy Part C4,203 (1962).

6. K.C. Rogers, D. Finkelstein, L.Ferrari, D. Caulfield, I. Mansfield, and G. Brucker, International Conf. on High-Energy Accelerators and Instrumentation CERN (1959).

7. J.G. Linhart, Proc. of the 4th Inter. Conf. on Ionization Phenomena in Gases, Uppsala, 981 (1959).

8. P. Reynolds, H.M. Skarsgard, Jour. Nuc. Energy Part C I,36 (1959).

9. J. Drees, Diplomarbeit, Bonn., July 1960.

10. L.T. Shepherd, and H.M. Skarsgard Phys. Rev. Letters 10, 121 (1963).

11. H.P. Furth, R.W. Waniek, Rev. Sci Inst 27, 195 (1956). Furth, H.P., M.A. Levine, R.W. Waniek, Rev Sci Inst. 28, 949 (1957).

12. D. Finkelstein A.E.C. Report NYO-7735, (1957),

13. H.Dreicer, Proceedings of the Second United Nations International Conference on the Peaceful Uses of Atomic Energy V#31, pg. 57

14. H. Dreicer, Phys. Rev. 115 238 (1959).

15. L.M. Kovrizhngkh, Soviet Physics JETP 37 989 (1960).

16. A.V. Gurevich, Soviet Physics JETP 12 904 (1961).

17. I.B. Bernstein, and I.N. Rabinowitz, Proc. of the 4th Int. Conf. on Ionization Phenomena in Gases. Uppsala. 634 (1959).

18. M.D. Kruskal and I.B. Bernstein, Physics of Fluids 7, 40 (1964).

19. E.C. Field, and B.D. Fried, Physics of Fluids 7, 1937 (1964).

20. D. Kerst and K. Serber, Phys. Rev. 60 53 (1941).

21. F.K. Goward, Proc. of the Phys. Soc. 61 284 (1948).

22. J.G. Linhart, Plasma Physics, North-Holland Publishing Company 1960, ch#1.

23. G. Schmidt, Plasma Physics Notes, Stevens Inst. of Technology. 1960, ch#1.

24. G.N. Glasor, and J.V. Lebacq Pulse Generators, V5 Radiation Laboratory Technical Series, McGraw-Hill.

25. M.H. Dazey, V. Josephson, R.F. Wuerker, Space Technology Lab. STL/TR 60-0000-09255.

26. D. Ridney, L. Kaaus, H. Malamud, Republic Aviation Corporation PPL-TR-61-4 (258).

27. E. Gill and A. von Engel Proc. Phys. Soc. A192 446 (1948).

28. H.J. Oskam, and V.R. Mittelstadt Phys. Rev. (to be published).

29. D.R. Inglis and E. Teller Astrophys. Jour. 90 439 (1939).

30. H. Margenau and M. Lewis Rev. of Mod. Physics 31 569 (1959).

31. W.S. Cooper et al. Univ. of California Lawrence RAD Lab UCRL-9509.

32. H. Huff Technical Memo #8 Vitro Laboratories.

33. D.Simon Private Communication.

34. R.D. Evans, The Atomic Nucleus, McGraw -Hill co. 1955 ch 21.

35. H.J. Huber and K.C. Rogers, Rev. Sci. Inst. 35 801 (1964).

36. G.W. Grodstein, National Bureau of Standards Circular #583.

37. E.B. Meservey and L.P. Goldberg Princeton University, Plasma Physics Lab.Rept. Matt.#68 (I96I)

38. W. Bernstein, F.F. Chen, M.A. Heald, A.Z. Kranz Physics of Fluids I 430 (1958).

39. K.C. Rogers
Theory of Space Charge Neutralized Betatrons.
Stevens Institute of Technology. Unpublished (I960)

40. L.I. Schiff Quantum Mechanics, Mc-Graw Hill Book Co. 1955, ch#7.

41. E.R. Harrison, Jour. of Nuc. Energy Part C 4,7 (1962).

42. D. Finkelstein, P.A. Sturrock, Plasma Physics, Mc-Graw Hill Book Co. (1961), Edited by J.E. Drummond. Ch#8.

43. R.W. Landau, PhD. Thesis, Stevens Inst. of Technology (1963).

44. T.H. Stix. Theory of Plasma Waves, Mc-Graw Hill Co. (1962), Ch#9.

45. I. Sneddon, Elements of Partial Differential Equations, Mc-Graw Hill Book Co. 1957 Ch#6.

46. F.W.Crawford, G.S.Kino, A.B.Cannara
J. Appl. Phys. 34, 3I68 (I963). An extensive list of references can also be found here.

EARLY-TIME COLLECTIVE EFFECTS

IN A PLASMA BETATRON

S.J. Lukasik
K.C. Rogers

ABSTRACT

Electrostatic collective effects occurring during startup have been examined numerically in a simple model of a plasma betatron having a uniform guide field, vector potential $A_\varphi(r,t) = 0.5\, B_o \left[r + 1.3\, r_1^2/r\right] \sin\omega t$. A region in the neighborhood of the equilibrium orbit, populated by an initially uniform zero temperature distribution of electrons and infinitely heavy ions, was divided into cells. The trajectory of each particle of a cell was taken to be that of the central particle. The electrostatic force acting on a particle during a time step was obtained by extrapolating the charge distributions obtained during preceding time steps. Typical values of parameters were: electron density $0 \le n \le 10^{12}$ cm^{-3}, $B_o = 50$ kilogauss, $\omega = 10^6$ sec^{-1}, $r_1 = 5$ cm. For $n \le 10^8$ cm^{-3}, the electrostatic forces on the electron beam are negligible and pure betatron motion ensues. Radial betatron oscillations are observed and the electron beam slowly collapses to the equilibrium betatron orbit. For $n \ge 10^{12}$ cm^{-3}, the electrostatic forces determine the radial motion of the beam. The collapse of the beam to the equilibrium betatron orbit is completely inhibited. Radial plasma oscillations $\omega_r \approx \omega_p = (ne^2/\varepsilon_o m)^{1/2}$ excited by the betatron oscillations $\omega_b = (e/m)B_o \sin\omega t$ are observed. Intermediate values of charge density lead to beam behavior that shows a gradual transition from the pure-betatron case to the pure-plasma oscillation case. In all cases the plasma oscillations were found to be stable. The presence of a sufficiently strong B_φ field completely suppressed the radial plasma oscillations.

BLANK PAGE

Early-Time Collective Effects in a Plasma Betatron

S.J. Lukasik and K.C. Rogers
Stevens Institute of Technology, Hoboken, New Jersey

I INTRODUCTION

Previous calculations related to the early-time conditions in a plasma betatron were concerned with the maximum allowable temperature of the plasma that would lead to the capture of electrons into stable betatron orbits.[1] The study consisted of calculating single-particle trajectories for a variety of initial kinematic conditions and magnetic field shapes and observing for what values of the various parameters the electrons escaped from the region of the vector potential well. For these calculations all collective effects such as the electric and magnetic self-fields of the beam were ignored.

In the work reported here, the effect of the collective electrostatic field that develops during the start-up of a plasma betatron is studied. In so doing, the initial temperature of the plasma has been largely ignored, being assumed to be $0^{o}K$.

A self-consistent calculation is performed in the following way. A finite width beam is divided into a number of "macroparticles" whose subsequent motion is taken to be identical to that of a single particle located at their center. At any time increment, the electrostatic force on a particle is calculated using the negative charge density distribution resulting from the positions of all of the macroparticles at the end of the previous time increment. The positive charge is assumed to remain fixed in its initial uniform distribution. A Runge-Kutta technique is used to advance each of the macroparticles by a time increment. As the new radial position of each macroparticle is calculated, it is distributed into radial accumulators, the sum in each becoming the charge distribution to be used during

This approach has been utilized recently to study several problems involving collective effects in plasmas. Buneman[2] and Dawson[3] considered the large amplitude limit of longitudinal plasma oscillations, the thermalization and ergodic behavior of an equilibrium plasma, and the development of the two-stream instability by means of a one-dimensional model. Similarly, Burger[4] has studied the charge distribution in a one-dimensional plasma diode with arbitrary boundary conditions. Hockney[5] has examined the oscillations of a two-dimensional plasma. Dunn and Ho[6] have calculated the approach to equilibrium in a one-dimensional diode as the result of an electron beam traversing and continually ionizing a background gas. In all of these numerical calculations the object has been to study the evolution in time of a system consisting of a number of charge elements each of which is acted on by the long-range electrostatic forces of all of the other charge elements.

II EQUATIONS OF MOTION

The non-relativistic Hamiltonian function for a single electron in an axially-symmetric magnetic field is given in cylindrical coordinates (r,φ,z) by

$$H = \frac{P_r^2}{2m} + \frac{1}{2m}(P_z + eA_z)^2 + \frac{1}{2m}\left(\frac{P_\varphi}{r} + eA_\varphi\right)^2 \tag{1}$$

This leads to the equations of motion

$$P_z = mv_z - eA_z = \text{const} \tag{2}$$

$$P_\varphi = mv_\varphi - erA_\varphi = \text{const} \tag{3}$$

$$m\ddot{r} = -\frac{\partial}{\partial r}\frac{1}{2m}\left[(P_z + eA_z)^2 + \left(\frac{P_\varphi}{r} + eA_\varphi\right)^2\right] \tag{4}$$

where the bracketed quantity in eq. (4) plays the role of an effective potential

$$V_{eff} = \frac{1}{2m}\left[(P_z + eA_z)^2 + \left(\frac{P_\varphi}{r} + eA_\varphi\right)^2\right]$$

For this work we have chosen the following model for the magnetic field

(a) the axial component of the magnetic field B_z

$$B_z(r,t) = \frac{1}{r}\frac{\partial}{\partial r}\left[r\,A_\varphi(r,t)\right]$$

and the associated component of the vector potential A_φ is shown in Fig. 1. The field has a value $B_1 \sin\omega t$ out to a radius r_1 and a value $B_2 \sin\omega t$ between r_1 and r_2. For the region $r_1 \le r \le r_2$, A_φ is given by

$$A_\varphi(r,t) = \frac{1}{r}\int_0^r B_z(r',t)\,dr' = \frac{B_2}{2}\left[r + (p-1)\frac{r_1^2}{r}\right]\sin\omega t \tag{5}$$

(b) the azimuthal component of the magnetic field B_φ also shown in Fig. 1 is independent of time. By Ampere's law

$$B_\varphi = B_3 r_1 / r$$

and hence

$$A_z(r) = -\int_{r_1}^{r} B_\varphi(r')dr' = -\, q\, B_2\, r_1 \ln r/r_1 \qquad (6)$$

where $q = B_3/B_2$

The azimuthal canonical angular momentum, P_φ, can be chosen arbitrarily. The axial canonical momentum, P_z, can be expressed using eq. (2) as

$$P_z = -\, eA_z(r(0)) \qquad (7)$$

where $r(0)$ indicates the initial radial position of the electron and where v_z has been set equal to zero initially.

The equations of motion can be conveniently non-dimensionalized by introducing the following quantities:

ω = angular frequency of the betatron guide field
$B(t) = B_o \sin\omega t$

ω_o = electron cyclotron angular frequency in the orbit region
$\omega_o = e\, B_2/m$

$x = \omega t$

$p = B_1/B_2$

$R = r/r_1$

$\beta = \omega_o/\omega$

$\alpha = P_\varphi/m\, \omega_o r_1^{\,2}$

In terms of these quantities, the radial and azimuthal equations of motion (3) and (4) for $1 \le R \le p-1$ can be written, using eqs. (5)-(7),

$$\frac{d^2R}{dx^2} = \frac{\beta^2}{R^3}\left[\alpha + \frac{p-1}{2}\sin x\right]^2 - \frac{\beta^2}{4} R \sin^2 x - \frac{q^2\beta^2}{R} \ln\left(\frac{R}{R(0)}\right) \tag{8}$$

$$\frac{d\varphi}{dx} = \frac{\beta}{R^2}\left[\alpha + \frac{1}{2}\left\{R^2 + (p-1)\right\}\sin x\right] \tag{9}$$

These can be solved numerically using a Runge-Kutta fourth-order technique. Writing the radial equation (8) as two simultaneous first-order equations, we have

$$\frac{dR}{dx} = S(x,R,S) \tag{10}$$

$$\frac{dS}{dx} = \frac{\beta^2}{R^3}\left[\alpha + \frac{p-1}{2}\sin x\right]^2 - \frac{\beta^2}{4} R \sin^2 x - \frac{q^2\beta^2}{R} \ln\left(\frac{R}{R(0)}\right) = T(x,R,S) \tag{11}$$

subject to the initial conditions

$$\begin{aligned} R &= R_o \\ S &= S_o \\ x &= x_o \end{aligned} \tag{12}$$

The evaluation of the azimuth $\varphi(x)$ is simple when $R(x)$ is known since all of the quantities on the right-hand side of eq. (9) are then known. According to the Runge-Kutta procedure that has been used, to fourth order in Δx, [7]

$$\Delta R = (\Delta' + 2\Delta'' + 2\Delta''' + \Delta^{iv})/6 \tag{13}$$

$$\Delta S = (\delta' + 2\delta'' + 2\delta''' + \delta^{iv})/6 \tag{14}$$

where

$$\Delta' = S(x_o, R_o, S_o)\Delta x \tag{15a}$$

$$\Delta'' = S(x_o + \tfrac{1}{2}\Delta x, R_o + \tfrac{1}{2}\Delta', S_o + \tfrac{1}{2}\delta')\Delta x \tag{16a}$$

$$\Delta''' = S(x_o + \tfrac{1}{2}\Delta x, R_o + \tfrac{1}{2}\Delta'', S_o + \tfrac{1}{2}\delta'')\Delta x \tag{17a}$$

$$\Delta^{iv} = S(x_o + \Delta x, R_o + \Delta''', S_o + \delta''')\Delta x \tag{18a}$$

$$\delta' = T(x_o, R_o, S_o)\Delta x \tag{15b}$$

$$\delta'' = T(x_o + \tfrac{1}{2}\Delta x, R_o + \tfrac{1}{2}\Delta', S_o + \tfrac{1}{2}\delta')\Delta x \tag{16b}$$

$$\delta''' = T(x_o + \tfrac{1}{2}\Delta x, R_o + \tfrac{1}{2}\Delta'', S_o + \tfrac{1}{2}\delta'')\Delta x \tag{17b}$$

$$\delta^{IV} = T(x_o + \Delta x, R_o + \Delta''', S_o + \delta''')\Delta x \tag{18b}$$

Thus, to advance one time step Δx, one must calculate ΔR and ΔS using eqs. (13) and (14). This is done by evaluating eqs. (15a) and (15b), (16a) and (16b), (17a) and (17b), and (18a) and (18b) in that order.

Equation (8) is an expression for the radial acceleration of an individual particle; i.e., it is the radial force per unit mass on a particle having as initial conditions eqs. (12). Suppose, however, that a region of space is filled with a neutral plasma all of whose particles are initially accelerated as described by eq. (8); due to the varying trajectories of the electrons and ions as a result of the differences in mass and initial conditions, there will be a tendency for an electrostatic space charge to develop. The resultant electrostatic field will then influence the subsequent motion of the individual particles making up the plasma. The object of the present calculation is a self-consistent solution of eq. (8) augmented by the electrostatic space-charge force.

To derive this additional force on the particle, note that by Gauss's law the electrostatic force for a charge distribution having radial symmetry and uniform in the z direction is purely radial and is given by

$$E_r = q_{in}/2\pi\,\epsilon_o r$$

where q_{in} is the net positive charge inside the radius r. Then

$$\text{acceleration} = e\,E_r/m = e\,q_{in}/2\pi\,m\,\epsilon_o r$$

where, for unit height in the z-direction

$$q_{in} = e \int_o^r (N_- - N_+)\ 2\pi r'\ dr'$$

The N's are positive and negative charge densities. The N's are written as

$$N_+ = n_+ N_o$$

$$N_- = n_- N_o$$

so that

$$\frac{F_e}{m} = \frac{e^2}{m \epsilon_o r} \frac{N_o}{r} \int_o^r (n_- - n_+)\ r'\ dr'$$

The quantity N_o represents the initial uniform charge density per unit volume and hence the n's represent the charge density relative to the initial charge density. Taking the plasma frequency ω_p as

$$\omega_p^2 = e^2 N_o / m \epsilon_o \tag{19}$$

the non-dimensional radial acceleration due to the electrostatic force is

$$\left.\frac{d^2R}{dx^2}\right|_{elect} = \frac{1}{r_1 \omega^2} \frac{F_e}{m} = \frac{\gamma^2}{R} \int_o^R (n_- - n_+)\ R'\ dR' \tag{20}$$

where

$$\gamma^2 = \omega_p^2 / \omega^2$$

Thus, electrostatic forces on the motion of any particle can be included by adding the right hand side of eq. (20) to the right-hand side of eq. (8). This amounts to replacing eq. (11) by

$$\frac{dS}{dx} = T(x,R,S) = \frac{\beta^2}{R^3}\left[\alpha + \frac{p-1}{2} \sin x\right]^2$$

$$- \frac{\beta^2}{4} R \sin^2 x - \frac{q^2\beta^2}{R} \ln\left(\frac{R}{R(0)}\right) + \frac{\gamma^2}{R} \int_o^R (n_- - n_+)\ R'\ dR' \tag{21}$$

The total negative charge present is

$$q_{total} = e\int_0^\infty N_- \, 2\pi r' \, dr' = eN_o 2\pi \int_0^\infty n_-(r') \, r' \, dr' \qquad (22)$$

The significant difference between eqs. (11) and (21) is that the former describes the trajectory of a single particle in a given magnetic field while the latter includes the collective effect of the instantaneous positions of all of the other particles on the trajectory of a single particle. The numerical solution of eq. (21) requires a fundamentally different procedure since now it is necessary to determine simultaneously the trajectories of an ensemble of particles.

III COMPUTATIONAL PROCEDURES

The calculation of the early-time behavior of a plasma betatron assumes an infinitely long cylindrical plasma annulus filled uniformly with electrons in a fixed matrix of positive charge as shown in Fig. 2(a). The total initial width of the plasma region, hereafter referred to as the beam, is divided into a number of equal radial width sections called macroparticles. Each macroparticle thus represents a part of the initial uniform charge distribution. Throughout the subsequent motion the width of each macroparticle is kept constant. The motion of each macroparticle is taken to be that of a characteristic electron located at the mid-radius of the macroparticle. Thus all the charged particles represented by a macroparticle are assumed to follow the same trajectory.

For the calculations reported here, it has been assumed that $p = B_1/B_2 = 2.3$. This means that the vector potential well has a (dimensionless) extent from an inner radius $R = 1.00$ to an outer radius $R = 1.30$. The initial charge distribution has been restricted to a region near the minimum of the vector potential well at $R = 1.14$ whose width is only 20 percent of the width of the well. This avoids complications arising from the possible loss of negative charge from the beam as a result of large amplitude transverse oscillations.

Since the positive charge is assumed to remain fixed at its initial position, only the negative charge density need be carried in the calculations as an explicit variable. An initial uniform charge density is specified by the value of γ^2 which is proportional to N_o , the number of charged particles per unit volume. The radial dependence of the charge distribution is given by the values of the relative negative charge density n_- in a number of equal width radial cells. These cells form a fixed radial network that assists in the charge "accounting" that must be performed

throughout the calculation. This network or mesh extends from some lower radial limit that is less than the inner radius of the beam to an upper radial limit that is greater than the outer radius of the beam. It is important for the successful operation of the program that the mesh always be at least as extensive as the radial charge distribution of the beam.

Since the motion of a charged particle depends on the radial dependence of the electrostatic charge distribution (see eq. (21)), it is necessary to specify this with as much accuracy as possible. On the other hand, running time and computer storage capacity place upper limits on the time and space resolution of the calculation. The time resolution is determined by the size of the time step while the space resolution is determined by both the number of macroparticles into which the beam is divided and by the radial mesh used in describing the charge density. For most of the work reported here, the beam was divided into six macroparticles and the radial mesh used to describe the charge density had a spacing one-tenth that of the width of a macroparticle. These geometric relationships are shown in Fig. 2(b).

On the basis of this description, the details of the calculation that are of importance for evaluating the results can be examined. It is especially important to be able to distinguish between computed results that are characteristic of the physical system under investigation and results that are simply characteristic of the numerical procedures involved.

The first step indicated in the flow chart in Fig. 3 is to read in the parameters needed to specify the calculation. Next the initial conditions for the first time step must be established. These are of two types: the initial charge distribution in the beam and the initial kinematic conditions for the macroparticles.

Setting the initial charge distribution consists of specifying the width of each of the radial intervals of the charge mesh, d, the radial position of the center of the innermost mesh point $\rho(1)$, zero values for the relative negative charge density in a number of inner "buffer" intervals $n_-(1)....n_-(j_\ell)$, unit values for the relative negative charge density $n_-(j_\ell+1)....n_-(j_u)$ corresponding to the initial position of the beam, and zero values for the relative negative charge density in a number of outer "buffer" intervals $n_-(j_u+1)....n_-(j_{max})$. The relative positive charge density for all time is understood to have the same distribution, viz.

$$\begin{aligned} n_+(j) &= 0 \qquad & 1 \le j \le j_\ell \\ n_+(j) &= 1 \qquad & j_\ell + 1 \le j \le j_u \\ n_+(j) &= 0 \qquad & j_u + 1 \le j \le j_{max} \end{aligned} \tag{23}$$

The initial kinematic conditions are the initial position and velocity of each macroparticle. Since z-motion is ignored in the model employed here, these consist of the radial and azimuthal positions and velocities. As shown in Fig. 2(b), the initial radial positions are simply the mid-radius of each macroparticle. The initial radial velocity of each macroparticle is assumed to be zero. The initial azimuthal velocity $v_\varphi(0)$, specified by α, has been set equal to zero in all of the calculations that have been performed.

After establishing the necessary initial conditions, a series of j_{max} variables called accumulators representing successive charge mesh intervals are set equal to zero. As each macroparticle is advanced to a new radial position during a time step, the values of the appropriate accumulator variables are suitably incremented. Since the beam width does not in general remain constant, the macroparticles may overlap and so during the course of a time step an accumulator may receive contributions from more than one macroparticle.

The contents of the accumulators at the end of a time step become the values of n_- that are used to calculate the electrostatic force on each macroparticle during the next time step. Thus there must be at least two sets of such variables representing the radial charge distribution. One set represents the charge distribution obtained during the previous time step and being currently used to determine the particle trajectories; the second set represents the accumulators being incremented during the current time step and whose values will be used to determine the particle trajectories during the next time step.

In order to advance a macroparticle by one time step, the Runge-Kutta procedure requires that $T(x,R,S)$ given by eq. (21) be evaluated at the points indicated in eqs. (15b), (16b), (17b) and (18b). The first three terms on the right hand side of eq. (21) present no problem. However, the last term in eq. (21) does present a problem due to the discreteness of the charge distribution mesh and to the implicit dependence of n_- and n_+ on the time.

The integral in this term is a function of R only through the upper limit of integration. It is required, therefore, to evaluate the quantity

$$C(R) = \int_0^R (n_- - n_+) R' \, dR' \tag{24}$$

for each macroparticle at the four points $R = R_i$, $R_i + 0.5\Delta'$, $R_i + 0.5\Delta''$, and $R_i + \Delta'''$ at or near the radial position of the i^{th} macroparticle. To do this values of the discrete variable $C(j)$ corresponding to $C(R)$ are calculated using the discrete values of the negative and positive relative charge densities $n_-(j)$ and $n_+(j)$. Based on eq. (24) these are calculated from the recursion relations

$$C(j) = C(j-1) + \left[n_-(j) - n_+(j)\right] \rho(j)\, d$$

$$\rho(j) = \rho(j-1) + d \qquad (25)$$

$$C(0) = 0$$

Proper handling of the implicit time dependence of the integral term in eq. (21) is also required in order to evaluate eqs. (15b)-(18b). To do this, values of the integral $C(j)$ for several past time steps must be saved and used in an extrapolation from x_o to $x_o + \Delta x/2$ and to $x_o + \Delta x$. In the work reported here, values of $C(j)$ for the last three time steps were preserved for use in the time extrapolation.

Advancing each macroparticle by one time step consists of a loop over all values of the macroparticle index i, for each of which the operations indicated by A in Fig. 3 are performed. First the radial position R_i of a macroparticle is located with respect to the charge mesh; that is, the value of j corresponding to the mesh interval containing R_i is determined. Next the nine nearest values of $C(j)$ at locations symmetrically distributed about R_i are fitted by a least squares polynomial. The degree of this polynomial is optional; the result of using polynomials of various orders will be discussed later. This continuous function fitted to the discrete values of $C(j)$ is then used in place of $C(R)$ when evaluating the right hand side of eq. (21).

In an early version of the program, difficulty was experienced in the least squares fitting due to an ill-conditioned matrix of coefficients in the set of linear algebraic equations that must be solved. This trouble was avoided and, at the same time computation time was decreased significantly by using the method of orthogonal polynomials in the least squares fitting[8,9].

An interpolation between the known values of C(j) is obviously necessitated by the Runge-Kutta procedure. The use of a least-squares polynomial is believed to be superior to an n-point interpolation formula because it provides a way to compensate for the finite spatial resolution imposed by the use of a digital computer. The charge distribution can be quite discontinuous, both near the edge of the beam and where there is only a small overlap between macroparticles. The latter situation is shown schematically in Fig. 4. If two macroparticles overlap slightly, which is the usual situation, a small step will develop in the charge distribution. Such a step does not mean that there would be a corresponding sharp discontinuity in the charge distribution in an actual physical device, however. The essential continuity in nature is put back into the calculation by distributing this step over the width of the macroparticle by means of the least-squares fitting. At the same time one does not want to spread the step uniformly because it is important to preserve the gradients of the charge distribution since it is these that determine the force on a charged particle. By fitting a low order polynomial to such a distribution a representation of the radial gradients is preserved in a way that still allows the use of a Runge-Kutta integration technique.

In the light of this discussion, it is also clear that the number of C(j) values used in the least-squares fit should be such as to approximately span one macroparticle. Thus the use of nine values is related to the choice of the macroparticle to charge mesh width ratio D/d , of 10. Or, to put the matter in a different perspective, the choice of D/d is related to the number of points and hence to the amount of computing time that one wishes to employ in the least-squares fit for each macroparticle at each time step.

Since the time variation of the $C(j)$ quantities is smooth, a simple polynomial extrapolation procedure could be used to evaluate the integral expression in eq. (24) at the points in time required by the Runge-Kutta procedure. Thus, after locating each macroparticle, a least-squares polynomial expressing the radial variation of $C(j)$ was fitted to each of the three sets of $C(j)$ representing the charge integral for the three past time steps. Whenever $C(R)$ is required at a future time, the fitted least-squares polynomials for the three past time steps are evaluated at the desired radi points and the resulting three values are used to extrapolate $C(R)$ to the desired time.

Calling the value of $C(R)$ at a given point R_k obtained using the values of $C(j)$ for the most recent time step $x_o, C_1(R_k)$, the value of $C(R)$ at R_k obtained using the values of $C(j)$ for the previous time step $x_o - \Delta x, C_2(R_k)$, and the value of $C(R)$ at R_k obtained using values of $C(j)$ for the next previous time step $x_o - 2\Delta x, C_3(R_k)$, then the value of $C(R)$ at R_k for $x_o + \frac{1}{2}\Delta x$ is

$$C_4(R_k) = \frac{15}{8} C_1(R_k) - \frac{5}{4} C_2(R_k) + \frac{3}{8} C_3(R_k)$$

The value of $C(R)$ at R_k for $x_o + \Delta x$ is

$$C_5(R_k) = 3 C_1(R_k) - 3 C_2(R_k) + C_3(R_k)$$

Once the integral $C(R)$ has been evaluated at the required points in space and time, the calculation of ΔR and ΔS for one time step using eqs. (15)-(18) is straightforward. When the new radial position has been obtained, the appropriate accumulators must be incremented. This requires that the new value of R_i be again located with respect to the charge mesh. The amount by which each accumulator is incremented is such that the total amount of charge represented by the macroparticle is conserved. Since each macroparticle represents a cylindrical annulus of mid-radius R_i and fixed

width D, the relative charge density per radial interval d, $n_-(x,R)$, must satisfy the relation

$$n_-(x,R)R_1(x) = R_1(0)n_-(0,R) \qquad (26)$$

where $R_1(0)$ is the initial position of the 1^{th} macroparticle and $n_-(0,R) = 1$. Thus, if the width of a macroparticle is, for computational convenience, to be kept fixed, the density of charge must be adjusted when the macroparticle departs from its initial radial position. When $R_1(x) > R_1(0)$, due to the cylindrical geometry the macroparticle represents a greater volume and so the charge density must be proportionally decreased. The opposite is the case when $R_1(x) < R_1(0)$. Thus the amount by which each accumulator is incremented is not unity as at the beginning of the problem but $R_1(0)/R_1(x)$. Also, since for $x > 0$ a macroparticle is not in general exactly aligned with D/d charge mesh intervals, the above accumulator increment is applied to only the $(D/d)-1$ intervals completely spanned by the macroparticle. The remaining charge increment $R_1(0)/R_1(x)$ is divided between the inner and outer accumulators that are only partially spanned by the macroparticle in the ratio of the overlap of the two mesh intervals.

When the last macroparticle has been advanced by one time step, the A loop in Fig. 3 is completed and the calculation enters the B loop. This consists of extracting the information of physical interest from the results, making the necessary preparations for the next time step and recycling the program to start the next time step.

Prior to these steps, however, the total amount of charge present in the accumulators is calculated and compared with that present initially. Due to the approximate way in which the accumulators are incremented these will not in general be identical. The contents in each accumulator are then

"corrected" by multiplying by the factor necessary to keep the amount of negative charge in the beam constant and thus preserve the overall neutrality of the plasma. At this point the relative negative charge distribution can be printed if desired. This information and the radial and azimuthal position and the radial velocity of each macroparticle are the primary output of the program for each time step.

It is difficult to form a clear picture of the behavior of the beam from this mass of detailed information. Therefore, the above information is edited to yield the mean radial position of the negative charge and the rms deviation of the negative charge from this mean. These quantities are referred to in the figures to follow as the beam position and the beam width. Specifically, they are defined as

$$\begin{matrix}\text{beam}\\ \text{position}\end{matrix} = \bar{R} = \frac{\int n_-(R')R'^2\,dR'}{\int n_-(R')R'\,dR'} \quad \frac{\Sigma\, n_-(j)\,\rho_j^2}{\Sigma\, n_-(j)\,\rho_j} \tag{27}$$

$$\left[\begin{matrix}\text{beam}\\ \text{width}\end{matrix}\right]^2 = \frac{\int n_-(R')(R'-\bar{R})^2\,R'\,dR'}{\int n_-(R')R'\,dR'} \quad \frac{\Sigma\, n_-(j)(\rho_j-\bar{R})^2\rho_j}{\Sigma\, n_-(j)\,\rho_j} \tag{28}$$

Finally, the contents of each of the accumulators are transferred to the $n_-(j)$ array, the time is incremented, and the program recycles to the point indicated in Fig. 3 where the accumulators are cleared and next time step is started.

The program terminates when some maximum time value is reached. One finds in many cases that the beam position undergoes a sinusoidal oscillation that is either exponentially growing or exponentially damped. In these cases the really significant quantities are the frequency, phase, amplitude, and e-folding rate of the beam position oscillations. Therefore, the calculated beam position information must be further edited to produce these quantities.

This is done by fitting the beam position as a function of time by an expression of the form

$$\bar{R}(x) = Ae^{Dx} \sin(\omega x + \Phi) + S \qquad (29)$$

During the course of the trajectory calculation, some of the values of $\bar{R}$ and x are saved for input into a final part of the program where the five adjustable constants, A, D, ω, Φ, and S, are fitted by an iterative non-linear least squares technique[10]. This has proven to be extremely useful in studying the validity of the numerical procedures used in the calculation. In the work that is reported here, about eighty set of $\bar{R},x$ values spanning about seven plasma periods have been used to determine the characteristics of the beam motion. Typically about thirty iterations are used to determine the five constants. Comparison of the fitted $\bar{R}$ values with those used in the fitting process shows that the two agree to at least seven significant figures. This indicates that the time behavior of $\bar{R}$ is very closely approximated by eq. (29). The number of iterations required to achieve such accuracy depends, in general, on the accuracy of the initial guess used to start the iterative process. This is a matter of experience. It has been found, for example, that good initial values for A, D, and Φ are not important but that ω should be specified to within about 25 percent of the correct value if the iterative process is to converge properly.

V. RESULTS

On the basis of previous single particle trajectory calculations[1], the effects of many of the variables on the early-time motion of a particle is reasonably well-understood. Therefore, the following physically realistic values have been chosen:

$$p = B_1/B_2 = 2.3$$

$$\omega = 10^6 \text{ sec}^{-1}$$

$$\beta = \omega_o/\omega = 10^6$$

The choice of p implies a vector potential well-depth of 1.73 percent for $\alpha = 0$. The choice of β implies a peak magnetic field in the orbit region of about 5 w/m^2. As indicated previously, the initial velocity of each particle was assumed to be zero and the initial position of the beam was chosen to be relatively narrow and located symmetrically with respect to the minimum of the vector potential well.

The first objective was to understand the effect of the charge density on the start-up behavior of the beam. This involved varying the value of γ. For all of these calculations, the azimuthal component of the magnetic field B_φ was set equal to zero (i.e. $q = 0$). Figure 5 shows a set of six macroparticle trajectories for the case where $N_o = 10^8 \text{ cm}^{-3}$. These trajectories do not differ significantly from the $N_o = 0$ case. That is, they are simply six single-particle trajectories; the radial oscillations are the familiar betatron oscillations about the equilibrium orbit at $R = 1.14$. The abscissa is the dimensionless time variable $x = \omega t$; for $\omega = 10^6 \text{ sec}^{-1}$, the dimensionless unit of time corresponds to one μsec.

The representation of this information in terms of the beam parameters, position and width, defined by eqs. (27) and (28), is shown in Fig. 6. Because the initial beam is located symmetrically about the equilibrium orbit,

the beam position does not vary significantly with time. The beam width undergoes a periodic oscillation of slowly decaying amplitude corresponding to the adiabatic damping of the betatron oscillations of the individual particles[11]. The minimum beam width at the cross-over points is not zero as implied by Fig. 5 because of the finite width of the macroparticles.

The set of trajectories in Fig. 7 for $N_o = 10^9$ cm^{-3} clearly shows the effect of the electrostatic force on the beam behavior. There is a tendency for the concentration of charge near the equilibrium orbit to repel further macroparticle penetration. Despite the apparent disorder of the trajectories, the beam position and beam width shown in Fig. 8 behave in a regular manner. The beam position undergoes larger amplitude oscillations than those for $N_o = 10^8$ cm^{-3} (Fig. 6) when a considerably more symmetric particle motion existed. The collapse of the beam still occurs and actually the collapse is more rapid at the larger charge density. Nevertheless, the essential features of the single-particle betatron oscillations are still present. The frequency of the position and width oscillations corresponds to the betatron frequency. The frequency of these oscillations increases with time and their amplitude decreases with time.

When the case of a charge density of $N_o = 10^{10}$ cm^{-3} is examined, the effect of the electrostatic forces on the beam motion is even more striking. The trajectories in Fig. 9 indicate that the beam collapse is considerably inhibited. In addition, there is now a high frequency radial oscillation by each macroparticle. From the fact that these radial oscillations for each macroparticle are in phase, it is clear that what is involved is a collective oscillation of the negative charge with respect to the fixed positive charge. The beam position and beam width shown in Fig. 10 summarize these observations. The beam collapse is smooth with no evidence of betatron oscillations. From the apparent approach of the

beam width to some minimum value, one infers that an equilibrium between betatron and electrostatic forces has been reached. One notes, however that the beam position oscillations, while decreasing in amplitude, still show an increase in frequency with time.

The period of the initial radial beam position oscillation in Fig. 10 is found to be very nearly the plasma frequency defined by eq. (19). Thus, the effect of the electrostatic space charge force on the early-time motion of a finite width beam in a plasma betatron is the following. The rapid collapse of the beam to the single-particle equilibrium orbit and the subsequent adiabatically-damped radial betatron oscillations are replaced by an inhibited spatial collapse of the beam and by a radial oscillation of the position of the beam with respect to the fixed positive charge at the plasma frequency. The inhibited collapse of the beam was expected; the appearance of a radial charge oscillation at the plasma frequency is not unreasonable either. The rising magnetic field excites radial betatron (single particle) oscillations which in turn drive the radial plasma (collective) oscillations. The energy source is the time-varying magnetic field. When the plasma frequency is much higher than the radial betatron frequency one expects the plasma oscillations to occur essentially at the "free" collective mode frequency which is very nearly the plasma frequency.

When $N_o = 10^{12}$ cm^{-3}, the charge density is sufficiently great that the collapse of the beam is completely inhibited, as shown by the macro-particle trajectories in Fig. 11. In this case the motion is completely characterized by the radial plasma oscillations. The beam position and beam width shown in Fig. 12 confirm this observation. Note that for these larger values of the charge density when the motion is dominated by electrostatic plasma oscillations, it is necessary to change the time scale of the calculation with the plasma period. Thus, between Figs. 10 and 12

there is a factor of 100 difference in the charge density. This means that the plasma frequency is higher by a factor of 10 in Fig. 12 and so the total amount of time shown in Figs. 11 and 12 is less by a factor of 10 than that shown in Figs. 9 and 10. For the lower values of charge density, the plasma frequency is less than the betatron frequency and so the time scale of the calculation, which is then determined by the betatron period, does not depend on the charge density.

Several supplementary investigations were made to assess the validity of the computed results. One of these consisted of solving a series of otherwise identical problems where the degree s of the least-squares polynomial used to interpolate between the available values of $C(j)$ was varied over the range $1 \leq s \leq 3$. It was found that the computed results were not dependent on s. Aside from the practical matters of computing time and the importance of truncation error in the determination of the coefficients of the least-squares polynomials, there is a logical necessity in keeping s small. As discussed previously the purpose of the least-squares interpolation is to smooth an otherwise irregular charge distribution; the use of a high degree polynomial tends to defeat this objective since the interpolation function then becomes an increasingly "better" fit to the irregularities one desires to smooth. For all of the calculations presented here, s was chosen to be two. It was felt that this was a reasonable compromise, smoothing $C(j)$ and still preserving its radial dependence.

The effect of the number of significant figures carried by the computer was examined by repeating some typical calculations on a computer that worked to sixteen figure accuracy instead of the eight figure accuracy of the machine used for all of the other calculations reported here. This could be a serious effect since as shown by eq. (25) the calculation of

$C(j)$ requires taking the difference between n_- and n_+. Since often these are both near unity, there can be a loss of three or four significant figures at this point. No significant effect on such integrated quantities as the beam parameters defined by eqs. (27) and (28) was observed; however such details as the macroparticle trajectories and the charge distributions showed some small but perceptible differences.

A most important supplementary investigation was that of the effect of the time step on the calculation. The earliest calculations of collective effects were required, because of computer limitations, to ignore the time dependence of the charge integral $C(t)$. It was found that the electron motion was quite unstable. Within a few plasma periods the beam position oscillations became quite large; coupled unstable oscillations in the beam width occurred also. Eventually, coherent beam motion ceased as macroparticles broke away from the positive charge entirely. However, it was observed that the magnitude of the growth rate of the instability decreased as the time step decreased indicating that the observed beam instability had a numerical rather than a physical origin.

It was at this point that time was made available on a computer that offered more memory capacity and greater speed. Not only could the time dependence of $C(j)$ be treated but also the time step could be made much smaller. The first step was to consider a linear extrapolation of $C(j)$ using the results of the previous two time steps. It was found that this procedure had an enormous effect in decreasing the growth rate of the instability. As before, it was found that decreasing the time step also decreased the growth rate.

However, the beam position oscillation was still unstable although for a sufficiently small time step the effect was barely perceptible. The next step was to perform a quadratic extrapolation of $C(j)$ using the

results of the previous three time steps. When this was done it was found that the beam position oscillation was no longer unstable. The coefficient of the exponential factor in eq. (29) was found to be negative indicating that the plasma oscillations were damped. Again it was found that the rate of this process decreased as the time step decreased. Therefore, the interpretation has been made on the basis of both the linear and quadratic extrapolation of $C(j)$ that the observed plasma oscillations are stable in the limit as the time step goes to zero. The residual growth or decay rate for a small finite time step is believed to be a purely numerical effect. These results are summarized in Table I. For all of the calculations reported here, quadratic extrapolation of $C(j)$ was employed and the time step was either 5×10^{-6} or 1/220 of the plasma period if that was smaller.

Finally, the effect of a B_φ field on the results was studied. A charge density $N_o = 10^{12}$ cm^{-3} was selected since this represents a case where the electrostatic forces completely dominate the beam behavior. When $q = B_3/B_2 = 10^{-2}$, corresponding to $B_\varphi(r_1) = 540$ gauss, there was virtually no effect on the radial position oscillation. The beam width remained constant at its initial value as shown in Fig. 12 for $q = 0$. However, when $q = 1$ i.e. when the B_φ field is essentially equal to the betatron field in the orbit region, the radial plasma oscillations were completely suppressed. The macroparticle radial positions were constant in time and the beam width was constant, therefore.

Table I

Dependence of time step and time-dependence of C(j) on results for $N_o = 10^{12}$ cm^{-3}

time-dependence of C(j)	$\frac{\text{plasma period}}{\text{time step}}$	$\frac{\text{e-folding time}}{\text{plasma period}}$
none	11	1.2
	22	2.3
	44	4.5
linear	22	41
	44	340
	110	5,600
	220	38,000
	440	150,000
quadratic	22	-40
	110	-2,500
	220	-27,000

V CONCLUSIONS

On the basis of the results reported here, the following conclusions can be drawn:

1. For charge densities less than about 10^9 cm^{-3}, the electrostatic field that develops during the start-up of a plasma betatron is ineffective in preventing the collapse of the beam to the single-particle equilibrium orbit

2. For charge densities in the range 10^9 - 10^{10} cm^{-3}, the beam behavior indicates a transition from that of a single-particle pure betatron character to a collective character dominated by long-range electrostatic effects

3. For charge densities greater than about 10^{10} cm^{-3}, a radial plasma oscillation appears. This consists of an oscillation of the center of charge of the electrons with respect to the relatively fixed positive charge. The frequency of this charge oscillation is the plasma frequency

4. This radial plasma oscillation appears to be stable if the space and time dependence of the charge integral term is handled sufficiently carefully and if the time step is sufficiently small

5. The addition of an azimuthal component of the magnetic field comparable to the betatron field at the orbit suppresses the radial plasma oscillation completely

ACKNOWLEDGMENTS

The work was supported by the Advanced Research Projects Agency under U.S. Army Signal Corps Contract. The calculations were performed on an IBM 7094 at New York University. Computer time was contributed by the U.S. Atomic Energy Commission under Contract Nr. AT(30-1)-2813.

REFERENCES

1. S.J. Lukasik, K.C. Rogers, G.W. Zepko, G.J. Brucker, "The Capture of Electrons into Stable Betatron Orbits", Nuclear Instruments and Methods 24 365 (1963)
2. O. Buneman, "Dissipation of Currents in Ionized Media", Phys. Rev. 115 503 (1959)
3. J. Dawson, "One-Dimensional Plasma Model", Phys. Fluids 5 445 (1962)
4. P. Burger, "Computer Simulation of One Dimensional Plasmas", presented at the meeting of the Plasma Physics Division, American Physical Society, 6-9 Nov 1963
5. R. Hockney, "Computer Simulation of a Plasma in Two Dimensions", presented at the meeting of the Plasma Physics Division, American Physical Society, 6-9 Nov 1963
6. D.A. Dunn and I.T. Ho, "Computer Model of a Beam-Generated Plasma", presented at the meeting of the Plasma Physics Division, American Physical Society, 6-9 Nov 1963
7. H. Levy and E.A. Baggott, Numerical Solutions of Differential Equations Dover Publications, Inc. 1950
8. G.E. Forsythe, "Generation and Use of Orthogonal Polynomials for Data-Fitting on a Digital Computer", J. Soc. for Industrial and Appl. Math 5 74 (1957)
9. P.H. Rank, Jr., "Fortran II Subroutine for Least-Squares Polynomial Fitting by Orthogonal Polynomials", Davidson Laboratory, Stevens Institute of Technology Note N-727, April 1965
10. S.C.Y. Chen, "A Fortran II Program for Least Squares Fitting of a Sinusoidal Function with Exponential Growth or Decay", Davidson Laboratory, Stevens Institute of Technology Note N-715, March 1964
11. D.W. Kerst and R. Serber, "Electronic Orbits in the Induction Accelerator", Phys. Rev. 60 53 (1941)

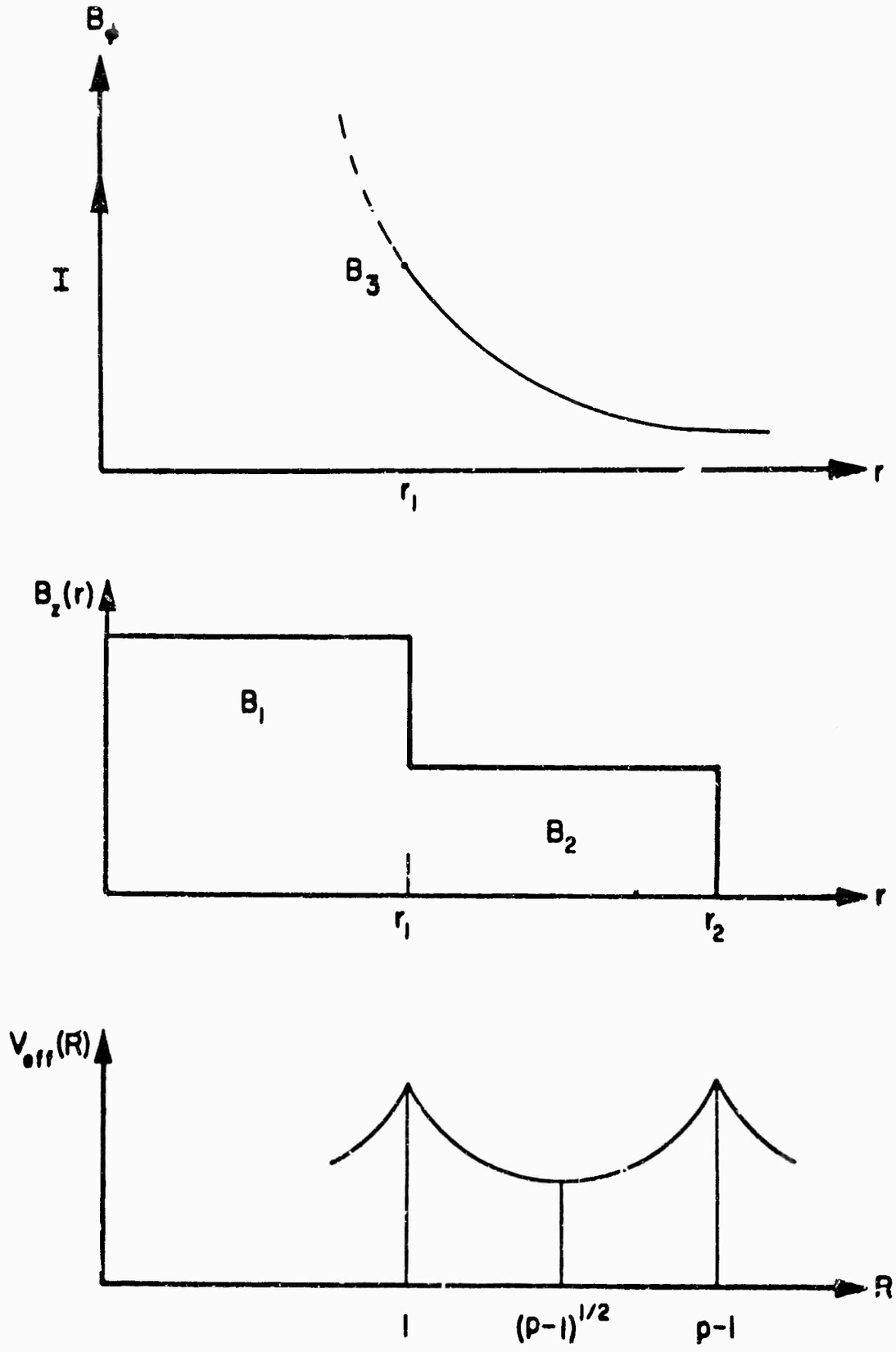

FIGURE 1

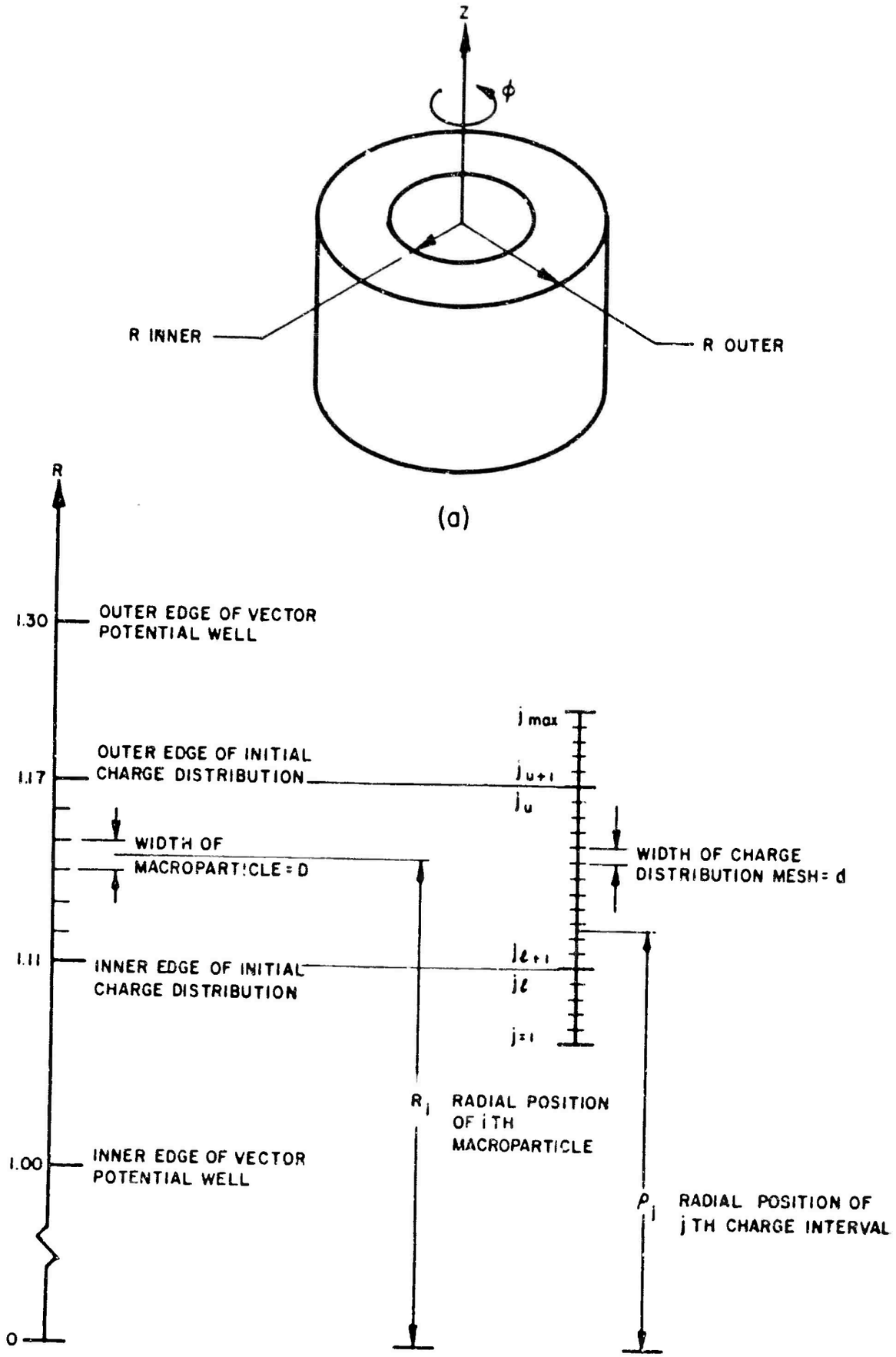
Z
φ
R INNER
R OUTER
(a)
R
1.30
OUTER EDGE OF VECTOR POTENTIAL WELL
1.17
OUTER EDGE OF INITIAL CHARGE DISTRIBUTION
WIDTH OF MACROPARTICLE = D
1.11
INNER EDGE OF INITIAL CHARGE DISTRIBUTION
1.00
INNER EDGE OF VECTOR POTENTIAL WELL
0
j max
j u+1
j u
WIDTH OF CHARGE DISTRIBUTION MESH = d
j ℓ+1
j ℓ
j=1
R i RADIAL POSITION OF i TH MACROPARTICLE
P j RADIAL POSITION OF j TH CHARGE INTERVAL
(b)

FIGURE 2

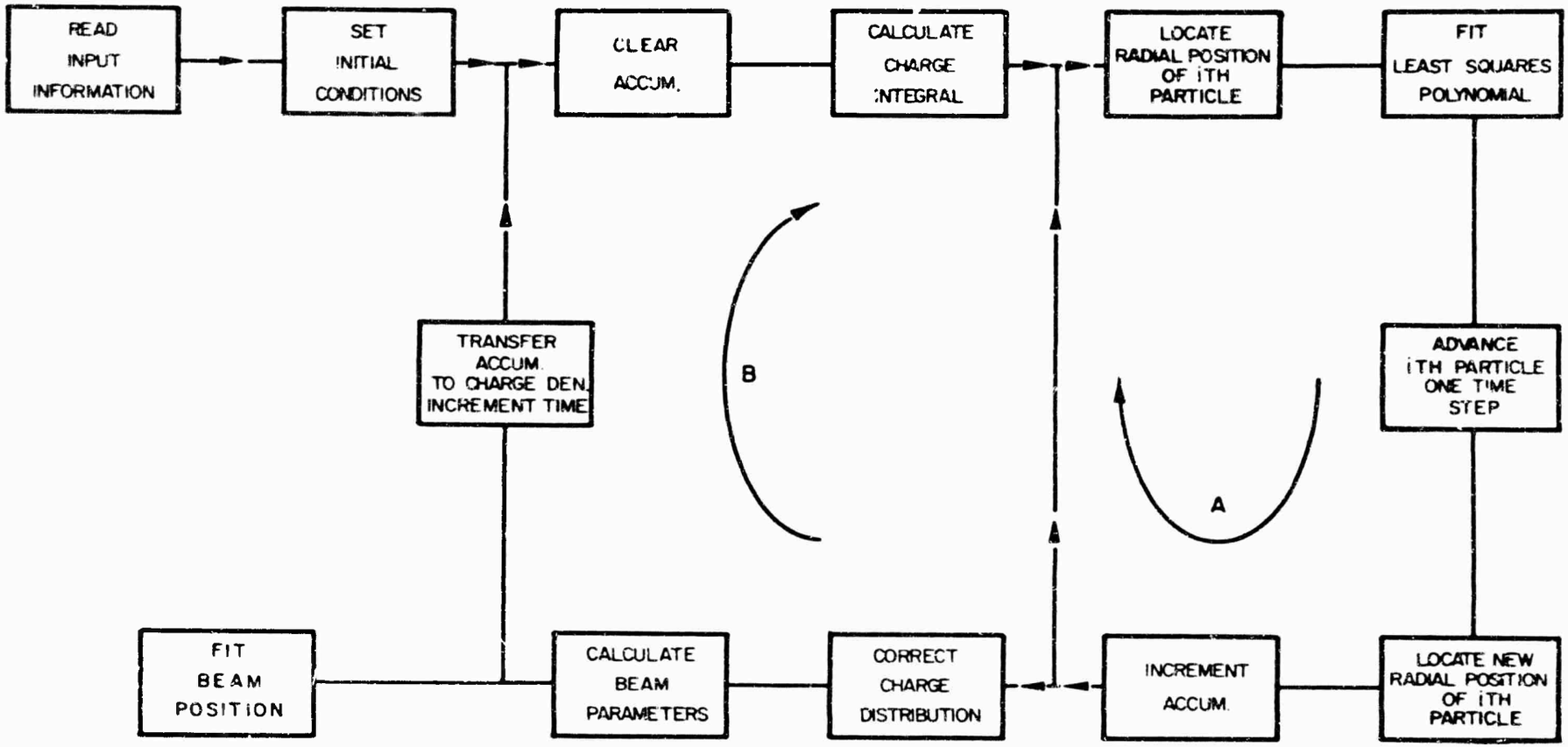

FLOW CHART FOR CALCULATIONS

FIGURE 3

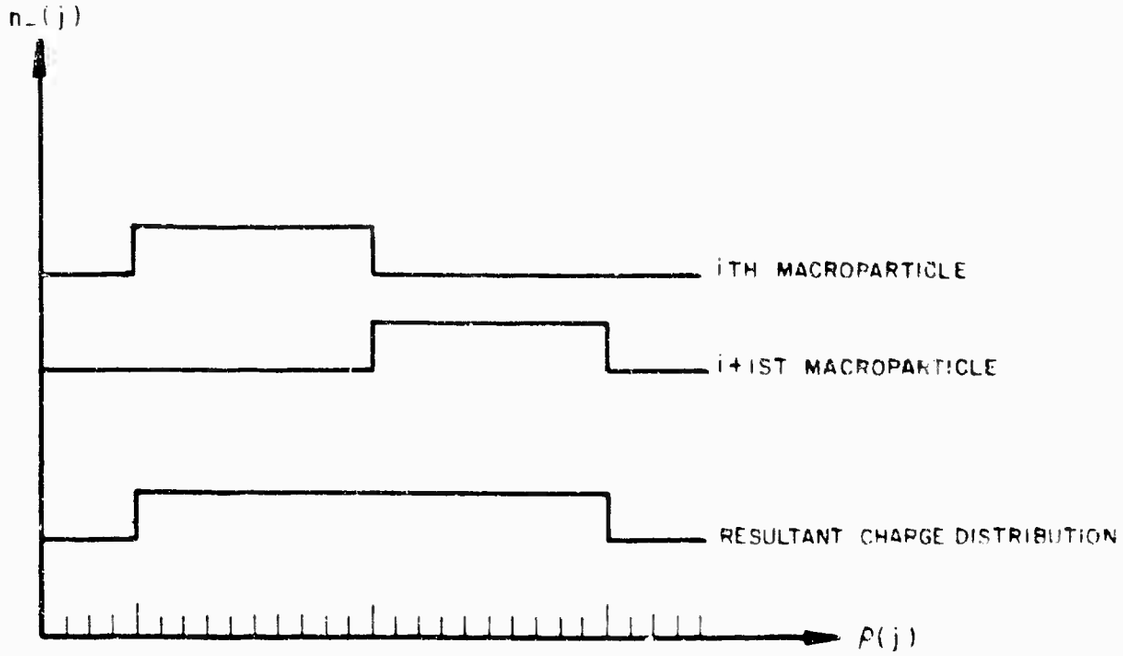

(a) EXACTLY CONTIGUOUS MACROPARTICLES

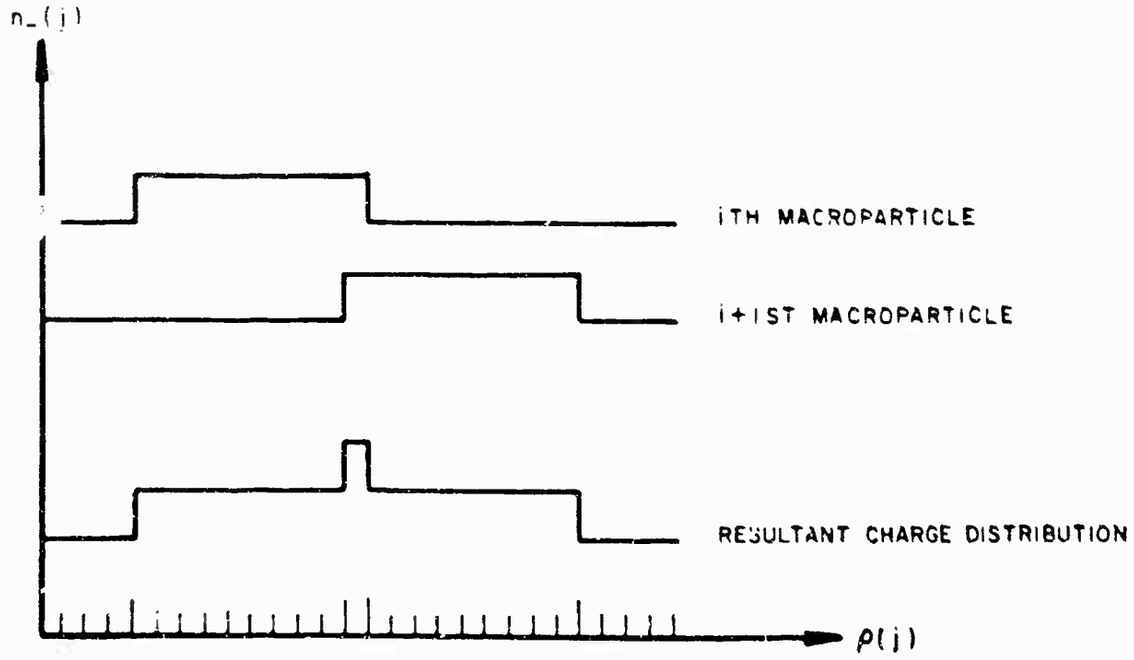

(b) SLIGHT OVERLAP BETWEEN ADJACENT MACROPARTICLES

FIGURE 4

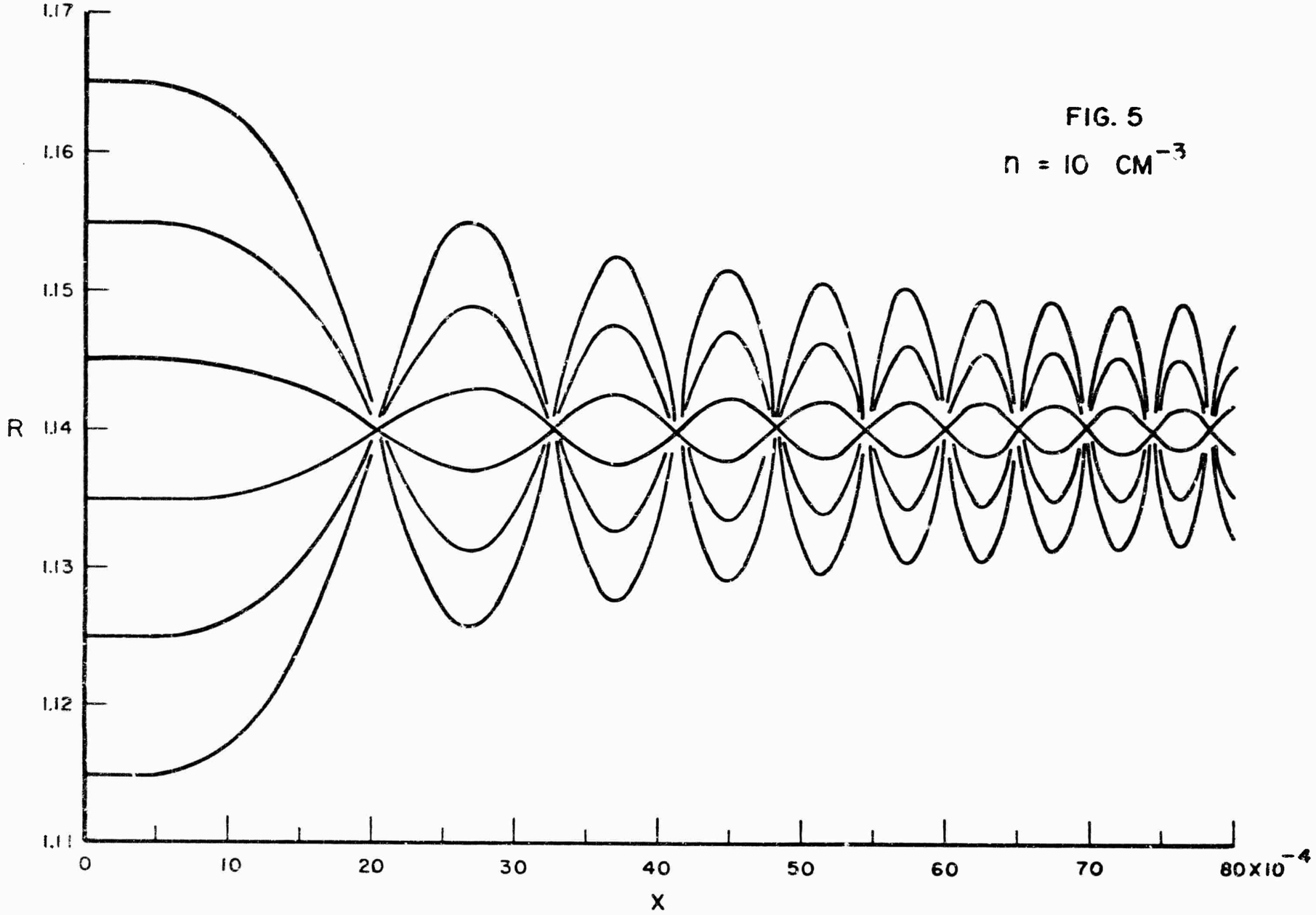

FIG. 5

$n = 10^{-3}$ CM

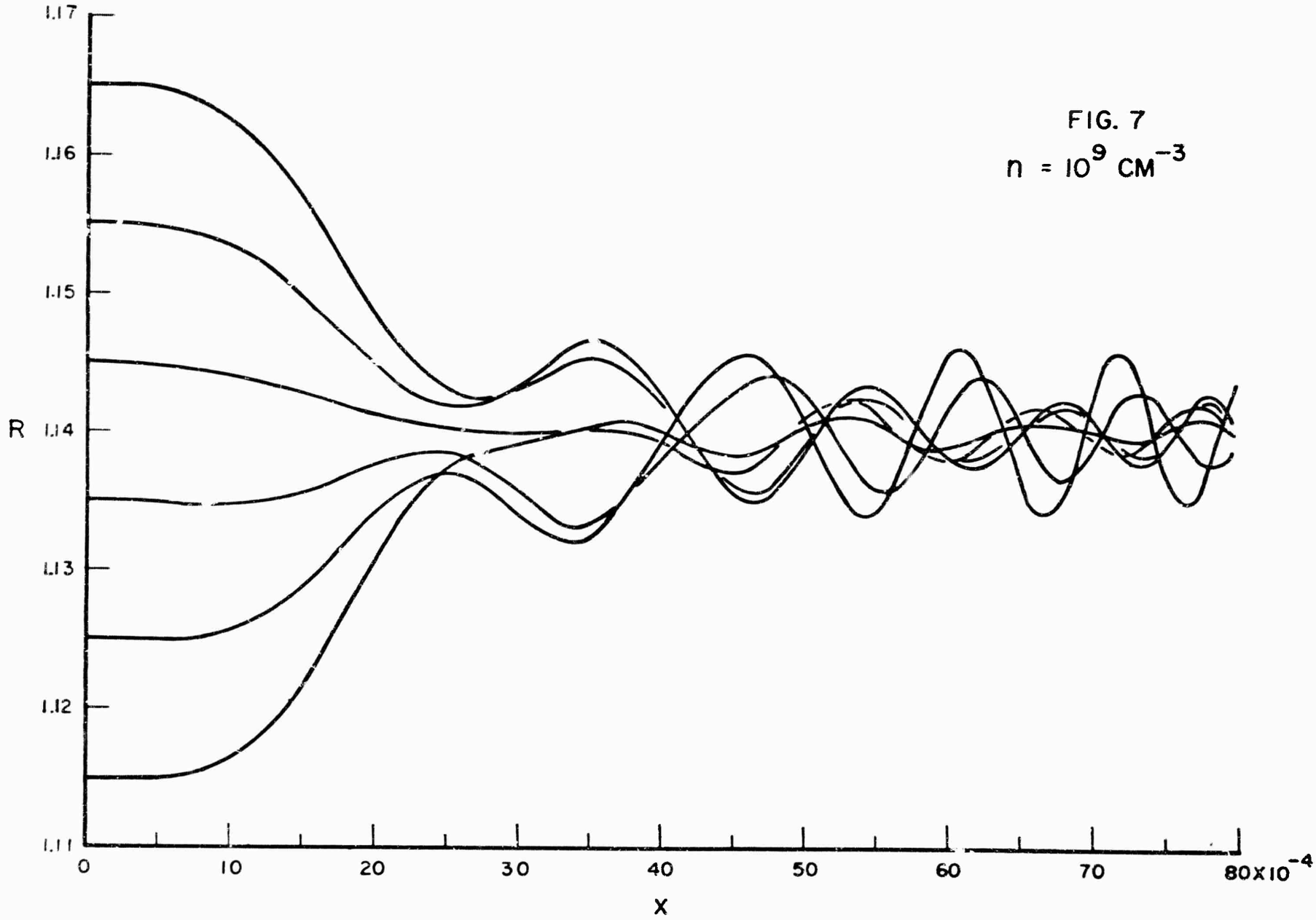

FIG. 7

$n = 10^9\ CM^{-3}$

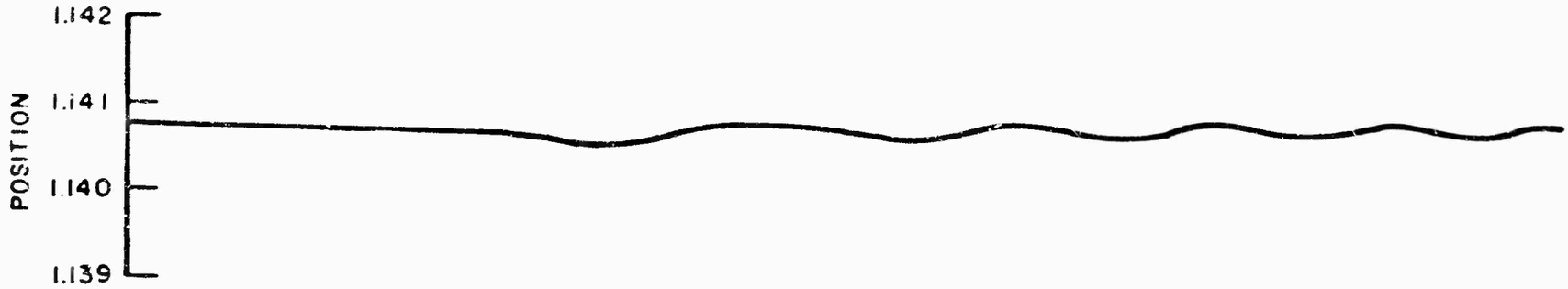

FIG. 6

$n = 10^{8}\ CM^{-3}$

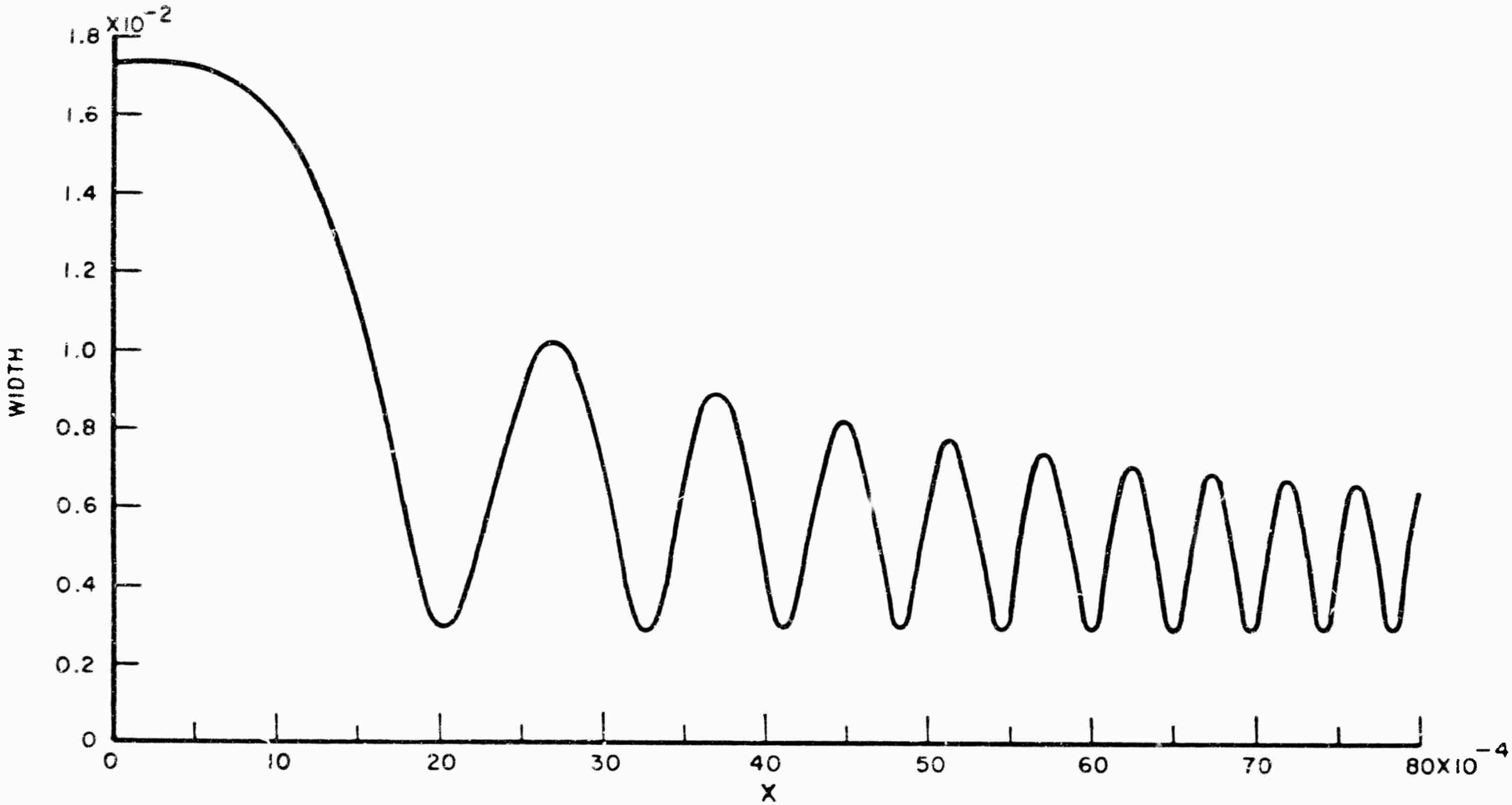

1.17

FIG. 9

$n = 10^{10} CM^{-3}$

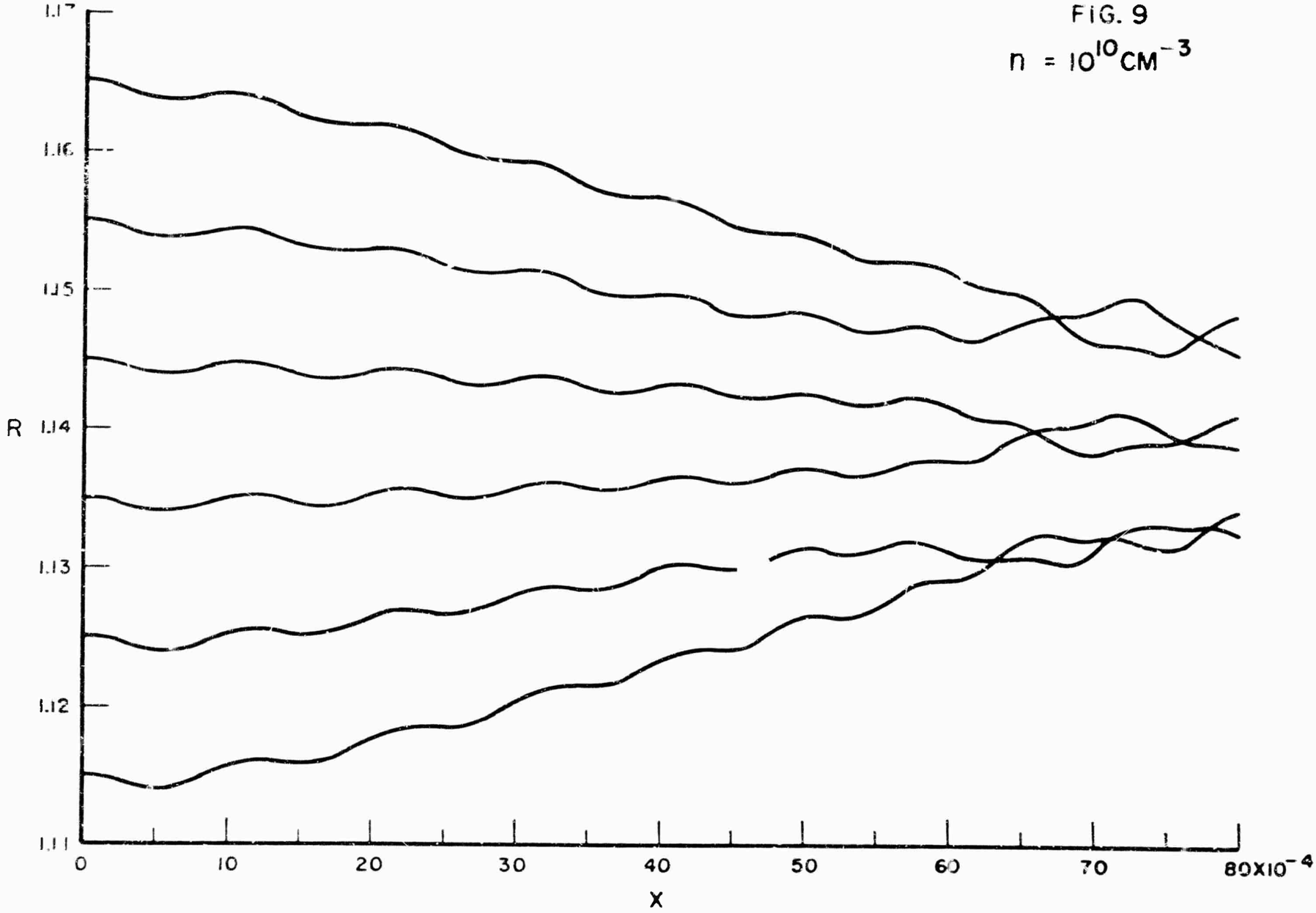

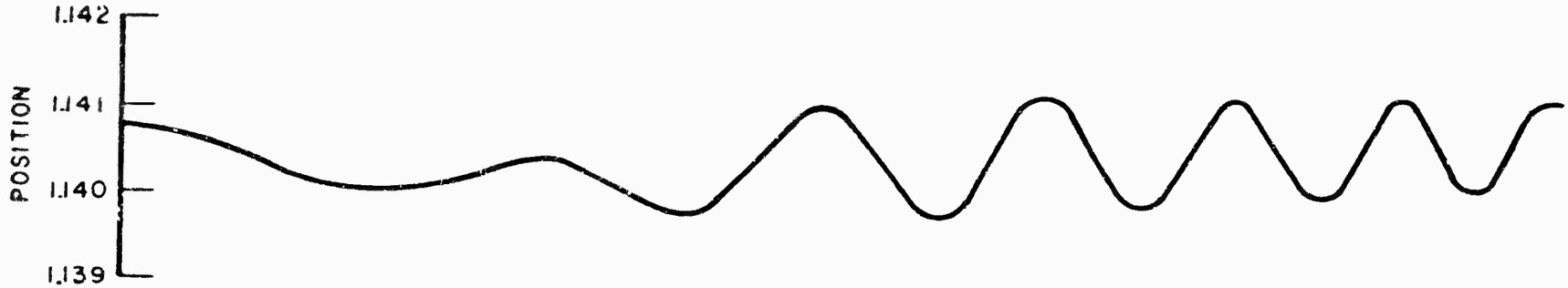

FIG. 8

$n = 10^9$ CM^{-3}

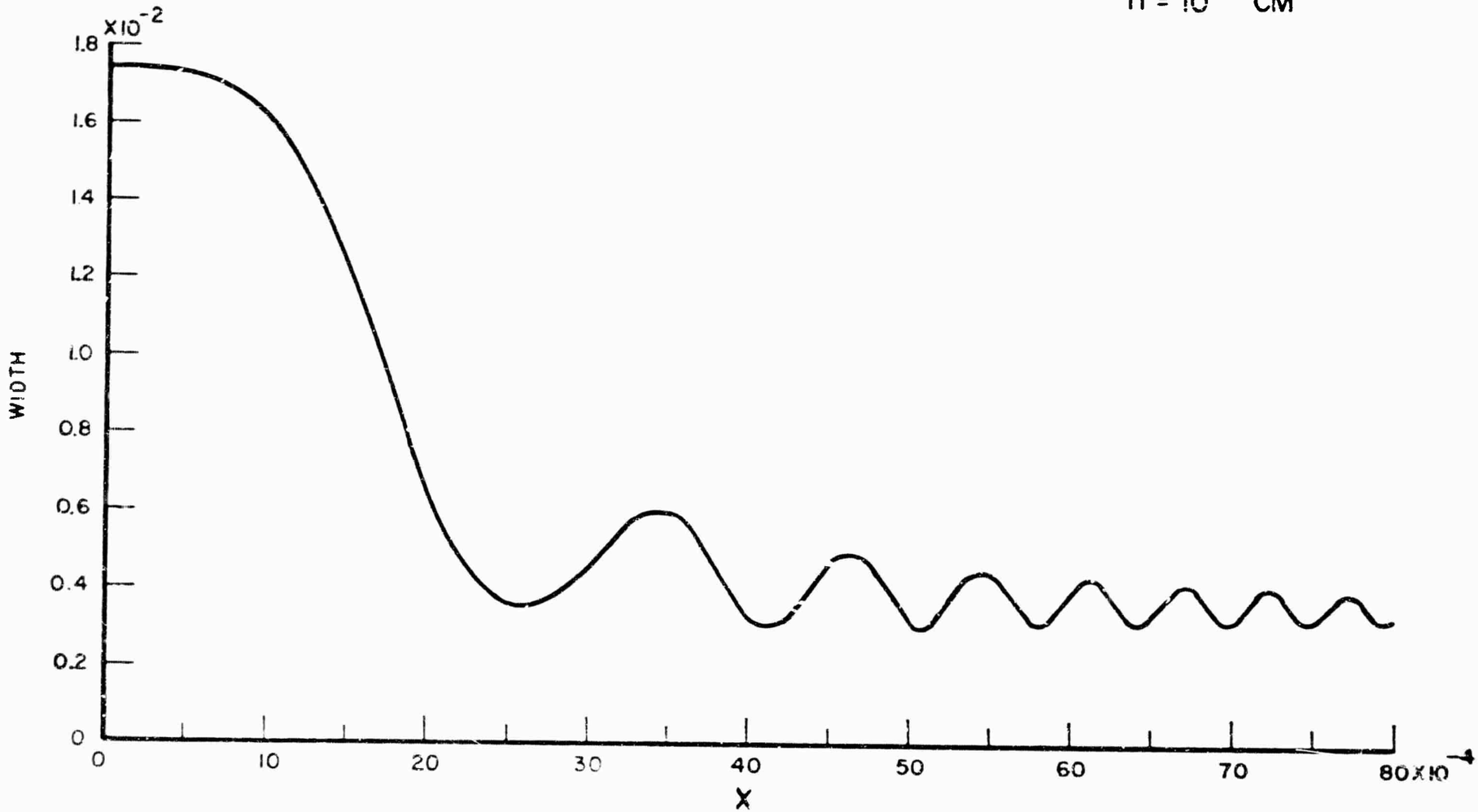

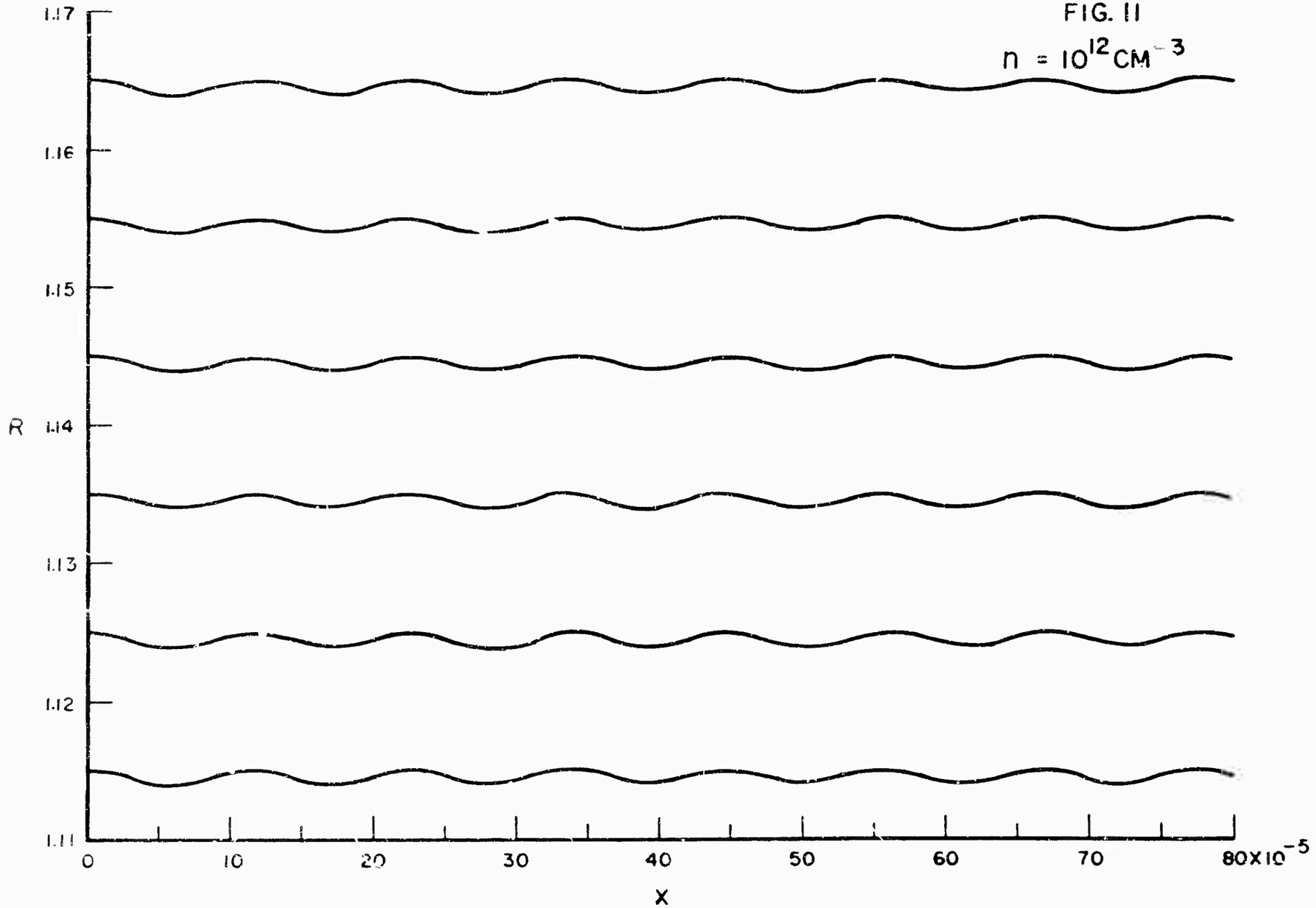
FIG. 11
n = 10^12 CM^-3
1.17
1.16
1.15
1.14
1.13
1.12
1.11
R
0
10
20
30
40
50
60
70
80X10^-5
X

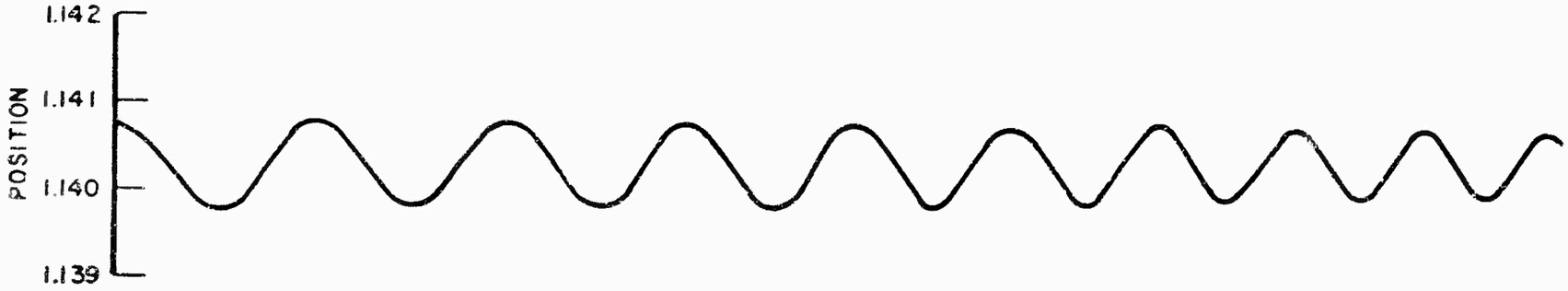

FIG. 10

$n = 10^{10}\ CM^{-3}$

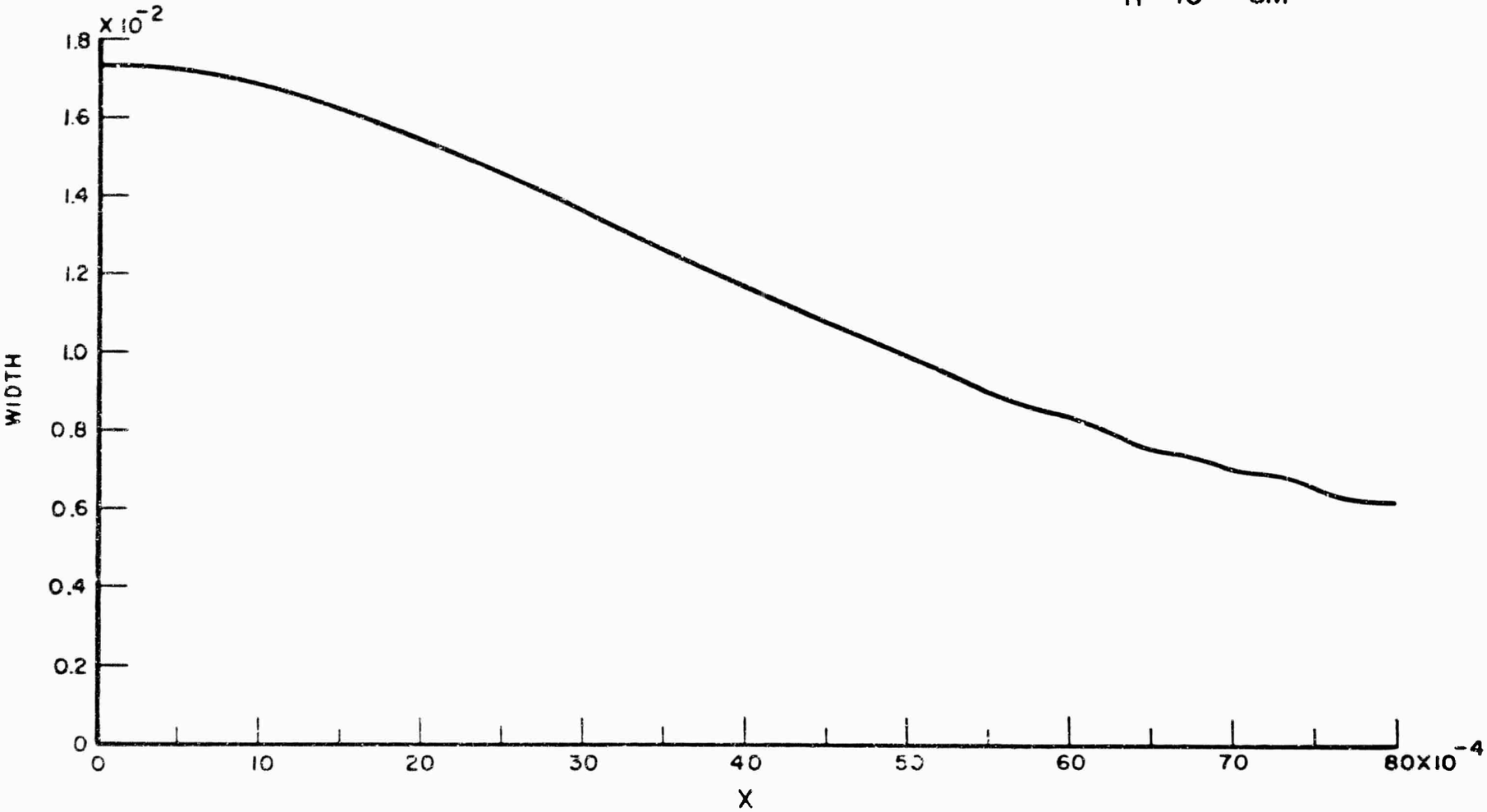

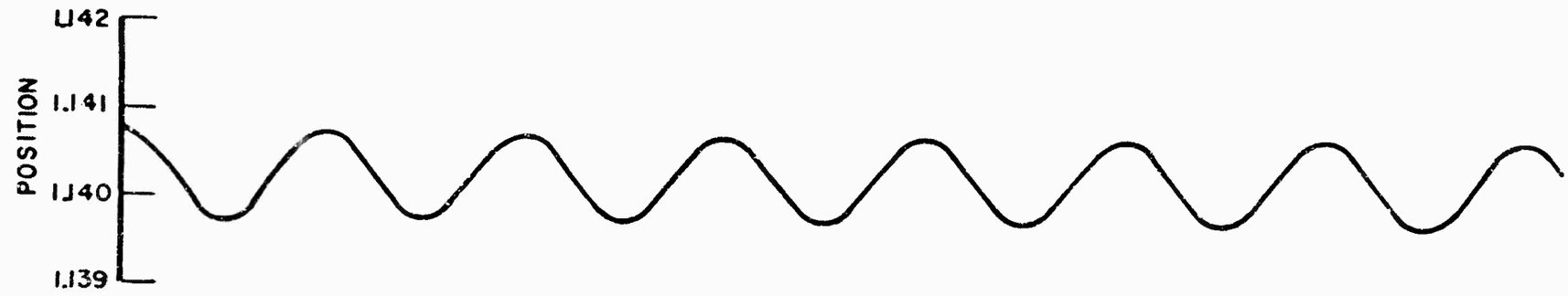

FIG. 12

$n = 10^{12}\ CM^{-3}$

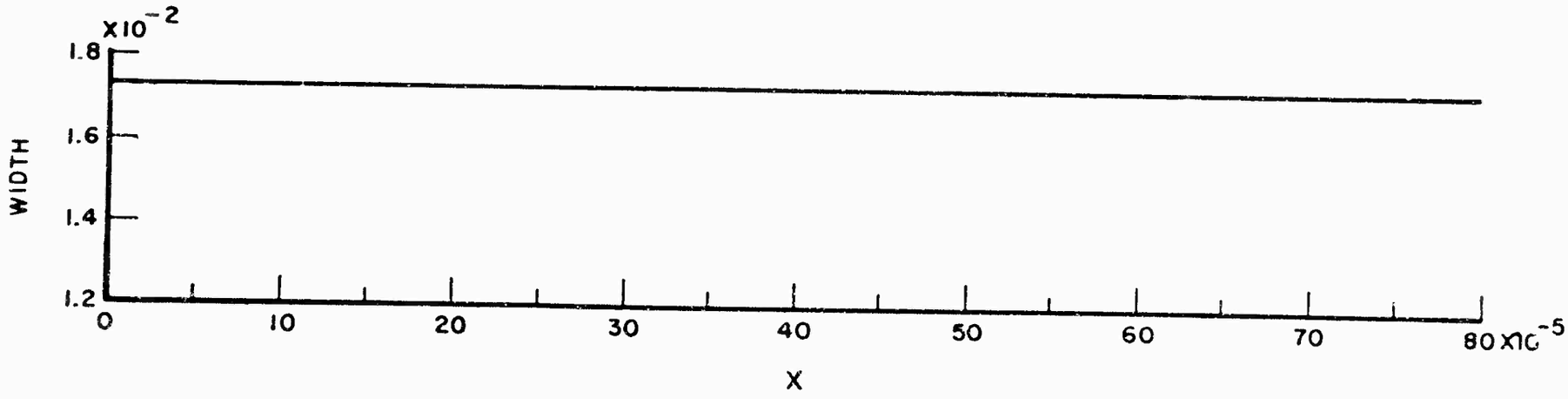

Papers and Publications Produced by Participants in the Megatron Project (Not Including Semi-Annual and Annual Progress Reports)

1. D. Finkelstein, The Megatron, NYO-7735, unpublished (1957).

2. D. Finkelstein, The Megatron, Second United Nations Intern. Conf. on the Peaceful Uses of Atomic Energy, Geneva (1958).

3. I. Mansfield, Measurements on a Low Inductance Capacitor, NYO-8647, unpublished (1958).

4. K. C. Rogers, D. Finkelstein, L. Ferrari, I. Mansfield, and G. Brucker, A High Efficiency Capacitor Bank Study, NYO-2378.

5. K. C. Rogers, D. Finkelstein, and G. Brucker, The Megatron - A High Field Plasma Betatron, Proc. of The Intern. Conf. on High-Energy Accelerators and Instrumentation - CERN 1959.

6. D. Finkelstein, Neutralized Electron Beams and Budker Accelerators, Proc. of The Intern. Conf. on High-Energy Accelerators and Instrumentation - CERN 1959.

7. K. C. Rogers, G. Brucker, and D. Finkelstein, The Megatron, Bull. of the Amer. Phys. Soc. Sec. II Vol. 5, 319 (1960).

8. K. C. Rogers, Plasma Betatrons and Relativistic Plasma Physics, Bull. of the Amer. Phys. Soc. Sec. II Vol. 5, 53 (1960).

9. G. Brucker and K. C. Rogers, A Kilovolt-Kiloampere Low Pressure Switch, Nuc. Instr. and Methods, 8, 236 (1960).

10. K. C. Rogers and D. Finkelstein, The Construction and Study of a High Field Plasma Betatron Accelerator, NYO-9101, SIT-P9 - 6/60 .

11. G. Schmidt, Self-Consistent Field Theory of Plasma Betatrons, J. of Nuc. Energy: Part C, 3, 156 (1961).

12. D. Finkelstein and P. A. Sturrock, Stability of Relativistic Self-Focusing Streams in "Plasma Physics" edited by Drummond, J. E. (McGraw-Hill, New York 1961) p 224.

13. S. J. Lukasik, K. C. Rogers, G. W. Zepko, The Capture of Particles into Stable Betatron Orbits, Nuc. Instr. and Methods, 24, 365 (1963).

14. Ronald W. Landau, Longitudinal Instabilities of Relativistic Beams in Axially Symmetric Magnetic Fields, Ph.D. thesis, Stevens Institute of Technology SIT P-98 (1963).

15. S. J. Lukasik and K. C. Rogers, Early-Time Collective Effects in a Plasma Betatron, Bull. of the Amer. Phys. Soc. Sec. II, 9, 330 (1964) and SIT-114.

16. H. J. Huber and K. C. Rogers, High Frequency Properties of Peaking Strip Probes, Rev. Sci. Instr. 35, 801 (1964)

17. H. J. Huber, Wide Voltage Range High Energy Solid Dielectric Switch, Rev. Sci. Instr. 35, 1067 (1964)

18. L. Ferrari and K. C. Rogers, Runaway Electrons in a Plasma Betatron, Bull. of the Amer. Phys. Soc. Sec. II, 10, 214 (1965)

19. Lawrence A. Ferrari, Behavior of Runaway Electrons in a Plasma Betatron, Ph.D. Thesis, Stevens Institute of Technology, Dept. of Physics (1965)

PERSONNEL

Scientific Personnel

Principal Investigator - K. C. Rogers, Ph.D., Professor of Physics, S.I.T.

Project Scientists:

G. Brucker, Ph.D.[a]	Scientist, USARDL, Fort Monmouth, N.J.
J.R.M. Coulter, Ph.D.[b]	Visiting Research Associate, S.I.T.
D. Finkelstein, Ph.D.[c]	Associate Professor of Physics, S.I.T.
S.J. Lukasik, Ph.D.	Head Fluid Physics Div., Davidson Laboratory S.I.T.

Graduate Students

L.A. Ferrari[e]	R. W. Landau[f]
A. Jermakian	I. Goldhar
N. Wolf	R. Intemann[g]

Engineers

I. Mansfield

T. Lunghard

H. Huber

G. Zepko

(a) At RCA Research Laboratories, Princeton, N.J., since 1963
(b) At Queens University, Belfast, Ireland, since 1963
(c) At Yeshiva University, New York, N.Y., since 1960
(e) At Plasma Physics Lab. Princeton University, since 1964
(f) At Lawrence Radiation Laboratory, Lawrence, Calif., since 1963
(g) At Temple University, Philadelphia, Pa., since 1963

BLANK PAGE

DOCUMENT CONTROL DATA · R&D

(Security classification of title, body of abstract and indexing annotation must be entered when the overall report is classified)

1. ORIGINATING ACTIVITY (Corporate author)
Stevens Institute of Technology
Hoboken, New Jersey

2a. REPORT SECURITY CLASSIFICATION
Unclassified

2b. GROUP

3. REPORT TITLE
Megatron Accelerator Final Report

4. DESCRIPTIVE NOTES (Type of report and inclusive dates)
Final Report - April 15, 1961 - June 15, 1964

5. AUTHOR(S) (Last name, first name, initial)
[illegible], [illegible], Lukasik, S. J., and L. Ferrari

6. REPORT DATE	7a. TOTAL NO. OF PAGES	7b. NO. OF REFS
	223	11

8a. CONTRACT OR GRANT NO.	9a. ORIGINATOR'S REPORT NUMBER(S)
DA 36-039-sc-87242 (E) b. PROJECT NO 1P0 14501.B11A c. Task No: 1P0 14501 B11A.00 d. Subtask No: 1P0 14501.B11A.00.33	SIT-P147 (5/65)
	9b. OTHER REPORT NO(S) (Any other numbers that may be assigned this report)

10. AVAILABILITY/LIMITATION NOTICES
Qualified requesters may obtain copies of this report from DDC.
This report has been released to CFSTI.

11. SUPPLEMENTARY NOTES	12. SPONSORING MILITARY ACTIVITY
	U. S. Army Electronics Command (AMSEL-XL-S) Fort Monmouth, N. J. 07703

13. ABSTRACT

Runaway electrons generated by induction acceleration in a plasma betatron with axially symmetric guide field $B_z(r,z,t)=B_o (r_o/r)^n x\ f(g) \sin 2\pi t/\tau$ ($n=0.6$, $\tau=16\mu$sec, $r=4.8$cm) together with auxilliary azimuthal guide field $B_\theta(r)=(k/r)$, (2 kG$\leq B_\theta(r)\leq$ 5kG) have been studied for a wide range of induction electric fields E_θ(2.5 v/cm$\leq$ $(E)_\theta\leq$26v/cm). Experiments have been carried out in argon and krypton at ambient pressures of 0.5-5 Torr. The ratio of the applied electric field to the critical electrical field for runaway was typically ~500 so that most of the electrons should run away. Runaway currents of ~1A were observed immersed in a background conduction current of 25-100 A. The runaway electrons strike the vacuum chamber walls at a time t_x after betatron acceleration has begun. The resulting x-rays are detected with a scintillation counter. The x-ray time t_x has been measured as a function of E_θ and B_θ for several half-cycles of the guide field. It is found that t_x decreases with E_θ but increases with B_θ. It is also found that t_x depends on the relative orientation of E_θ with respect to B_θ. This is shown to be due to a small transverse magnetic field associated with the B_θ guide field. The small runaway current is consistent with that determined from the self electric field generated by the adiabatic constriction of the runaway stream or the Negative-Mass-Instability. The reason for the beam disruption and subsequent x-ray emission are unexplained but the mechanism of Field and Fried appears to describe the process.

The betatron guide field was generated in a low inductance (50×10^{-9}h) single-turn coil using flux-concentrators. Techniques used to construct the flux-concentrators and measure the resulting pulsed magnetic field distribution are also described.

DD FORM 1 JAN 64 1473

14 KEY WORDS	LINK A		LINK B		LINK C	
	ROLE	WT	ROLE	WT	ROLE	WT
Electron Accelerators Plasma Instabilities Runaway Electrons						

INSTRUCTIONS

1. ORIGINATING ACTIVITY: Enter the name and address of the contractor, subcontractor, grantee, Department of Defense activity or other organization *(corporate author)* issuing the report.

2a. REPORT SECURITY CLASSIFICATION: Enter the overall security classification of the report. Indicate whether "Restricted Data" is included. Marking is to be in accordance with appropriate security regulations.

2b. GROUP: Automatic downgrading is specified in DoD Directive 5200.10 and Armed Forces Industrial Manual. Enter the group number. Also, when applicable, show that optional markings have been used for Group 3 and Group 4 as authorized.

3. REPORT TITLE: Enter the complete report title in all capital letters. Titles in all cases should be unclassified. If a meaningful title cannot be selected without classification, show title classification in all capitals in parenthesis immediately following the title.

4. DESCRIPTIVE NOTES: If appropriate, enter the type of report, e.g., interim, progress, summary, annual, or final. Give the inclusive dates when a specific reporting period is covered.

5. AUTHOR(S): Enter the name(s) of author(s) as shown on or in the report. Enter last name, first name, middle initial. If military, show rank and branch of service. The name of the principal author is an absolute minimum requirement.

6. REPORT DATE: Enter the date of the report as day, month, year, or month, year. If more than one date appears on the report, use date of publication.

7a. TOTAL NUMBER OF PAGES: The total page count should follow normal pagination procedures, i.e., enter the number of pages containing information.

7b. NUMBER OF REFERENCES: Enter the total number of references cited in the report.

8a. CONTRACT OR GRANT NUMBER: If appropriate, enter the applicable number of the contract or grant under which the report was written.

8b, 8c, & 8d. PROJECT NUMBER: Enter the appropriate military department identification, such as project number, subproject number, system numbers, task number, etc.

9a. ORIGINATOR'S REPORT NUMBER(S): Enter the official report number by which the document will be identified and controlled by the originating activity. This number must be unique to this report.

9b. OTHER REPORT NUMBER(S): If the report has been assigned any other report numbers *(either by the originator or by the sponsor)*, also enter this number(s).

10. AVAILABILITY/LIMITATION NOTICES: Enter any limitations on further dissemination of the report, other than those imposed by security classification, using standard statements such as:

(1) "Qualified requesters may obtain copies of this report from DDC."

(2) "Foreign announcement and dissemination of this report by DDC is not authorized."

(3) "U. S. Government agencies may obtain copies of this report directly from DDC. Other qualified DDC users shall request through

_____ "

(4) "U. S. military agencies may obtain copies of this report directly from DDC. Other qualified users shall request through

_____."

(5) "All distribution of this report is controlled. Qualified DDC users shall request through

_____ _____."

If the report has been furnished to the Office of Technical Services, Department of Commerce, for sale to the public, indicate this fact and enter the price, if known.

11. SUPPLEMENTARY NOTES: Use for additional explanatory notes.

12. SPONSORING MILITARY ACTIVITY: Enter the name of the departmental project office or laboratory sponsoring *(paying for)* the research and development. Include address.

13. ABSTRACT: Enter an abstract giving a brief and factual summary of the document indicative of the report, even though it may also appear elsewhere in the body of the technical report. If additional space is required, a continuation sheet shall be attached.

It is highly desirable that the abstract of classified reports be unclassified. Each paragraph of the abstract shall end with an indication of the military security classification of the information in the paragraph, represented as *(TS), (S), (C), or (U)*.

There is no limitation on the length of the abstract. However, the suggested length is from 150 to 225 words.

14. KEY WORDS: Key words are technically meaningful terms or short phrases that characterize a report and may be used as index entries for cataloging the report. Key words must be selected so that no security classification is required. Identifiers, such as equipment model designation, trade name, military project code name, geographic location, may be used as key words but will be followed by an indication of technical context. The assignment of links, rules, and weights is optional.

GPO 886-551